Monash University

Developing biomaterials with non-linear elasticity using core/shell electrospinning technology

Bing Xu

Thesis submitted to the Monash University in conformity with the requirements of the degree of Doctor of Philosophy

Department of Materials Engineering

Australia

January 2015

Declaration

I declare that this thesis contains no material which has been accepted for the award of any other degree or diploma at any university or any other institution. To the best of my knowledge, this thesis contains no materials published or written by another person previously, except where due reference is made in the thesis.

Signed:

Date:

Notice 1

Under the Copyright Act 1968, this thesis must be used only under the normal conditions of scholarly fair dealing. In particular no results or conclusions should be extracted from it, nor should it be copied or closely paraphrased in whole or in part without the written consent of the author. Proper written acknowledgement should be made for any assistance obtained from this thesis.

Notice 2

I certify that I have made all reasonable efforts to secure copyright permissions for third-party content included in this thesis and have not knowingly added copyright content to my work without the owner's permission.

Acknowledgements

First and foremost, I would like to thank my supervisors A/Professor John Forsythe, Professor Wayne Cook and A/Professor Qizhi Chen for their supervision, invaluable help, patience and encouragement throughout my PhD study.

I would like to thank all my colleagues Yuan Li, Chenghao Zhu, Nicholas Boyd and Andrew Rodda for their training and tremendous help in my experiments.

I would like to extend my thanks to material engineering staffs, in particular Mr. Silvio Mattievich, Ms. Karla Contreras, Mr Roderick Mackie, Dr Tara Schiller, Dr Jack Wang for their patient training and technical assistance in the usage of instruments. And thanks a lot to Dr Matteo Altissimo from the Melbourne Centre for Nanofabrication for his training and help in SEM.

I would also like to thanks my collaborators Dr Xiya Fang from the Monash Centre for Electron Microscopy, Dr Ben Rollo, Dr Dongcheng Zhang, Dr Donald Newgreen from The Royal Children's Hospital, and Dr Lincon Stamp Dr George Thouas from University of Melbourne for their great contribution to this project. It has been always very happy to work with you.

Last but not least, I would like to show my deepest gratitude to my parents for their unconditional love and endless support throughout during my study.

Abstract

One of the major challenges in the field of biomaterials engineering is the replication of the non-linear elasticity of soft tissues. In this PhD thesis project, non-linearly elastic biomaterials have been successfully fabricated from a chemically cross-linked elastomeric poly (glycerol sebacate) (PGS) and thermoplastic poly (L-lactic acid) (PLLA) or polyvinyl alcohol (PVA). PGS/PLLA fibre mats were fabricated using the core/shell electrospinning technique and the spun fibrous materials, containing a PGS core and PLLA shell, demonstrated J-shaped stress-strain curves, having ultimate tensile strength, rupture elongation, and stiffness constants comparable to muscle tissue properties. *In vitro* evaluations have shown that the PGS/PLLA fibrous biomaterials possess excellent biocompatibility, and are capable of supporting human stem-cell-derived cardiomyocytes over several weeks in culture or supports, and they can foster the growth of enteric neural crest (ENC) progenitor cells. [1]

Controlled enzymatic degradation is a major requirement of polyester implants *in vivo* and excessively rapid degradation speed is the major drawback for PGS. *In vitro* degradation of PGS/PLLA core/shell fibre mats were explored in tissue culture medium with and without enzyme, and were compared with cast PGS sheets. Both pH change and weight loss results have proved that the degradation rates of these core/shell fibre mats are much slower than PGS sheet in media with or without enzyme.

It has been previously shown that aligned fibre mats can guide neurite and stem cell growth along the aligned fibres [2]. Therefore in this project, aligned PGS/PLLA core/shell fibre mats collected on a rotating drum under different rotational speeds were fabricated, and their alignment and mechanical properties measured. The stiffness of fibre mats dramatically increased with higher rotation speed, while UTS elongation and resilience initially increased with the degree of alignment, but then decreased.

PLLA cannot be easily removed by solvent dissolution and so pure PGS fibre mats could not be obtained from PGS/PLLA core/shell fibre mats. However more pure PGS porous mats were fabricated by dissolution of the water soluble poly (vinyl alcohol) shell surrounding the PGS core in core-shell electrospun fibres, and these mats were studied. For these experiments, a different PGS was synthesized with a stoichiometric glycerol:sebacic acid ratio of 2:3

(rather than the more common 1:1 ratio) and it was found that this overcame the rapid degradation kinetics normally found with 1:1 PGS. Tensile tests showed these porous $PGS_{2:3}$ mats had superior mechanical properties than cast $PGS_{2:3}$ polymers and they demonstrated J-shaped stress-strain curves when tested in the wet state. *In vitro* evaluations revealed that the spun porous $PGS_{2:3}$ have excellent biocompatibility.

Table of Contents

Declaration ..... **II**

Acknowledgements ..... **III**

Abstract ..... **IV**

Table of Contents **1**

List of Figures **6**

List of Tables **13**

List of Abbreviations **14**

List of Publications **15**

Chapter 1 .....

Introduction **16**

Chapter 2 .....

Literature Review **19**

2.1 Introduction 19

2.2 Polymeric materials used in soft tissue engineering 20

2.2.1 Naturally occurring polymers 20

2.2.2 Synthetic polymers 20

2.2.3 Materials Summary 26

2.3 Electrospinning 27

2.3.1. Electrospinning parameters 28

2.3.2 Core/shell electrospinning 42

2.3.3 Aligned electrospinning 45

2.3.4 Mechanical properties of fibre mats 48

2.3.5 Summary 50

2.4 Project Goal 50

Chapter 3 .....

Materials and Experiments 52

3.1 Materials 52

3.2 Solution miscibility 52

3.2.1 PGS/PLLA solution miscibility 52

3.2.2 $PGS_{2:3}$/PVA solution miscibility 53

3.3 Polymer synthesis 53

3.3.1 Synthesis of PGS polymers sheets 53

3.3.2. Synthesis of PGS-co-LA polymer and PGS-PLLA blends 53

3.3. Electrospinning 54

3.3.1 PLLA electrospinning 54

3.3.2 PVA electrospinning 55

3.3.3. PGS/PLLA core shell electrospinning 55

3.3.4 Fabrication of $PGS_{2:3}$ fibre mats using core/shell electrospinning 56

3.4 Characterization 57

3.4.1 Scanning electron microscopy (SEM) 57

3.4.2. Determination of the degree of esterification in PGS 57

3.4.3. Rheology of PVA and $PGS_{2:3}$ solutions 58

3.4.4. Fourier Transform Infrared (FTIR) spectroscopy 58

3.4.6 Differential Scanning Calorimetry (DSC) 58

3.5 Tensile testing 58

3.6 Cytocompatibility assay 60

3.7 Cell proliferation 61

3.8. Cell culture work 62

3.8.1 Viability of human embryonic stem cell (hESC)-derived cardiomyocytes 62

3.8.2 Isolation and culture of enteric neural crest (ENC) cells 63

3.9 Enzymatic degradation *in vitro* 63

3.10 Statistical analysis 64

Chapter 4 .....

Mechanically tissue-like elastomeric PGS/PLLA core/shell fibres and their potential applications 65

4.1 Introduction 65

4.2. Results and Discussion 67

4.2.1 PLLA electrospinning 67

4.2.1. Miscibility of the PLLA and the PGS solutions 68

4.2.2. Mechanical properties of PGS/PLLA blends 69

4.2.3. Mechanical properties of PGS-co-LA copolymers 69

4.2.4. Optimisation of the core/shell electrospinning conditions 72

4.2.5. Mechanical properties of fibrous mat materials 76

4.2.6. *In vitro* evaluation: cellular viability and proliferation 79

4.2.7. Viability and function of hESC-derived cardiomyocytes 81

4.2.8. ENC cell delivery capabilities *ex vivo* 82

4.3. Conclusions 85

Chapter 5 .....

Enzymatic degradation of $PGS_{1:1}$/PLLA core/shell fibre mats and comparison with PGS sheets 86

5.1 Introduction 86

5.2 Results and discussion 87

5.2.1 Improvement in the protocol for measuring mass loss during *in vitro* degradation 87

5.2.2 Mass loss during *in vitro* degradation 89

5.2.3 Reduction in sheet and fibre mat thickness during *in vitro* degradation 92

5.2.4 Change in pH during exposure of materials to culture medium 93

5.3 Conclusions 94

Chapter 6 .....

Aligned core/shell electrospinning of PGS/PLLA with tuneable structural and mechanical properties.....96

6.1 Introduction 96

6.2 Results and discussion.....97

6.2.1 Alignment and diameter measurements 97

6.2.2 Mechanical properties.....102

6.3 Conclusions 105

Chapter 7 .....

Fabrication, mechanical properties and cytocompatibility of elastomeric nanofibrous mats of $PGS_{2:3}$.....107

7.1. Introduction 107

7.2. Results and discussion.....109

7.2.1. Rheology.....109

7.2.2. Optimisation of PVA fibre fabrication conditions 110

7.2.3. Optimisation of $PGS_{2:3}$/PVA core/shell fibre fabrication conditions 113

7.2.4. Fabrication of $PGS_{2:3}$ fibre mats.....116

7.2.5. Characterisation results of FTIR and DSC 117

7.2.6 Mechanical properties of fibrous mats 121

7.2.7. *In vitro* evaluation of cytotoxicity 127

7.3. Conclusions 129

Chapter 8 .....

Summary and future work.....131

8.1 Summary 131

8.1.1 Characterization and cell culture of PGS/PLLA core/shell fibre mats.....131

8.1.2 *In vitro* enzymatic degradation of PGS/PLLA core/shell fibre mats.....132

8.1.3 Characterization of aligned PGS/PLLA core/shell fibre mats.....133

8.1.4 Fabrication and characterization of porous $PGS_{2:3}$ mats made by $PGS_{2:3}$/PVA core/shell electrospinning 133

8.2 Recommendations for future work 134

8.2.1 Improvement of the electrospinning conditions 134

8.2.2 Possible future work on the degradation kinetics 135

8.2.3 Extension of cell culture work and *in vivo* studies 135

8.2.4 Development of additional electrospun core/shell polymer systems 136

References 137

List of Figures

Chapter 2

Figure 2. 1 Molecular structure of PGA 21
Figure 2. 2 Molecular structure of PLA 22
Figure 2.3 Molecular structure of PCL 22
Figure 2.4 Typical polyurethane thermoplastic elastomers showing a) hard and soft segments b) secondary bonding interactions between chains (dotted lines) 24
Figure 2.5 Polyhydroxyalkanoate (PHA) structure where n is usually 1 or 2 and R is usually either hydrogen, methyl, ethyl, propyl or butyl 24
Figure 2.6 PGS synthesised from sebacic acid and glycerol 25
Figure 2.7 A simplified schematic of the electrospinning process. Reproduced with permission from American Chemical Society [57] 27
Figure 2.8 PLA fibre with porous surface produced using dichloromethane as solvent. Reproduced with permission from John Wiley & Sons [61].....29
Figure 2.9 SEM images of electrospun PLLA (a) 2 wt% and 14 kV, (b) 4 wt% and 10 kV, (c) 6 wt% and 10 kV, (d) 8 wt% and 10 kV, (e) 9 wt% and 11 kV, (f) 10 wt% and 18 kV. Reproduced with permission from John Wiley & Sons [71].....33
Figure 2.10 (a) Increasing the solution concentrations of the outer shell PLLA or (b) increasing the flow rate ratio (FRR) of inner and outer solutions could (c) increase the size of the stable region. Reproduced with permission from Elsevier [63].....35
Figure 2.11 (a) At high viscosity, the solvent molecules are distributed evenly around the entangled polymer molecules. (b) At a lower viscosity, the solvent molecules tend to aggregate due to surface tension. Reproduced with permission from World Scientific [56]. .36
Figure 2.12 SEM photographs of electrospun PLLA. Surfactant content: (a) none (b) 5wt% triethyl benzyl ammonium chloride (ionic salt) (c) 5wt% poly(propylene oxide-ethylene oxide) ether (non-ionic surfactant) (d) 5wt% sodium dodecyl sulfate (ionic surfactant). Reproduced with permission from Elsevier [77]. 38
Figure 2.13 Nylon 6,6 at (a) 2 cm and (b) 0.5 cm deposition distances. Reproduced with permission from Elsevier [67]. 41
Figure 2.14 Polysulfone/tetrahydrofuran fibres under varying humidity (a) <25% (b) 31-38% (c) 40-45% (d) 50-59% (e) 60-72%. Reproduced with permission from American Chemical Society [57].....42

Figure 2.15 Schematic of (a) emulsion electrospinning (dark grey spheres and dark grey line represents the second phase) Reproduced with permission from American Chemical Society [87] and (b) coaxial electrospinning Reproduced with permission from American Chemical Society [88].....43
Figure 2.16 Electrospun fibre collection using (a) parallel plates. Reproduced with permission from American Chemical Society [96]and (b) a rotating mandrel. Reproduced with permission from Elsevier [99] 46
Figure 2.17 Using the frequency of the angle between each fibre and the preferred direction to indicate fibre alignment of PLLA hollow fibrous membranes prepared to different (a) outer solution concentrations and (b) flow rate ratios (in/out). Reproduced with permission from Elsevier [63].....47
Figure 2.18 SEM of alignment of PLLA fibres using different rotation speeds and their analysis [99] using FFT. 48
Figure 2.20 (a) The Young's modulus tested in parallel and perpendicular directions from PCL fibre-aligned scaffolds produced at varying speeds (*p<0.05 vs. parallel at the same speed, **p<0.05 vs. parallel fibres produced a t different speeds) [101], and (b) the stress strain curves of randomly collected (indicated as R) and aligned (indicated as A) gelatin fibre mats. Reproduced with permission from Elsevier [14] 50
Chapter 4
Figure 4.1 SEM image of PLLA with different concentrations (a) 12.5 g/100 ml solvent and (b) 20 g/100 ml solvent (spun at +12 and -2 kV, feeding rate 1 ml/h and collection distance 200 mm). The arrow in (a) points at a droplet or bead on the fibre.....68
Figure 4.2 The Young's modulus (a), UTS (b), elongation at break point (c) and the resilience (d) of the PGS-co-LA polymer with a 1:1 or 2:3 G:S molar ratio and synthesised in a vacuum at 130°C for three days.....71
Figure 4.3 SEM images of PGS/PLLA core/shell fibres fabricated at different core to shell feed flow rates: 0.10 ml/h vs. 2 ml/h at 10 kV (a), 0.20 ml/h vs. 0.80 ml/h at 12kV (b), 0.30 ml/h vs. 0.90 ml/h at 12kV (c) and 0.50 ml/h vs. 1.0 ml/h at 13kV (d). The material was heat treated for crosslinking at 130 °C for 72 h. The optimal conditions are shown in (b) and (c). The ratios of core solution radius and shell solution thickness in spinning (calculated from concentrations and relative flow rates) for (a)-(d) are 0.28, 0.81, 1.00 and 1.37, respectively. 73

Figure 4.4 Cross-sectional SEM image of a PGS/PLLA core/shell fibrous sheet. The inset shows the core/shell structure at a high magnification. The fibres were spun at a core feed flow rate of 0.20 ml/h and a shell feed flow rate of 0.80 ml/h at 12 kV. The material was crosslinked at 130 °C for 72 h. The specimen was sectioned at -120°C in a cryogenic microtome. 75
Figure 4.5 SEM image of the porous microstructure within the PLLA shell of a PGS/PLLA core-shell fibre. The fibres were spun at a core feed flow rate of 0.2 ml/h and a shell feed flow rate of 0.8 ml/h at 12 kV. The material was crosslinked at 130 °C for 72h. The specimen was sectioned at -120°C in a cryogenic microtome. 75
Figure 4.6 Stress-strain curves of the PGS (core)/PLLA (shell) fibre sheets fabricated at three core to shell feed flow conditions: 0.20 ml/h vs. 1.0 ml/h, 0.20 ml/h vs. 0.80 ml/h and 0.30 ml/h vs. 0.90 ml/h, having PLLA contents of 67, 62 and 55 wt% respectively. 77
Figure 4.7 Stiffness-stress relationship of the PGS/PLLA fibrous mat material spun at different core/shell feeding rates 1:3 1:4 and 1:5 having PLLA contents of 67, 62 and 55 wt% respectively. The stiffness constant of this stiffness-stress relationship is given in Table 4.3. For the 1:5 specimens, Equation 3.5 (Chapter 3) only fitted the data until a strain of approximately 7±1%, for the 1:4 specimens the fit was reasonable until 11±2%, while for the 1:3 specimens the Equation fitted the data up to 17±3%. 78
Figure 4.8 A cyclic stress-strain curves of a PGS/PLLA core/shell fibrous mat spun at a core feed flow rate of 0.30 ml/h and a shell feed flow rate of 0.90 ml/h at 12 kV. 79
Figure 4.9 SNL cells cultured for 2 days in a material-free culture medium (negative control) (a), PGS/PLLA fibre mat soaked with culture medium, produced from spinning at a core feed flow rate of 0.30 ml/h and a shell feed flow rate of 0.90 ml/h at 12 kV followed by PGS crosslinking at 130 °C for 72 h (b), and PLLA fibre mat soaked with culture medium and used as a positive control (c). 80
Figure 4.10 SNL cell proliferation kinetics measured by the AlamarBlue™ technique (detecting the chemical reduction of AlamarBlue). The initial plating density was 2000 cells per well in a 48-well plate (n = 5). Overall, there were no significant differences between any two of the three groups that were analysed ($p > 0.05$). The PGS/PLLA fibre mat was spun at a core feed flow rate of 0.30 ml/h and a shell feed flow rate of 0.90 ml/h at 12 kV followed by PGS crosslinking at 130 °C for 72 h. 80
Figure 4.11 Cytotoxicity of PGS/PLLA core/shell spun materials, detected by measuring the release of lactate dehydrogenase (LDH) from the cells after 4 days of cultivation (n = 5). No

significant differences existed between any two of the three groups ($p > 0.05$). The PGS/PLLA fibre mat was spun at a core feed flow rate of 0.30 ml/h and a shell feed flow rate of 0.90 ml/h at 12 kV followed by PGS crosslinking at 130 °C for 72 h. 81
Figure 4.12 Average beating rate of cardiomyocytes in basal media compared with cardiomyocytes cultured in the presence of PGS/PLLA core-shell spun fibrous sheet (n = 5). 82
Figure 4.13 An *ex vivo* cell transplant trial using the PGS/PLLA fibrous mat. (a) EDNRB-Kikume mouse ENC cells cultured on PGS/PLLA fibrous mat maintain expression of ENC-lineage antigens SOX10 (glial and progenitor cell marker) and TUJ1 (neuron and neurite marker). (b) On the mat EDNRB-Kikume mouse ENC are able to proliferate as assessed by EDU uptake exclusively in Sox10 expressing cells. (c) Assembly of the ex-vivo trial: ENS-deficient quail hindgut (outlined by the black dotted line) is attached to (i.e. on the top of) the PGS/PLLA fibre mat (the background of the image) seeded with EDNRB-Kikume mouse ENC cells (light grey background). (d) Following removal of the hindgut after 3 days of *ex vivo* growth, the mouse ENC cells have migrated through the serosa (dotted line) and have formed a *de novo* chain-like network in the interior of the embryonic colonic wall (as shown in the enlarged image).....84
Chapter 5
Figure 5.1 SEM of the surface of PGS/PLLA fibre mat cleaned using the methodology of Li et al. [130] and Liang et al. [131] after exposure to hog liver esterase enzyme. The mass change during 35 days of exposure to culture medium is also shown.....88
Figure 5.2 PGS/PLLA fibre mat removed from the hog liver esterase enzyme degradation media then washed in floating warm water at 37 °C for 24 hr 89
Figure 5.3 Percentage mass of PGS sheet and PGS/PLLA core/shell fibre mats after incubation at 37°C in (a) tissue culture medium DMEM and (b) tissue culture medium DMEM with the addition of hog liver esterase enzyme (0.3 units enzyme per mg biomaterial) for up to 35 days. The PGS sheet and in the mats was pre-polymerised at 130°C for 24 h and cross-linked at 130°C for 3 days.....90
Figure 5.4 SEM of (a) PGS sheet after incubation for 35 days in standard tissue culture media, (b) PGS sheet after incubation for 35 days in media with esterase, (c) PGS/PLLA fibre mat after incubation for 35 days in culture medium (d) PGS/PLLA fibre mat after incubation for 35 days in culture medium with esterase (e) accidentally exposed PGS core from PGS/PLLA fibre mat after incubation for 35 days in standard tissue culture media.....91

Figure 5.5 Mass change (a) and thickness change (b) of PGS/PLLA fibre mats and PGS sheets after 35 days immersion in culture media or in culture media with enzyme. 93
Figure 5.6 pH_{biomat} - $pH_{biomat\text{-}free}$ versus incubation time at 37°C for up to 35 days. pH_{biomat} represents the pH values of the (a) DMEM medium, (b) DMEM medium with enzyme (0.3 units per mg of biomaterial), whereas $pH_{biomat\text{-}free}$ represents those culture media cultured under the same condition but without materials. 94
Chapter 6
Figure 6.1 SEM and distribution of angular orientation of PLLA fibres collected using a mandrel with 16 cm circumference at different rotation speeds (a) 0 prm, (b) 1000 rpm, and (c) 2000 rpm.....99
Figure 6.2 SEM and angle distribution of PGS/PLLA fibres collected using a mandrel with 16 cm circumference at different rotational speeds (a) 0prm, (b) 1000 rpm, and (c) 2000 rpm. 101
Figure 6.3 Stress-strain curves of PLLA fibre mats collected at different rotational speeds using a mandrel with 16 cm circumference. 102
Figure 6.4 Stress-strain curves of PGS/PLLA fibre mats collected using a mandrel with a 16 cm circumference at different rotation speeds at and heat treated after purging the vacuum oven with nitrogen. 104
Figure 6.5 Surface SEM of PGS/PLLA fibre mats collected at (a) 0 rpm and (b) 1000 rpm using a mandrel with a 16cm circumference 105
Chapter 7
Figure 7.1 Shear rate dependence of the viscosity of the aqueous PVA solutions and $PGS_{2:3}$ prepolymer solution. 110
Figure 7.2 SEM images of electrospun fibres from PVA of M_w (a) and (a′) 31,000-50,000 g/mol (20g/100ml PVA in water, voltages: +12 and -2 kV). (b) and (b′) 89,000-98,000 g/mol (12 g/100ml PVA in water, voltages: +15 and -2 kV), (c) and (c′) 146,000-186,000 g/mol (8 g/100ml PVA in water, voltages: +17 and -2 kV). Feeding rate: 1ml/h, collection distance: 18cm for (a)-(c). The fused regions of the fibres shown by the dotted circles in (a′)-(c′) are close-up views of (a)-(c) 112
Figure 7.3 SEM images of $PGS_{2:3}$/PVA core/shell electrospun mat after heat treatment at 130°C for 3 days under vacuum. The core solution was 50% v/v $PGS_{2:3}$ in DMF, and collection distance was 18cm.(a) and (a′) PVA of M_w 31,000-50,000 g/mol. The shell solution was 20g PVA in 100ml water: positive/negative voltages were +12/-2 kV, and the

core/shell feeding rates were 0.1:1ml/h. (b) and (b′) PVA of M_w 89,000-98,000 g/mol. The shell solution was 12g PVA in 100ml water, positive/negative voltages were +15/-2 kV, and the core/shell feeding rates were 0.2:1.2ml/h. (a′) and (b′) are close-up views of (a) and (b), respectively which reveal fused regions of the fibres shown by the dotted circles. 114

Figure 7.4 SEM images of $PGS_{2:3}$/PVA core/shell electrospun mat after heat treatment at 130°C for 72 h. The core solution was $PGS_{2:3}$100g/100ml THF and collection distance was 18 cm. Note that regions to the left and right of the micrographs appear blurry and this was caused by leaking of PGS from the fibres which is shown in the SEM as a featureless surface. (a) PVA of M_w 31,000-50,000 g/mol. The shell solution was 20g PVA in 100 ml water, positive/negative voltages were +12/-2 kV, and the core/shell feeding rates were 0.1:0.8 ml/h. (b) PVA of M_w 89,000-98,000 g/mol. The shell solution was 12g PVA in 100ml water, positive/negative voltages were +15/-2 kV, and the core/shell feeding rates were 0.2:1.0 ml/h. 115

Figure 7.5 $PGS_{2:3}$/PVA fibres spun using PVA M_w 89,000-98,000 g/mol, after PGS curing and following removal of the shell. The shell solution was 12g PVA in 100ml water, the core solution was $PGS_{2:3}$ 50g/100ml THF, and core/shell feed/flow rates were 0.3 and 1.2ml/h, respectively, using positive/negative voltages of +15 and -2 kV, respectively, and with a collection distance of 18 cm. After rinsing the spun mat in hot water at 95 °C for (a) 2 hours or (b) 4 hours, to wash off most of the PVA, the above SEM images were obtained. 117

Figure 7. 6 ATR-FTIR absorbance spectra for PVA (M_w 89,000-98,000 g/mol), $PGS_{2:3}$/PVA core-shell fibre mat, $PGS_{2:3}$ fibre mat (formed from the $PGS_{2:3}$/PVA fibre mat by soaking in hot water for 4h) and $PGS_{2:3}$ sheet. The spectra have been normalized by the area under the CH peaks near 2900 cm^{-1} but the same trends in the intensity of ester, hydroxyl and C-O-C peaks is observed as in the un-normalized spectrum (see inset for comparison). 118

Figure 7.7 DSC curve for PVA (M_w 89,000-98,000 g/mol), $PGS_{2:3}$/PVA core-shell fibre mat, $PGS_{2:3}$ fibre mat (formed from the $PGS_{2:3}$/PVA fibre mat by soaking in hot water for 4h) and $PGS_{2:3}$ sheet.....120

Figure 7.8 Stress-strain curves of $PGS_{2:3}$ solid sheet and of spun $PGS_{2:3}$ fibrous mat (spun at feed rates of 0.2(core)/1.2 (shell) ml/h) , after PGS curing and after the PVA shell (PVA M_w 89,000-98,000 g/mol) had been removed by washing in 95°C water for 4h , tested in dry and wet conditions. 122

Figure 7.9 The Young's modulus (a), UTS (b), elongation (c) and resilience (d) comparison of $PGS_{2:3}$ solid sheet, dry $PGS_{2:3}$/PVA fibre mat (after PGS curing), dry $PGS_{2:3}$ fibre mat

(after PGS curing) and water-saturated $PGS_{2:3}$ fibre mat (after PGS curing) saturated with water . The PGS/PVA fibres were spun at feed rates of 0.2(core)/1.2 (shell) ml/h using PVA with a M_w of 89,000-98,000 g/mol. With the exception of Chart (d), the error bars show the standard deviations; for Chart (d) the bars give the variation in resilience obtained after the first cyclic (left part) and the average of the following cyclic (right part) loadings and unloadings. 123

Figure 7.10 The stress-strain curve of water-saturated $PGS_{2:3}$ fibre mat (a) compared with the fit given by Equation 4 (with k=2.5, α=0.61 MPa up to 40% elongation, and of dry $PGS_{2:3}$/PVA mat (b) compared with the fitted curve using Equation 4 (where k=21.9, α=53 MPa) up to 5% elongation The PGS/PVA fibres were spun at feed rates of 0.2(core)/1.2 (shell) ml/h using PVA with a M_w of 89,000-98,000 g/mol and the PGS in the core-shell fibres cured at 130°C under vacuum for 72 h. 124

Figure 7.11 (a) Resilience tests of $PGS_{2:3}$ solid sheet (glycerol and sebacic acid, molar ratio 2:3, heated at 130°C for 3 days), (b)$PGS_{2:3}$/PVA fibre mat (glycerol and sebacic acid molar ratio 2:3, core/shell electrospinning with PVA M_w of 89,000-98,000 g/mol at feeding rates of 0.2(core)/1.2 (shell) ml/h after heated at 130°C for 3 days), (c) dry $PGS_{2:3}$ fibre mat (glycerol and sebacic acid molar ratio 2:3, core/shell electrospinning with PVA M_w of 89,000-98,000 g/mol at feeding rates of 0.2(core)/1.2 (shell) ml/h after heated at 130°C for 3 days, washed in 95°C water for 4 hours) and (d) wet $PGS_{2:3}$ fibre mat 126

Figure 7.12 Images of SNL cells cultured for 2 days in (a) material-free culture medium (negative control), adjacent to (b) PLLA fibre mat (positive control) (c), PGS2:3 solid sheet, and (d) PGS2:3 fibre mat obtained from the core-shell fibres after removal of the PVA. 128

Figure 7.13 Cytotoxicity of material-free culture medium (negative control), PLLA fibre, PGS2:3 solid sheet and PGS2:3 fibre mat (obtained from the core-shell fibres after removal of the PVA) detected by measuring the release of lactate dehydrogenase (LDH) from the cells after four days of cultivation (n=5). No significant differences existed between PGS2:3 fibre mat and PLLA fibre mat and PGS2:3 fibre mats but PGS2:3 fibre mat is better than the control. 129

List of Tables

Chapter 2

Table 2.1 Biomaterials used in soft tissue engineering scaffolds 26

Table 2.2 Electrospun polymer fibres with porous surface structure.....31

Table 2.3 Electrical conductivity of solvents. Reproduced with permission from World Scientific [56].....37

Table 2.4 Applications of core/shell electrospinning.....44

Chapter 4

Table 4.1 Mechanical properties of PGS/PLLA blends/copolymers after heat treatment in vacuum at 130°C for three days to crosslink the PGS component. 69

Table 4.2 Optimal core/shell electrospinning conditions under a voltage potential of 12 kV. 74

Table 4.3 Mechanical properties of the core/shell mats. 76

Chapter 6

Table 6.1 Diameters and angle standard deviation of PLLA and PGS/PLLA fibre mats collected at different speeds.....100

Table 6.2 Mechanical properties of PLLA fibre mats collected at different rotation speed (using a mandrel with 16 cm circumference). 103

Table 6.3 Mechanical properties of PGS/PLLA mats with different alignments 104

Chapter 7

Table 7.1 Optimal electrosinning conditions that produced stable PVA fibres, and diameters of spun PVA fibres*. The positive voltage was the minimum to form fibres and neither drops (at low voltages) nor spray (high voltages).....111

Table 7.2 Optimal electrospinning conditions that produced stable $PGS_{2:3}$/PVA core/shell fibres 114

List of Abbreviations

3D	3-dimensional
DCM	Dichloromethane
DMF	Dimethylformamide
DSC	Differential Scanning Calorimetry
ECM	Extracellular matrix
ENC	Enteric neural crest
FDA	Food and Drug Administration
FTIR	Fourier Transform Infrared
hESC	Human embryonic stem cell
LDH	Lactate dehydrogenase
P4HB	Poly(4-hydroxy butyric acid)
PCL	Polycaprolactone
PDLA	Poly-D-lactic acid
PDLLA	Poly-D,L-lactic acid
PEUU	Poly(ester urethane) urea
PGA	Polyglycolic acid
PGS	Poly(glycerol sebacate) with molar ratio of glycerol and sebacic acid 1:1
$PGS_{2:3}$	Poly(glycerol sebacate) with molar ratio of glycerol and sebacic acid 2:3
PHAs	Polyhydroxyalkanoates
PLA	Polylactic acid
PLLA	Poly(L-lactic acid)
PPS	Poly(polyol sebacate)
PU	Polyurethanes
PVA	Polyvinyl alcohol
SEM	Scanning electron microscope
TEBAC	Triethyl benzyl ammonium chloride
THF	Tetrahydrofuran
UTS	Ultimate tensile strength

List of Publications

- Xu, B., Rollo, B., Newgreen, D.F., Chen, Q.Z. Non-linearly elastic nanobiomaterials for soft tissue engineering, Journal of tissue engineering and regenerative medicine, 2012, 6, 215-215
- Xu, B., Li, Y., Fang, X.Y.,, Thouas, G.A. Cook, W. D., Chen, Q.Z. Mechanically tissue-like elastomeric polymers and their potential as a vehicle to deliver functional cardiomyocytes., Journal of the mechanical behaviour of biomedical materials, 2013, 28, 354-365.
- Xu, B., Rollo, B., Stamp, L.A., Zhang, D.C., Fang, X.Y., Newgreen, D.F., Chen, Q.Z. Non-linear elasticity of core/shell spun PGS/PLLA fibres and their effect on cell proliferation, Biomaterials, 2013, 34, 6306-6317.
- Xu, B.; Li, Y.; Zhu, C.; Cook, W.D.; Forsythe, J.S.; Chen, Q. Fabrication, mechanical properties and cytocompatibility of elastomeric nanofibrous mats of poly(glycerol sebacate) , accepted for Publication in Euro. Polym. J. (2014)

Chapter 1

Introduction

The ability of biological tissues to stretch in a non-linear elastic manner is a major mechanical property [3] that thermoplastic (linear or branched) polymers, such as polylactic acid and polyglycolic acid, cannot provide since they undergo plastic deformation when exposed to cyclic-strain testing. One of the major challenges in developing biomaterials used for tissue engineering is the replication of this non-linear elasticity [4]. To date, the clinical applications of synthetic polymers in the repair of soft tissues are, in general, disappointing [5]. The mechanical dissimilarities between synthetic biomaterials and the biological tissue are believed to be the major cause of graft failure in experimental animal studies and preclinical trials [6]. Over the past decade, a number of soft elastomers have been developed as transplantable biomaterials for tissue engineering [4]. Among these elastomers, poly (polyol sebacate) (PPS) is a relatively new family of crosslinked biodegradable elastomers that have been developed for applications in soft tissue engineering [7-9].

The majority of *in vivo* trials demonstrate that PPS has good biocompatibility [7-12]. However, these studies also revealed two critical drawbacks of using solid PPS patches. First, the poly(glycerol sebacate) (PGS, a member of PPS) used as grafted patches were completely absorbed in 1-2 months [4]. This time frame is too short for the recovery of many diseased soft tissues, which can take several months for regeneration [11]. Second and more significantly, physical damage was observed in the local tissue due to the friction between the host myocardial tissue and grafted synthetic polymers. This friction was attributed to the mechanical mismatch between the grafted material and the muscle [11]. The stress-strain curves of synthetic elastomers are linear, especially up to 15% corresponding to the maximal strain of living tissues, but biological tissues all exhibit non-linear J-shaped stress-strain curves in this range [4]. The main reason for these different elastic behaviours is that synthetic polymers are composed entirely of randomly tangled molecular chains, while proteins are made of aligned nanofibres. Hence, the production of a partially aligned nanofibrous structure within a synthetic polymer would be an approach to achieve the nonlinear elasticity in soft tissues.

The production of nanofibres from chemically crosslinked elastomers is technically challenging. Major hurdles include the fact that once crosslinked these polymers cannot be dissolved in solvents used for electrospinning, but fibres spun from uncrosslinked pre-polymers will flow when they undergo a thermal crosslinking treatment. However, the recent development of a core/shell electrospinning technique could offer an opportunity to address these problems [13, 14].

In this project, nonlinearly elastic biomaterials has been successfully fabricated from a chemically crosslinked PGS elastomer and a thermoplastic PLLA using the core/shell electrospinning technique. The optimal electrospinning conditions were established and the mechanical properties of the resultant fibre mats were comparable to those of muscular tissues. *In vitro* evaluations showed that the PGS/PLLA fibrous biomaterials possessed excellent biocompatibility, capable of supporting human stem-cell-derived cardiomyocytes over several weeks in culture or supports, and fostered the growth of enteric neural crest (ENC) progenitor cells. In addition, the PLLA shell decreased the degradation speed of these PGS/PLLA fibre mats compared with PGS sheets especially in the presence of enzyme, thus overcoming a major drawback of PGS. Also aligned PGS/PLLA fibre mats with different alignments were engineered to provide a wide range of mechanical properties which may broaden the application of these elastic biomaterials. Finally, by using a removable PVA shell in place of the PLLA shell, PGS (with glycerol and sebacic acid ratio 2:3) fibre mats were successfully fabricated and their mechanical properties were improved compared with cast PGS sheets.

This thesis is comprised of seven chapters as follows:

Chapter 2 reviews the relevant biomaterials and electrospinning techniques.

Chapter 3 is the description of the experimental procedures.

Chapter 4 focuses on the synthesis, characterisation and application of PGS/PLLA fibre mats.

Chapter 5 compares the degradation speeds of PGS/PLLA fibre mats with normal cast PGS sheets with and without enzyme.

Chapter 6 investigates the effects of alignments on the mechanical properties of PGS/PLLA fibre mats.

Chapter 7 describes how almost pure PGS fibre mats were fabricated from PGS synthesized with a 2:3 glycerol/sebacic acid ratio and shows that the mechanical properties were dramatically improved compared with normal cast PGS sheets.

Chapter 8 summaries the main findings in this thesis and recommends possible future work.

Chapter 2

Literature Review

2.1 Introduction

Tissue engineering is a multidisciplinary field that combines medicine, biology, biomaterials science and engineering. The goal of tissue engineering is to develop medical implants that can assist the regeneration of impaired or injured tissues. Over the past 30 years, tissue engineering has drawn considerable attention as an alternative medical treatment [15-19].

The classic tissue engineering strategy usually involves seeding a 3-dimensional (3D) porous matrix (scaffold) with autologous cells before implantation. As the cells invade the scaffold and produce extracellular matrix (ECM), thus increasingly lending structure and stability to the tissue, the scaffold is gradually absorbed *in vivo*. Once absorption is complete, only the newly created functioning tissue remains [20].

Porous scaffolds play a critical role in tissue engineering by accommodating cells and guiding their growth and the resulting tissue regeneration in three dimensions. Among various scaffolds, the elastomeric scaffolds which could further improve the recovery speed of tissues, has received increasing attention [21-23]. Over the past two decades, numerous scaffolding techniques have been used to develop porous structures including fusion-based methods, solvent-based methods, gas-foaming and rapid prototyping [24-30]. Compared with other techniques, electrospinning is a facile method to fabricate aligned, 3D-textured scaffolds for tissue engineering applications [1, 21, 31]. All biological tissues have elastic behaviour so their artificial substitutes should also be elastic. However, at the moment most of the polymers used in electrospun scaffolds are thermoplastic, such as polylactic acid (PLA), polyglycolic acid (PGA), polycaprolactone (PCL) and their copolymers. Such thermoplastic scaffolds will therefore undergo permanent deformation when stretched [21].

The following literature review will provide an update on polymeric materials used in soft tissue engineering and regeneration, with a focus on electrospinning. The review will provide a rationale for developing nanofibrous elastomeric biomaterials, which is the research topic of this thesis.

2.2 Polymeric materials used in soft tissue engineering

2.2.1 Naturally occurring polymers

The extracellular matrices of soft tissues are composed of various types of collagen. It is not surprising that a great deal of biomaterials research has focussed on naturally occurring polymers, such as collagen [30, 32] and chitosan, for tissue engineering applications, and collagen, fibrin, gelatin and alginate have been extensively investigated for myocardial tissue engineering [33]. In some cases, naturally occurring polymers can be biocompatible, and they could provide a natural substrate for cellular attachment, proliferation, and differentiation [34]. Although naturally occurring polymers possess the above-mentioned advantages, their poor mechanical properties and variable physical properties have hampered these materials' progress. The immunogenic problems associated with collagen has also caused concern [35].

2.2.2 Synthetic polymers

The challenges in using naturally occurring polymers as scaffold materials have brought considerable attention to synthetic polymer alternatives. Synthetic polymers are essential for tissue engineering, not only due to their excellent processing characteristics, which can ensure off-the-shelf availability, but also because of their potential biocompatibility and biodegradability [35]. Synthetic polymers have predictable and reproducible mechanical and physical properties and they can also be manufactured with great precision. Although these materials do not provide a natural environment to cells and can suffer shortcomings, such as eliciting persistent inflammatory reactions, erosion, mismatched mechanical compliance or non-integration with host tissues, if they are biodegradable they can also be replaced *in vivo* by cell-derived extracellular matrices in a timely fashion.[12]. An ideal tissue-engineered substitute could be made from a synthetic polymer scaffold, because they are similar to natural tissue structures and have tuneable mechanical properties [36]. In fact, aliphatic polyesters have been widely applied as scaffolding materials for 3D tissue engineering constructs.

2.2.2.1 Degradable Thermoplastics

Poly(glycolic acid) (PGA)

PGA (**Figure 2.1**) is a thermoplastic of relatively high crystallinity (45-55% crystallinity). PGA has a high Young's modulus (between 6.9 and 12.5 GPa), low solubility in organic solvents and bulk bio-degradation kinetics, all being associated with the high level of crystallinity [37]. The bulk degradation of PGA results in a non-linear loss in strength with time; the polymer loses its strength in 1 to 2 months and its mass within 6 to 12 months as a result of hydrolysis [38]. In the body, PGA is broken down into glycolic acid, which can be excreted in the urine or converted into carbon dioxide and water via the citric acid cycle, giving PGA excellent biocompatibility [38]. However, its uncontrolled degradation kinetics and acidic degradation products can cause unsatisfactory levels of inflammation, which limit its biomedical applications. The glycolic acid unit is usually used in a copolymer which improves the biomedical performance.

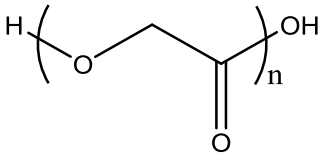

Figure 2. 1 Molecular structure of PGA

The cultivation of primary neonatal rat cardiomyocytes on highly porous PGA scaffolds in bioreactors results in 3D cardiac-like tissue consisting of cardiomyocytes with cardiac-specific structural and electrophysiological properties that contract spontaneously and synchronously. However, the visible spontaneous contractions in these constructs were inferior to those of native ventricles and eventually ceased after 4 days of cultivation [39].

Poly(lactic acid) (PLA)

Lactic acid is a chiral molecule that exists in two optically active forms: L-lactide and D-lactide. Hence, polylactides actually refer to a family of polymers, including isotactic poly-L-lactic acid (PLLA), isotactic poly-D-lactic acid (PDLA), and heterotactic of poly-D,L-lactic acid (PDLLA), as shown in **Figure 2.2**. The L-lactide polymer in particular has been extensively researched because the monomer is naturally occurring. PLLA polymers are semi-crystalline, with a crystallinity of approximately 37% and a Young's modulus of approximately 4.8 GPa. PLLA has a much slower rate of biodegradation; high molecular weight PLLA takes 2 to 5.6 years to be completely absorbed *in vivo* [40]. PLA has been

approved by the US Food and Drug Administration (FDA) for a variety of clinical applications and their applications in tissue engineering have also been investigated, for example used as a scaffold matrix for ligament replacements [41]. PLLA has some limitations, such as non-controllable degradation kinetics, acidic degradation products, slow degradation rate and poor flexibility, that limit its application in soft tissue healing [42]. Therefore L-lactide is usually copolymerised with other monomers to achieve optimal performance.

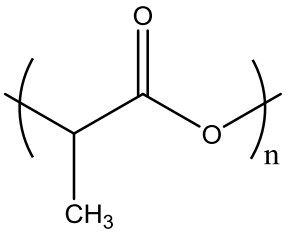

Figure 2. 2 Molecular structure of PLA

Polycaprolactone (PCL)

PCL (**Figure 2.3**) is a semi-crystalline polyester that has a low Young's modulus (0.21-0.34 GPa) but can tolerate an extremely high elongation before breaking (>700%) [37]. PCL undergoes hydrolytic degradation by scission of the ester backbone. A PCL implant usually takes 2-3 years to degrade due to its hydrophobic backbone. The advantages of PCL include its low cost, easy processing, ability to form miscible blends with a wide range of polymers, and its approval by the FDA [43]. In one study [44], PCL nanofibrous mats were produced by electrospinning and found to have an extracellular matrix-like topography for cardiomyocytes. The average fibre diameter of this scaffold was approximately 250nm, well below the size of an individual cardiomyocyte but *in vitro* investigations demonstrated that cardiomyocytes attached well to these PCL mats [44].

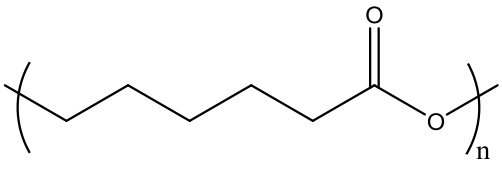

Figure 2.3 Molecular structure of PCL

2.2.2.2 Elastomers

Although thermoplastics used in implants have been well characterised and can be fabricated to biochemically match the biological system, they generally lack mechanical compatibility with soft tissues. In living tissues, elastic stretchability is the major mechanical property of soft tissues; thermoplastic polymers cannot replicate this behaviour because they undergo plastic deformation at low strain and fail when exposed to cyclic strain. Indeed, one of the major problems encountered by biomaterials scientists for repairing most soft tissue types is the need to replicate the innate elasticity of soft tissues [12]. Over the past decade, degradable soft elastomers have drawn a great deal of attention from the field of biomaterials as promising artificial substitutes for tissue engineering because of their mechanical compatibility [12].

Elastomers (also called rubbers) can usually undergo high deformation under stress without rupturing and can almost fully recover to their original state when the stress is removed. Synthetic elastomers can be divided into two categories based on the type of bonding used to crosslink the chains together: thermoplastic elastomers and cross-linked elastomers.

Thermoplastic elastomer: polyurethanes (PU)

Thermoplastic PU (**Figure 2.4**) elastomers are segmented copolymers that have thermoplastic characteristics while maintaining their elastomeric properties. The Young's modulus of PU is typically in the range of 5-60 MPa [45], which is much higher than those of typical soft tissues. However, PU can be processed into very thin films and highly porous networks, which makes the product flexible and compliant. Three dimensional poly(ester urethane) urea (PEUU) scaffolds have been fabricated by electrospinning. The electrospun PEUU is elastomeric and allows for the control of fibre diameter, porosity, and degradation rate by varying the fabrication parameters [45]. Muscle cells have been successfully cultured on PEUU scaffolds, but no research in myocardial tissue engineering has been performed using these materials.

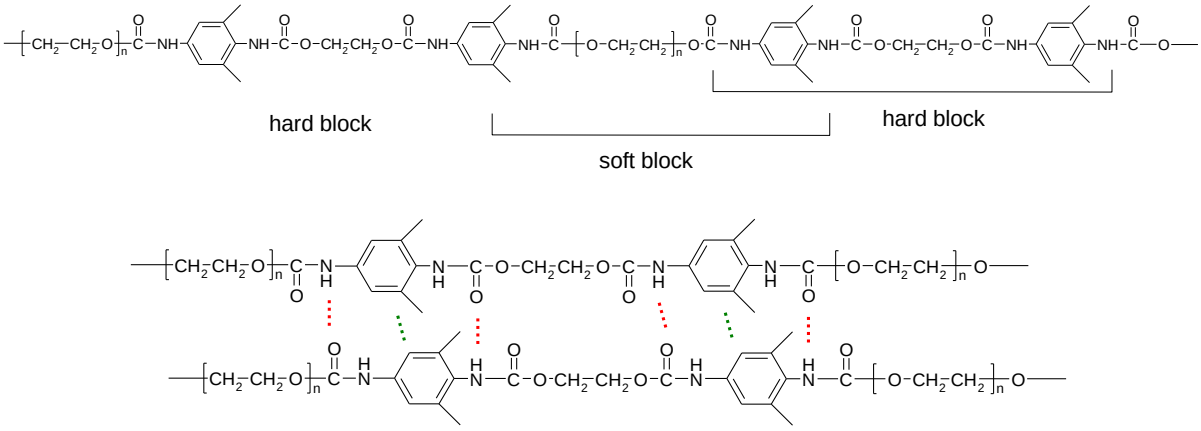

Figure 2.4 Typical polyurethane thermoplastic elastomers showing a) hard and soft segments b) secondary bonding interactions between chains (dotted lines)

Thermoplastic elastomer: Polyhydroxyalkanoates (PHAs) and copolymers

PHAs are polyesters produced by various microorganisms as a carbon and energy storage compound under unbalanced growth conditions. Their general chemical formula is shown below:

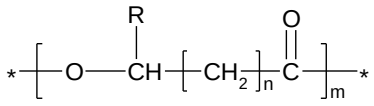

Figure 2.5 Polyhydroxyalkanoate (PHA) structure where n is usually 1 or 2 and R is usually either hydrogen, methyl, ethyl, propyl or butyl

Over 100 different types of PHAs have been produced offering a wide range of physical properties from rigid polymers to rubber-like elastomers. The polymer properties can be modified by varying the length of the side chain and the distance between ester linkages in the polymer back bone to achieve the desired properties (see **Figure 2.5**). Typically, PHAs with short side chains tend to be hard and crystalline, whereas PHAs with long side chains are generally soft and flexible, exhibiting elastomeric behaviour [46].

Among the PHA-based elastomers, poly(4-hydroxy butyric acid), P4HB, is of most interest because it is tough but flexible. Its Young's modulus, UTS and elongation at breaking point can reach 50 MPa, 70 MPa, and 1000%, respectively[47]. The degradation rate of P4HB is slower than that of PGA, but it is still faster than PLLA, PCL and some other PHAs. P4HB typically undergoes a gradual change in mechanical properties rather than an abrupt reduction

in strength during degradation [48], which is desirable because a sudden loss in mechanical properties can cause catastrophic failure in the growing host tissue. Evidence from various studies increasingly confirms that P4HB has excellent biocompatibility *in vivo* [46, 47, 49]. Though PHA elastomers have been studied for cardiovascular tissue engineering, wound healing, orthopaedics, sutures, and drug delivery, these polymers are currently only used as research materials because of PHAs' expensive microbial production costs.

Poly(glycerol sebacate) (PGS) and other Poly(polyol sebacate) (PPS)

PPS is a family of elastomers which are cross-linked via ester linkages. Unlike thermoplastic elastomers, chemically cross-linked elastomers gain their elasticity from a chemical bonding process that occurs between polymer chains when the compound is subjected to heat or radiation. Among the family of PPS polymers, poly(glycerol sebacate) (**Figure 2.6**) is the most well-studied as a biomaterial. PGS has a three dimensional, loosely cross-linked polymeric structure that is designed to provide mechanical stability and structural integrity to tissues and organs without causing mechanical irritation to the host. The Young's modulus of PGS ranges from 0.056 to 1.2 MPa, whereas its elongation at breaking point ranges from 41% to 448%, depending on the synthesis conditions [4]. These Young's moduli values cover the average moduli of soft tissues. PGS is predominantly degraded through surface erosion *in vivo* as shown by its steady and linear mass loss, its preservation of implant geometry, its gradual and slow loss of mechanical strength (approximately 8% per week), the absence of surface cracks and holes, and the minimal water uptake over the test period [10]. PGS completely resorbs in 6 weeks *in vivo* when used as a cardiac elastomeric tissue scaffold biomaterial [11].

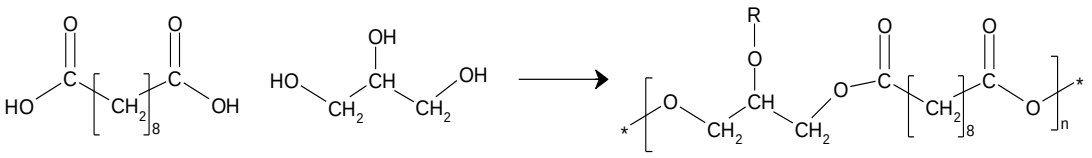

Figure 2.6 PGS synthesised from sebacic acid and glycerol

Accordion-like honeycomb microstructured PGS scaffolds have been made using an excimer laser microablation technique [50]. This new process produces a porous, elastomeric 3D scaffold that matches the mechanical stiffness of heart tissue. Furthermore, the PGS scaffold itself can intrinsically orient healthy cardiac cells.

2.2.3 Materials Summary

Polymeric biomaterials are currently dominated by thermoplastic polyesters, such as PLA, PGA, PCL and their blends or copolymers. However, thermoplastic polymer implants have mechanical mismatches with elastic soft tissues. **Table 2.1** lists the mechanical properties of some biomaterials and biological tissues. The elastic stretchability is a major mechanical property of biological tissues that cannot be provided by thermoplastic polymers because they undergo plastic deformation at low strain. Hence, elastomers are more suitable for soft tissue engineering scaffold materials compared with thermoplastic polyesters.

Table 2.1 Biomaterials used in soft tissue engineering scaffolds

Polymer	**Elastic (E) or Plastic (P): Strain at rupture**	**Young's modulus**	**Tensile strength**	**Degradation (months)**	**Refs**
PGA	P	7-10 GPa	70 MPa	2-12	[40]
PLLA	P	1-4 GPa	30-80 MPa	2-12	[51]
PCL	P	0.21-0.34 GPa	10.5-16.1 MPa	24-36	[52]
PU	E: 50-570%	5-60 MPa	20-45 MPa	Surface erosion	[53]
PGS	E: 40-500%	0.04-0.282 MPa	0.5 MPa	Surface erosion	[9]
Collagen	E: 10-20 %	2-46 MPa	1-7 MPa	Undergoes enzymatic degradation	[52]
Elastin	E: 100-150 %	300-1000kPa	1-15 MPa	Non-degradable	[54]

2.3 Electrospinning

Electrospinning is a simple, low-cost fabrication process that can form non-aligned and aligned fibrous structures. This technique is important because it can create fibres of small diameter that can match the size-scale of the extracellular matrix, and their high porosity and high surface area-to-volume ratio is ideal for cell attachment, proliferation and differentiation [55]. In addition, the spun fibre mats exhibit nonlinear elasticity that resembles the performance of soft tissues [14]. Hence, electrospinning was chosen as the fabrication technique in this thesis; its description is therefore worthy of a separate section.

Electrospinning is a process that creates micro/nanofibres through an electrically charged jet of monomer, polymer solution or polymer melt. Generally, in electrospinning, a high voltage is applied to a monomer/polymer fluid to induce charges on the surface of the fluid. When the amount of accumulated charge on the fluid reaches a critical level, a fluid jet erupts from the droplet at the tip of the needle, forming a Taylor cone. The electrospinning jet will travel toward the region of lower potential [56]. The electrospinning process commonly consists of a syringe and pump containing the monomer/polymer solution, two electrodes and a DC voltage supply in the kV range (**Figure 2.7**).

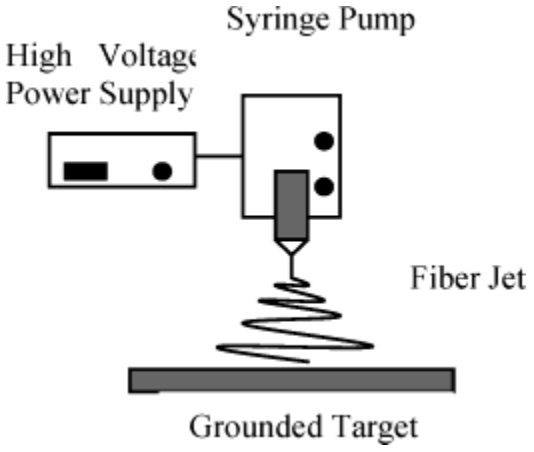

Figure 2.7 A simplified schematic of the electrospinning process. Reproduced with permission from American Chemical Society [57]

A monomer/polymer solution/melt in a syringe is fed to a metal needle. A high voltage power supply is connected to the needle, producing a fine jet of monomer/polymer solution/melt. This jet solidifies by solvent evaporation, by polymerization of monomer or by polymer cooling during transit, resulting in fine fibres that are collected on a grounded target.

One electrode is placed into the spinning solution/melt, and the other is attached to a collector. The electric field is applied to the end of a capillary tube that contains the monomer/polymer fluid held in by its surface tension, which induces a charge on the solution's surface. Mutual charge repulsion generates a force directly opposite to the surface tension. As the intensity of the electric field increases, the hemispherical surface of the fluid at the tip of the capillary tube elongates to form a conical shape, known as a Taylor cone. As the field increases, the charge in the solution reaches a critical value, where the repulsive electrostatic force overcomes the surface tension, causing a charged jet of fluid to be ejected from the tip of the Taylor cone. The discharged polymer solution jet undergoes a whipping process wherein the solvent evaporates, leaving behind a charged polymer fibre that lays itself randomly on a grounded metal collecting screen. In the case of a polymer melt, the discharged jet solidifies as it travels through the air and is cooled, and is collected on the grounded metal screen, while for a reactive monomer, polymerization (usually photopolymerization) occurs between the tip and the collector.

2.3.1. Electrospinning parameters

Although electrospinning has been carried out on polymerizable monomers [58] and molten polymer [59], most electrospinning is carried out using polymer solutions. The parameters that affect electrospinning and the resulting fibres may be broadly classified into polymer solution parameters (such as viscosity, molecular weight, and surface tension) and processing conditions (voltage and temperature) [31]. Different kinds of parameters and their effect on fibre morphology will be discussed in the following section.

2.3.1.1 Solution parameters

Polymer solution parameters exert the greatest influence on the overall characteristics of the final fibres[60]. Increases in factors that contribute to the cohesive strength, such as molecular weight and surface tension, and which produce thicker fibre diameters, tend to require higher critical voltages. It is interesting to note that, whereas increased molecular weight and surface tension produce thicker fibre diameters, the large critical voltages required tend to produce very large stretching forces, producing mechanically weaker fibres per cross sectional area.

Choice of polymers and solvents

The choice of polymer and solvent, as well as the concentration, has a range of impacts on the fibre structure. In many applications, the surface morphology can alter a scaffold's characteristics and functionality. As a result, the appropriate choice of polymer solution/melt for electrospinning can allow the creation of porous fibres, among other morphologies. Porous fibres can be produced using the traditional electrospinning setup by employing a ternary polymer-solvent system, where two immiscible polymers and a solvent are electrospun simultaneously. Using a bimodal or spinodal phase separation process, a desired phase can be selectively removed during electrospinning [61]. Binary systems using one polymer and one solvent with the same relationship have also been explored. This technique was used to produce porous PLA fibres using dichloromethane as the solvent [62]. **Figure 2.8** shows an example of a porous structure created on the surface of polymer fibres during electrospinning. The size of the surface structures ranged from tens of nanometres to 1 micron and was influenced by the type of polymers and solvents used, as well as the electrospinning conditions listed in **Table 2.3**.

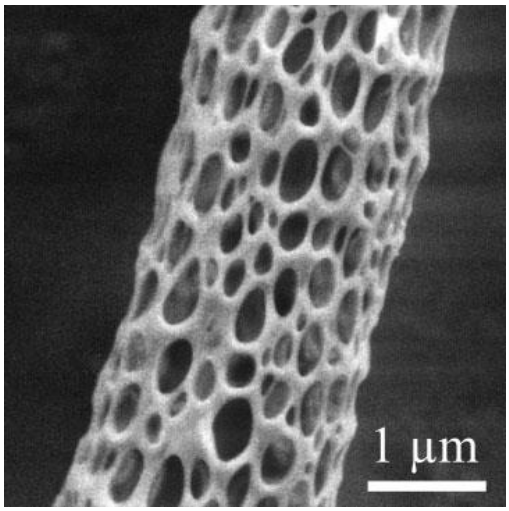

Figure 2.8 PLA fibre with porous surface produced using dichloromethane as solvent. Reproduced with permission from John Wiley & Sons [61]

The mechanism that forms porous surfaces on cast polymer films also applies to the phenomenon that occurs with electrospun nanofibres [62]. When a polymer solution is cast on a support, convective evaporation takes place and as the solvent evaporates, the solution

becomes thermodynamically unstable, causing it to separate into two phases, a polymer-rich phase and a polymer-deficient phase. The concentrated polymer-rich phase solidifies shortly after phase separation and forms the matrix, and the polymer-deficient phase forms the pores. Because of this phenomenon, the solvent vapour pressure has a critical influence on pore formation. For PLLA porous nanofibres, replacing dichloromethane (DCM) with chloroform or dimethylformamide (DMF), which have lower vapour pressures, effectively reduces pore formation. Another drawback of using high vapour pressure dichloromethane is that it clogs the spinneret due to premature solution solidification [63]. To decrease the solvent's volatility and mitigate solidification, DMF can been added to the DCM in the PLLA solution [63].

Table 2.2 Electrospun polymer fibres with porous surface structure

Polymer	**Molecular Weight**	**Solvent**	**Electrospinning Conditions**	**Pore Size (Fibre Diameter)**	**Reference**
PLLA	150,000	Dichloromethane	5 wt%	100-250 nm (<1 μm)	[62]
PLLA	Not given	Dichloromethane	Not given	<250 nm (0.3-3.5 μm)	[64]
PLLA	360,000	Chloroform	4 g/dL, -12 kV	Approximately 1μm (1.7-2.7 μm)	[65]
PLLA/PDLA	360,000/390,000	Chloroform	4 g/dL, -25 kV	No pores (400-970 nm)	[65]
PVP/PLA (core/shell)	Not given	DMF and Acetone	22 wt%, 6kV	No pores	[66]

Cohesive strength

The cohesive strength of the solution is characterised by two interactions: the interaction of the solvent molecules with other solvent molecules and the interaction of the solvent molecules with polymer chains. The polymer chains are long so that when they become solvated with solvent molecules, interactions between polymer chains tends to be minimal [56]. Interactions between solvent molecules are measured by surface tension, while the interactions between solvent and polymer molecules are measured by viscosity.

Molecular weight, viscosity and cohesive strength

The polymer chain's molecular weight affects the viscosity of the solution, and almost invariably a higher molecular weight polymer will have higher viscosity in solution than its lower molecular weight counterparts [56]. Once the jet leaves the needle tip, the polymer solution stretches as it travels towards the collection plate. Sufficient molecular weight and viscosity prevents the jet from breaking up, thus maintaining a continuous solution jet. As a result, in general, monomeric solutions are not easily formed into fibres by electrospinning [67].

The molecular weight of the polymer affects the polymer solution's viscosity primarily because the polymer length determines the amount of entanglement of the polymer chains in the solvent. Also increasing the polymer's concentration will result in more polymer chain entanglements within the solution and increase the viscosity. The polymer chain entanglements significantly impact whether the electrospinning jet breaks up into small droplets or whether the resultant electrospun fibres contain beads [68]. Although there is a minimum amount of polymer chain entanglements and thus, viscosity, necessary for electrospinning, a solution with an excessive viscosity can be very difficult to pump through the syringe needle [69]. Moreover, when the viscosity is too high, the solution may dry at the needle tip before electrospinning can be initiated.

Many experiments have shown that each polymer solution has a minimum viscosity necessary to yield fibres without bead formation [70]. For a low viscosity polymer solution, beads are commonly found along the fibres deposited on the collection plate. When the viscosity is steadily increased, the bead shape gradually changes from spherical to spindle-like and then a smooth fibre is obtained (**Figure 2.9**) [71]. For solutions with lower viscosities, surface tension is the dominant property controlling electrospinning behaviour, causing beads to form along the fibre due to the larger number of solvent molecules and

fewer chain entanglements. When the viscosity increases, there are more polymer chains that can entangle in solution, allowing the charges on the electrospinning jet to fully stretch the solution, with the solvent molecules distributed evenly among the polymer chains.

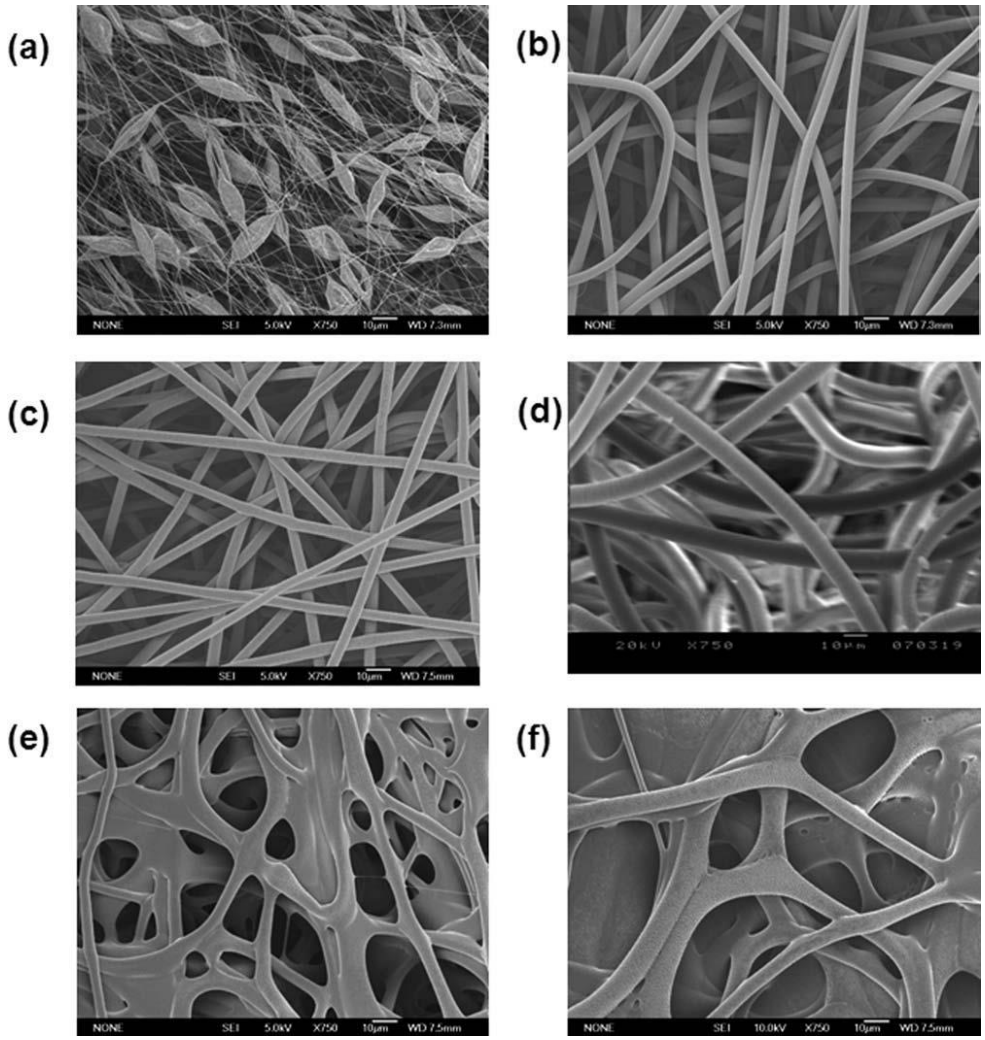

Figure 2.9 SEM images of electrospun PLLA (a) 2 wt% and 14 kV, (b) 4 wt% and 10 kV, (c) 6 wt% and 10 kV, (d) 8 wt% and 10 kV, (e) 9 wt% and 11 kV, (f) 10 wt% and 18 kV. Reproduced with permission from John Wiley & Sons [71]

More viscous solutions require larger electrostatic forces for spinning to be successful, and so larger applied voltages are required. Demir et al. [72] demonstrated that the critical voltage increased proportionally with increased viscosity of a polyurethaneurea solution, and the viscosity increased proportionally with polymer concentration.

Increased solution viscosity also affects fibre diameter. Viscous solutions have strong cohesive forces; in other words, the molecules stick together with greater force than those in less viscous solutions. As a result, high viscosities provide large resistance to the electrostatic

forces drawing the fibre through the spinneret, leading to larger fibre diameters. In addition, at intermediate viscosities, a secondary jet can erupt from the main electrospinning jet [73] to yield smaller diameter fibres. This phenomenon may explain the differential fibre diameter distribution observed in some cases [72]. However, when the viscosity is sufficiently high, it can discourage secondary jets from forming, contributing to the increased but uniform fibre diameter [74].

Higher polymer concentrations also lead to a smaller deposition area because the viscosity of the solution is strong enough to discourage bending instability over longer distances as it emerges from the needle tip. As shown in **Figure 2.10**, the jet path length is reduced with increased concentration or feeding rate, and the bending instability spreads over a smaller area [75], which also means that there is less solution stretching, resulting in a larger fibre diameter.

Surface tension

Surface tension plays an important role in determining the critical voltage required to electrospin the fibre. Electrospinning is initiated when the electrostatic force overcomes the surface tension of the solution at the tip [56]. Thus, large surface tensions directly lead to the requirement of large critical voltages for successful spinning. More obviously, the solution's surface tension can introduce necking or beading into the fibre. The shape of the fibre affects the free energy of the system. If the attraction between the solvent and polymer molecules dominates the solution's interactions, the solvent molecules will solvate the polymer, and the smaller solvent molecules will simply conform to the lowest free energy state of the polymer coil under these conditions (**Figure 2.11(a)**). However, if the forces between the solvent particles are dominant, the system will start to conform to the lowest energy state of the solvent, namely spherical drops, which decreases the surface area per unit mass. As the surface tension becomes larger, the beading becomes more pronounced (**Figure 2.11(b)**). Solvents such as ethanol have a low surface tension; adding these solvents can encourage the formation of smooth fibres [76]. The surface tension can also be reduced by adding surfactant to the solution, which has been found to yield more uniform fibres. Addition of insoluble surfactant to a solution as a fine powder also improves the fibre morphology [77].

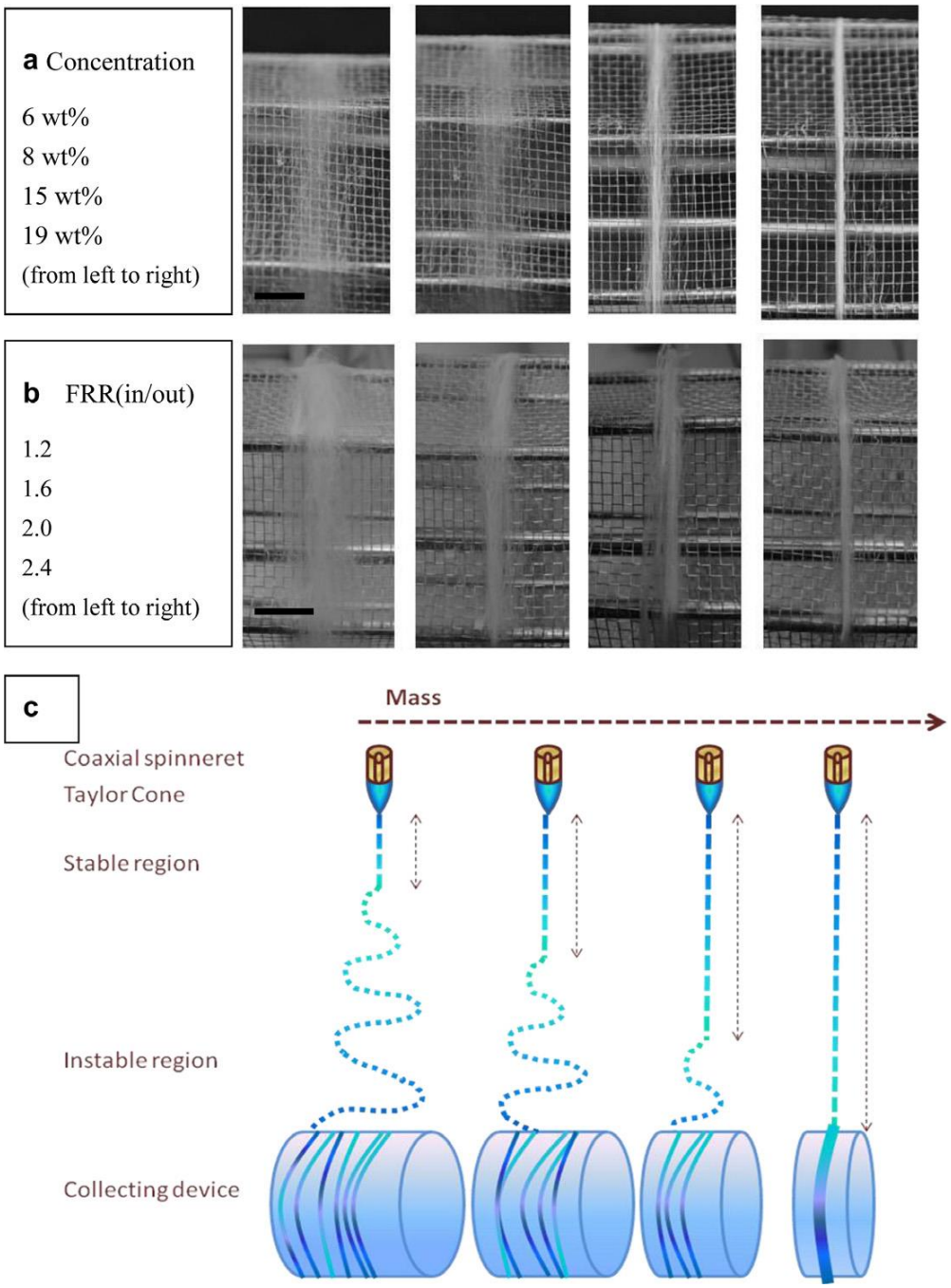

Figure 2.10 (a) Increasing the solution concentrations of the outer shell PLLA or (b) increasing the flow rate ratio (FRR) of inner and outer solutions could (c) increase the size of the stable region. Reproduced with permission from Elsevier [63]

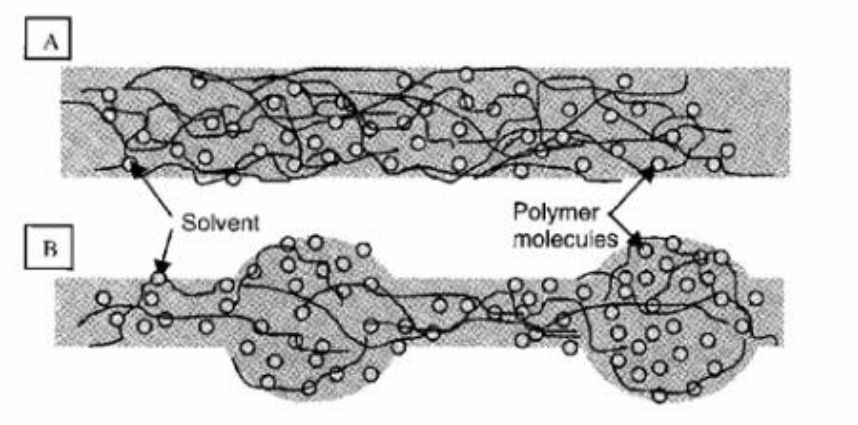

Figure 2.11 (a) At high viscosity, the solvent molecules are distributed evenly around the entangled polymer molecules. (b) At a lower viscosity, the solvent molecules tend to aggregate due to surface tension. Reproduced with permission from World Scientific [56].

Stretching forces

Stretching forces are responsible for the fibre's elongation from the spinneret tip. As the voltage is applied, the external electric field interacts with the surface charge, generating repulsive forces [31]. These forces overtake the cohesive forces of viscosity and surface tension at the critical voltage. At this point, the fibre is first extruded, or more literally, the fluid is simultaneously stretched and thinned until the droplet becomes conically shaped with the fibre elongating from its tip. Because the repulsive forces are directly due to the interactions between the spinneret electric field and the jet's surface charge, it follows that the solution conductivity can significantly affect the magnitude of the stretching force at a given applied voltage. Additionally, the dielectric constant can exert a similar effect. Thus, researchers [63] have often used mixtures of solvents to attain conductivities and dielectric properties that are highly conducive to smooth, uniform fibres. By varying these properties, researchers are not only able to vary the magnitude of the stretching force but are also able to apply it more uniformly.

Solution conductivity

The solution is stretched into a fibre by repulsion charges at the jet surface. Thus, if a solution has zero conductivity, fibres cannot be formed by electrospinning [56]. Increased conductivity amplifies the elongational force at a given applied voltage. This increased force, in turn, has several implications. Fibres can be produced at lower critical voltages for solutions with higher conductivity because greater repulsive forces are generated at the jet surface [56]. Consequently, the increased drawing force tends to produce fibres with smaller

diameters. Other researchers [78] have also demonstrated that the increased stretching that results from increased solution conductivity can be exploited to smooth out beaded fibres. **Table 2.3** shows the conductivities of common solvents used in electrospinning.

Table 2.3 Electrical conductivity of solvents. Reproduced with permission from World Scientific [56]

Solvent	**Conductivity (mS/m)**
1,2-Dichloroethane	0.034
Acetone	0.0202
Butanol	0.0036
Dichloromethane/Dimethylformamide(40/60)	0.505
Dichloromethane/Dimethylformamide (75/25)	0.273
Dimethylformamide	1.090
Distilled water	0.447
Ethanol	0.0554
Ethanol (95%)	0.0624
Ethanol/Water (40/60)	0.150
Methanol	0.1207
Propanol	0.0385
Tetrahydrofuran/Ethanol (50/50)	0.037

Solution conductivity is generally modified by adding metal salts, although adding ions in any form will usually increase the conductivity. Smaller ions, which have greater mobility, can generate greater drawing forces than larger ions for a given level of conductivity. As a result, at the same level of conductivity, ions with smaller ionic radii will result in slightly smaller fibre diameters than that obtained with ions with larger ionic radii. For example, at a

given conductivity, solutions containing the smaller sodium ion produced finer fibre diameters than solutions that used potassium [79].

To increase the conductivity of the solution while reducing the surface tension, ionic surfactants can be added [80]. The ions increase the conductivity, and the surfactant reduces the surface tension. Both of these characteristics contribute to smoother fibres with less beading. An example of this type of compound is triethyl benzyl ammonium chloride (TEBAC). **Figure 2.12** summarises the effect of this ionic surfactant and on chloroform/acetone fibres. As shown, the uneven beading is removed, producing smooth, uniform fibres with narrowed diameter distribution.

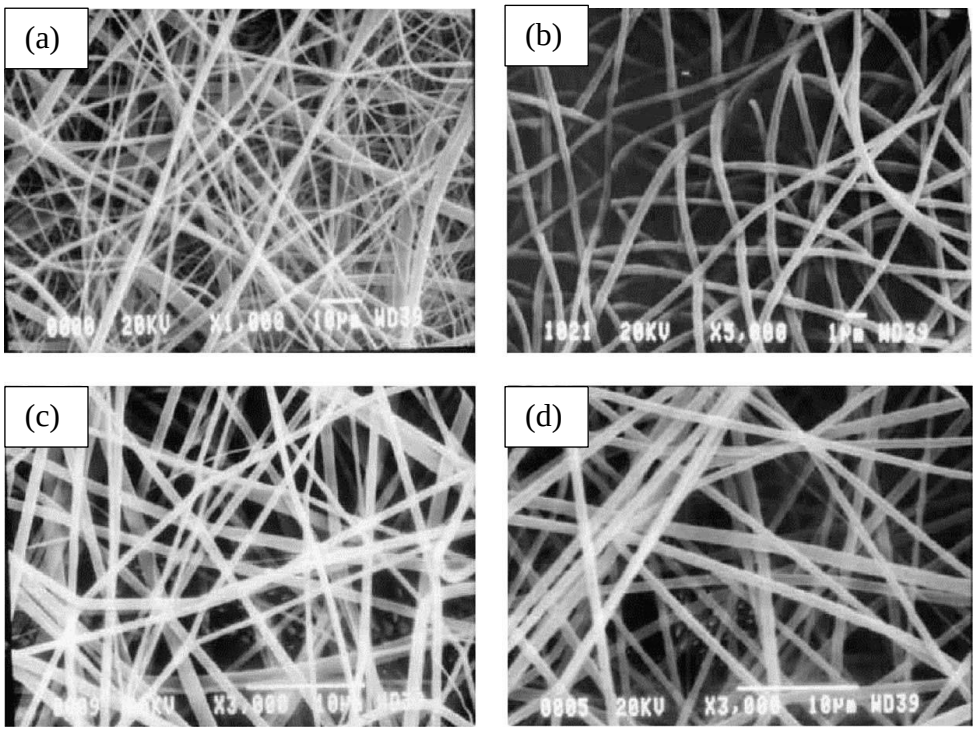

Figure 2.12 SEM photographs of electrospun PLLA. Surfactant content: (a) none (b) 5wt% triethyl benzyl ammonium chloride (ionic salt) (c) 5wt% poly(propylene oxide-ethylene oxide) ether (non-ionic surfactant) (d) 5wt% sodium dodecyl sulfate (ionic surfactant). Reproduced with permission from Elsevier [77].

Finally, pH is often varied to alter conductivity. Son et al. [60] demonstrated that cellulose acetate produces smaller fibre diameters as conditions become more basic. However, the effects of all parameters must be considered when adding chemicals to a solution. Son et al. demonstrated that cellulose acetate formed smaller fibre diameters under basic conditions and larger fibres in acidic conditions. Although the acidic solution had a higher conductivity than the neutral pH solution, the fibres produced were larger because the addition of ionic salts

may cause an increase in the viscosity of the solution. Thus, although the conductivity of the solution is improved, the viscoelastic force is stronger than the columbic force, resulting in increased fibre diameter [75].

2.3.1.2 Process parameters and conditions

Applied voltage

The applied voltage can be used to modify fibre diameter. The applied voltage works in two ways [81]. First, the supplied voltage amplifies the inherent columbic forces present in the jet, and secondly, the resultant electric field interacts with the charge on the jet's surface. Both of these actions serve to further increase the stretching forces and to accelerate the jet, producing larger throughput and reducing the final fibre diameter. However, a critical voltage limits this effect before the fibre is turned into a spray. As the applied voltage increases, the Taylor cone shrinks [81], eventually becoming unstable or even receding into the spinneret. However, as a general rule, increasing the applied voltage stretches out beading and generates smooth uniform fibres. Consequently, techniques can be used to control the jet path as a result of the forces between the electric field and the surface charge. Thus auxiliary electrodes can be used to manipulate the electric field surrounding the flow path. Electrospinning designs have been implemented that produce aligned parallel fibres and even patterned non-woven mats. The applied voltage amplifies the columbic charge and creates an external field, both of which can be varied to change the throughput rate and fibre diameter.

Temperature

The temperature can be controlled during the electrospinning process and usually requires an enclosure around the jet path that spans the distance from the spinneret to the collector. The temperature can be controlled using an environmental chamber. Controlling the temperature has several advantages. For example, the molecular mobility can be increased, which tends to reduce surface tension and can lead to stronger fibres being produced at lower critical voltages, similar to that achieved by vibration technology [56]. Additionally, controlling the temperature allows more precise control over solvent evaporation, which directly affects the drying process and indirectly weakens the cohesive strength by reducing the viscosity. These changes all lead to potentially more uniform fibres. Demir et al. [82] reported that polyurethane electrospun at higher temperatures had more uniform diameters and Mit-uppatham [75] suggests that smaller fibre diameters can be produced due to reduced viscosity.

Temperature may be an extremely important parameter in the electrospinning process, but further research is required to confirm these speculations.

Spinneret orifice

Spinneret tip diameters are usually on the order of tenths of millimetres. Ultimately, the orifice diameter can influence the amount of clogging, the critical voltage, and the throughput. Mo et al. [83] reported that smaller tip diameters seemed to clog less frequently than larger ones, possibly by reducing the area of atmospheric exposure and slowing the rate of extrusion. However, the smaller orifices provide a larger resistance to fluid flow increasing the required critical voltage, and smaller orifices decelerate the jet causing the jet to be suspended longer between the spinneret and the collector and allowing more time for thinning of the fibre. Thus, the fibre diameter can be influenced by the orifice's diameter.

Distance between the tip and the collector

Varying the distance between the spinneret tip and the collector directly influences the flight time. Controlling the flight time is critical because evaporation occurs during this stage. The flight time must be long enough for most of the solvent to evaporate to avoid forming joints between the fibres which would result in mat fusion (see **Figure 2.13**) [67]. A longer flight time has confounding effects on the fibre diameter. On one hand, increasing the distance increases the flying and stretching time of solution jets before the fibres are deposited on the collector which could decrease fibre diameters [74]. Conversely, increasing the distance will decrease the electrostatic field strength, and this could decrease the stretching of jets and increase the diameter of the fibres [84].

The variation in jet path length can influence the electric field, depending on the particular setup. In a simple setup with a constant applied voltage, the electric field strengthens as the jet length decreases. Thus, the variation in jet path length is crucial to the evaporative process as well as to fibre diameters.

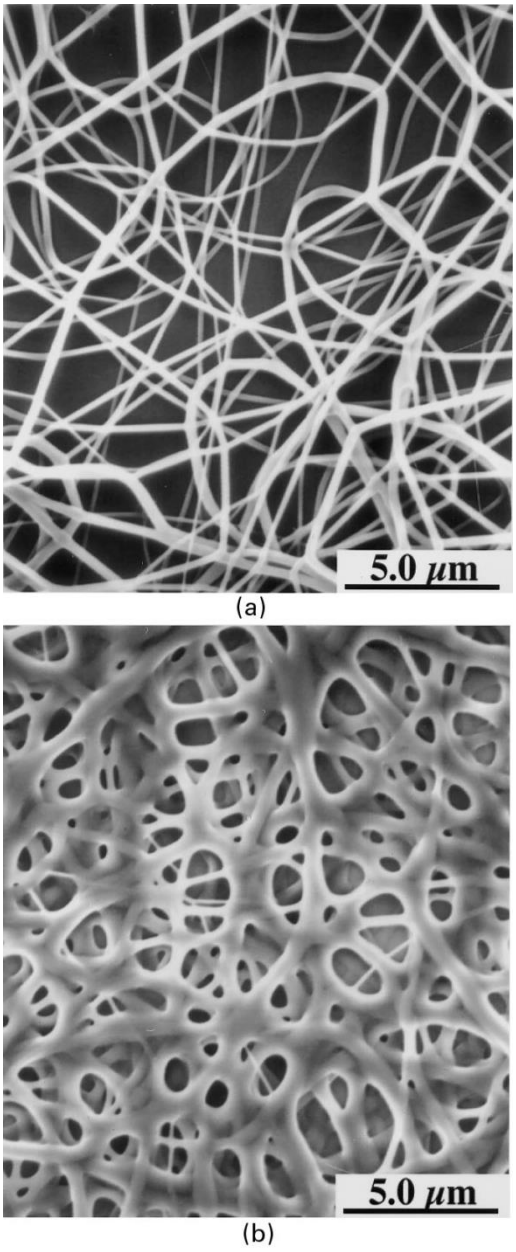

Figure 2.13 Nylon 6,6 at (a) 2 cm and (b) 0.5 cm deposition distances. Reproduced with permission from Elsevier [67].

Humidity

At high humidity, water condenses on the surface of the fibre when electrospinning is carried out under normal atmospheric conditions. The water content may influence the fibre morphology, especially for polymers dissolved in volatile solvents [70]. Experiments using PS dissolved in THF show that a humidity of less than 50% creates fibres with smooth surfaces. However, increasing the humidity causes circular pores to form on the fibre surfaces, which increase in diameter with increasing humidity until they coalesce to form large, non-uniformly shaped structures (**Figure 2.14**). The depth of the pores also increases with

increasing humidity, as determined by atomic force microscopy. However, above a certain humidity level, the pore depth, diameter and numbers reach a plateau [57].

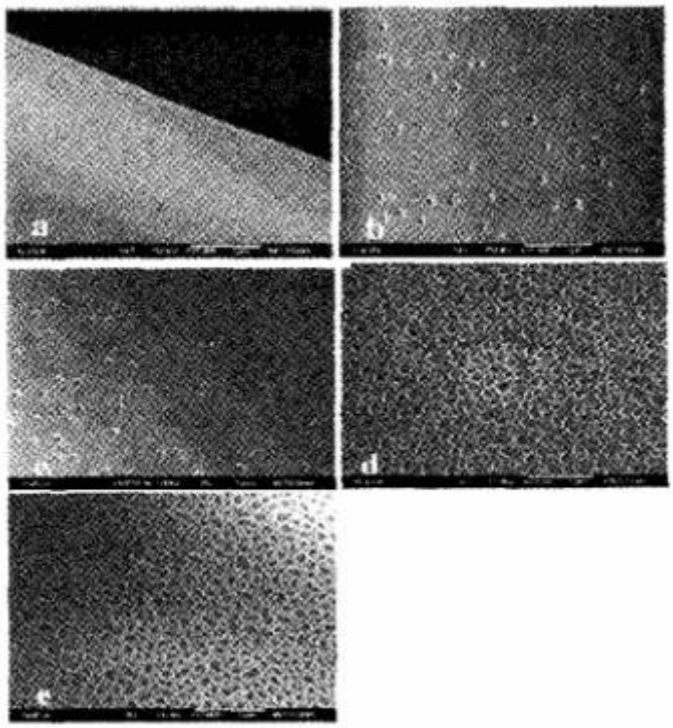

Figure 2.14 Polysulfone/tetrahydrofuran fibres under varying humidity (a) <25% (b) 31-38% (c) 40-45% (d) 50-59% (e) 60-72%. Reproduced with permission from American Chemical Society [57]

The humidity of the environment can determine the solvent's evaporation rate in the solution. At a very low humidity, a volatile solvent can dry up very rapidly. This could increase the formation of pores but the electrospinning process under these conditions can only be carried out for a short time because the needle tip becomes clogged.

2.3.2 Core/shell electrospinning

2.3.2.1 Methods of core/shell electrospinning

The fabrication of core/shell fibres using electrospinning technology was developed only in recent years [85]. The two methods of emulsion electrospinning and coaxial electrospinning techniques were developed from normal electrospinning, and are both useful for producing core/shell fibres [55].

Emulsion electrospinning is a simple way to fabricate a core/shell structure. Using a single nozzle, as demonstrated in **Figure 2.15(a)**, a core solution was dispersed in the shell solution

during electrospinning and results in a core/shell jet [55]. The problem with this method is that core/shell jets are only formed when the core solution droplet is entrained into the tip of shell solution Taylor cone. This entrainment is periodic and so the as spun fibres may contain large sections of the fibres containing only shell solution along with smaller sections of core/shell material. As a result, the core/shell structures produced by this method are often non-uniform and in-complete [85]. On the other hand, coaxial electrospinning using a coaxially placed inner and outer needle as indicated in **Fig 2.15(b)** can produce nanofibres with a well-organized core/shell structure [55]. In this method, the shell solution is ejected through the outer needle while the core solution is injected through the inner needle, resulting in stable core/shell jets. The core and shell solutions in this process do not have to be immiscible because the solidification time of core/shell jet is short and the mixing of fluids during this time is insignificant [55, 86].

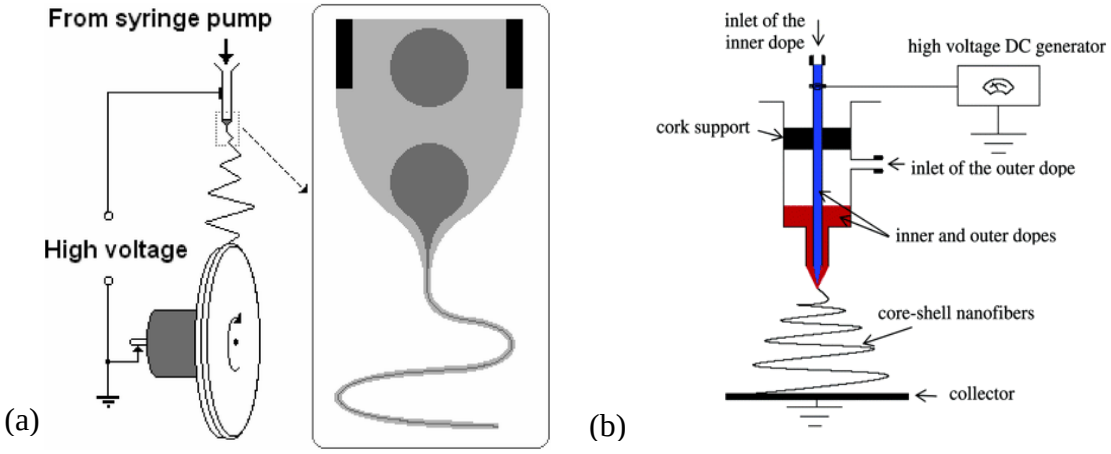

Figure 2.15 Schematic of (a) emulsion electrospinning (dark grey spheres and dark grey line represents the second phase) Reproduced with permission from American Chemical Society [87] and (b) coaxial electrospinning Reproduced with permission from American Chemical Society [88]

2.3.2.1. Applications of core/shell electrospinning

The first advantage of core/shell electrospinning is that this method can be used to process elastomer-forming prepolymers which cannot be spun using normal electrospinning [13, 89]. Unlike thermoplastics that can be easily spun into fibres by melting or dissolving in solvents, chemically cross-linked elastomers cannot be shaped by melting or solution casting because of their permanently cross-linked networks. Core/shell electrospinning has been developed to address this challenge [13]. Second, the properties of final core/shell fibres combine the properties of the individual core and shell polymers [55, 63, 90, 91]. Some applications of core/shell electrospinning are listed in **Table 2.4**.

Table 2.4 Applications of core/shell electrospinning

Method	Core	Shell	Achievement	Reference
Emulsion electrospinning	Tetraethyl orthosilicate (TEOS)	Poly(vinyl pyrrolidone) (PVP)	Polymer nanotubes were fabricated	[92]
Emulsion electrospinning	Poly(ethylene oxide)	Chitosan	Core/shell fibre with controllable shell thickness were fabricated	[93]
Emulsion electrospinning	Poly(ethylene oxide)	Mineral oil	Proved the feasibility of oil-in-water emulsion electrospinning	[94]
Coaxial electrospinning	PGS	PLLA	PGS nanofibres were fabricated	[95]
Coaxial electrospinning	Polyacrylonitrile (PAN) with carbon nanotubes	Cellulose acetate	Carbon nanotubes increased thermal stability	[88]
Coaxial electrospinning	PCL	Gelatin	Core shell fibres were fabricated	[66]
Coaxial electrospinning	Poly(N-vinyl pyrrolidone) (PVP)	PLA	The core/shell membranes were softer with twice water uptake than PLA membrane	

2.3.3 Aligned electrospinning

2.3.3.1 Method of aligned electrospinning

There are two commonly used methods in electrospinning to fabricate aligned fibre scaffolds. The first method is to use parallel electrodes as collectors that manipulate the electric field to orient the deposited fibres. The second method is the use of a high speed rotating mandrel as the collector [1].

Using the parallel plate method as shown in **Figure 2.16(a)** [96], the electrodes create an electric field so that when highly charged electrospun jets were directed at this electric field, the spun jets land perpendicular to the electrodes and so make aligned fibre scaffolds. One drawback of this method is that only a certain degree of alignment can be achieved. If the electric field strength is increased to produce more aligned fibre mats, the increased instability of the spinning jets caused by the increasing voltage will act to decrease the fibre alignment [97].

Using the rotating mandrel method shown in **Figure 2.16(b)**, a high speed grounded rotating mandrel was used as the collector. The diameter of the mandrel is usually a few centimetres and the rotational speeds range from zero to several thousand revolutions per minute (rpm). In this method, the speed of rotation is a key factor. At low mandrel rotational velocity, it is not possible to initiate fibre alignment. An increase in the rotational speed can initiate and increase the fibre alignment to maximum. But when the velocity at the edge of the rotating mandrel exceeds the stretching speed of spun jets, fibre alignment and quality will decrease due to fibre fracture [98].

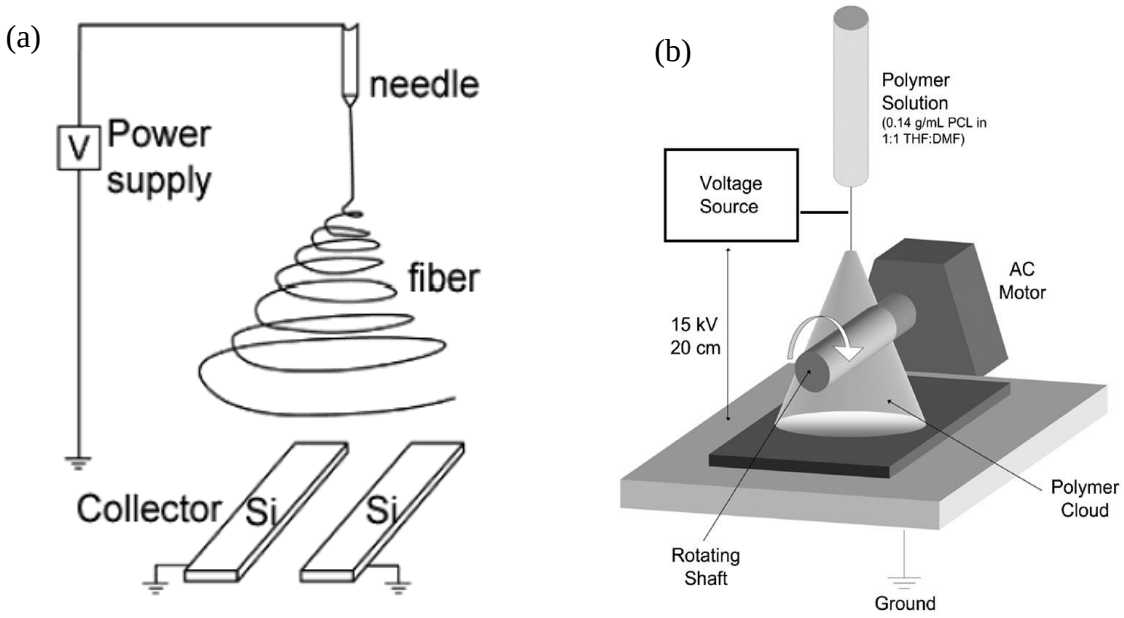

Figure 2.16 Electrospun fibre collection using (a) parallel plates. Reproduced with permission from American Chemical Society [96]and (b) a rotating mandrel. Reproduced with permission from Elsevier [99]

2.3.3.2 Alignment characterization

Analysis of scanning electron microscopy (SEM) images of aligned fibres with comparison with randomly collected fibres can be used to indicate the orientation of aligned fibres [96, 100]. However to compare the alignments of fibres fabricated at different conditions the frequency of angles between each fibre and the preferred direction (the collection direction) needs to be measured and calculated [63, 99, 101]. As shown in **Figure 2.17**, Ou et al [63] plotted the distribution of angles between each fibre and the preferred direction. The narrower distribution correlates with an increase in the aligned fibres.

The characterization of fibre alignment can also be carried out by Fast Fourier Transform (FFT) [99, 102, 103]. In this method, a SEM image of fibres is converted to a frequency plot of fibres orientated in each direction [104].

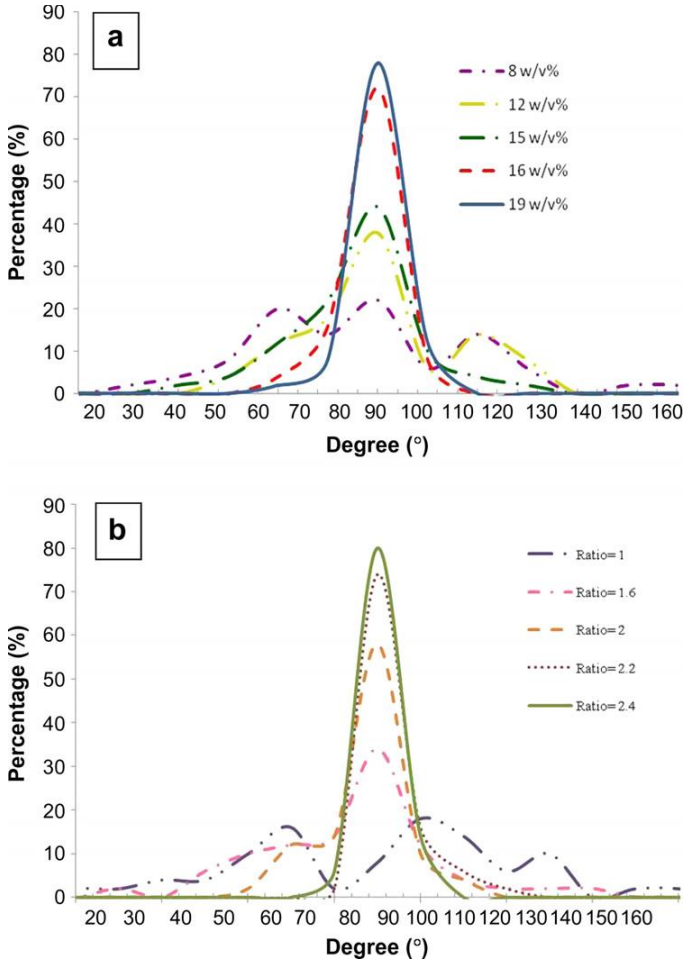

Figure 2.17 Using the frequency of the angle between each fibre and the preferred direction to indicate fibre alignment of PLLA hollow fibrous membranes prepared to different (a) outer solution concentrations and (b) flow rate ratios (in/out). Reproduced with permission from Elsevier [63].

In **Figure 2.18,** Wang et al. [99] used Scion Image Beta 4.0.3 software (Scion Corporation; Frederic, MD) to convert SEM images of fibres collected with rotation speeds of (A) 250 rpm, (B) 500 rpm and (C) 1000 rpm into FFT output images (D)-(F) respectively. The centre area of Figures (D)-(F) depicts the alignment of the fibres, while the narrower areas represent the most highly aligned fibre specimens. Figures (G)-(I) are histograms of angle differences of SEMs (A)-(C). Figures (G)-(I) indicated the alignments of fibres were increased with rotation speeds and the best fibre alignment was obtained at a rotational speed of 1000 rpm. The result proved that a high collection disk rotation rate stretches the fibres into an aligned and uniform orientation.

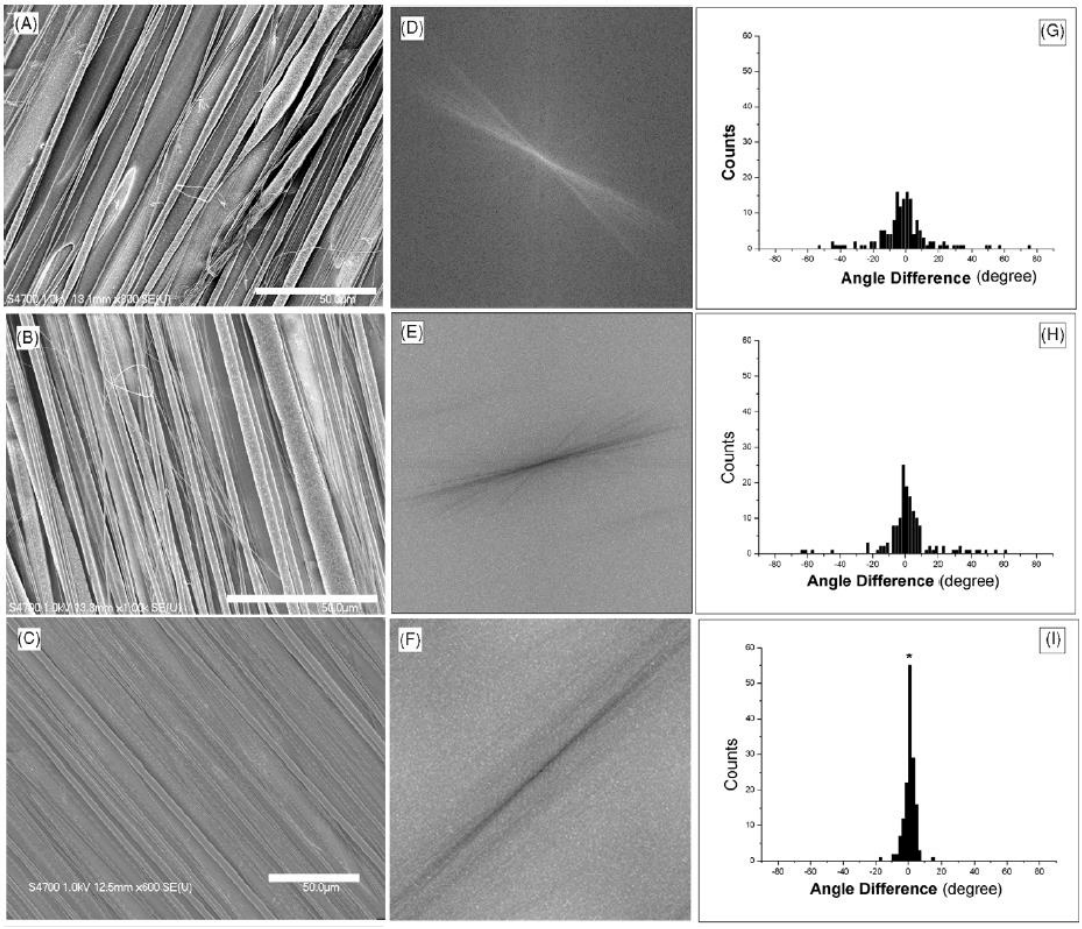

Figure 2.18 SEM of alignment of PLLA fibres using different rotation speeds and their analysis [99] using FFT.

Also the angular deviation of the fibre orientation can be used to described the alignment of fibre mats [2]. After a SEM image was processed with a digital image processing technique [105] and transformed into a distribution of fibre orientation, the angular deviation of certain fibre mats can be calculated using circular statistics [106]. The degree of angular deviation quantifies the alignment of fibres while a smaller angular deviation correlates to more aligned fibres.

2.3.4 Mechanical properties of fibre mats

The measurement of individual electrospun fibres using standard uniaxial tensile testing machines is very challenging because electrospinning yields fibres in the nanoscale range. For this reason, many studies have focused on measuring the electrospun non-woven fibre mats. Tensile tests of specimens from fibre mats punched using a standard mould is a

common approach to obtain the mechanical properties of non-woven mats of electrospun fibres [78].

It is interesting to find that the stress-strain curves of fibrous sheets were J-shaped (stress rises at an increasing rate as the strain is raised) [13, 89, 101] which could mimic the performance of nature biological tissues [107]. In contrast, the solid polymer sheet demonstrated a decreasing rate of rise in stress prior to plastic deformation, and these mechanical dissimilarities between synthetic biomaterials and natural tissue are believed to be the major cause of graft failure [6]. The effects of alignment on the fibre mats have also been studied and an increase in the fibre alignment of the mat was found to increase the strength on the collection direction but reduce the elongation. [78]

Li et al. [101] showed that nanofibre organisation in PCL fibre mats was dependent on the rotational speed of the target, and thus controlled the anisotropy of the scaffold. Non-aligned scaffolds of PCL fibre mats had an isotropic tensile modulus of 2.1±0.4 MPa, whereas highly anisotropic scaffolds had a modulus of 11.6±3.1 MPa in the presumed fibre direction, thus demonstrating that fibre alignment has a profound effect on the mechanical properties of scaffolds [101]. **Fig 2.20(a)** summarises the mechanical characteristics of electrospun gelatin fibres under different target rotation speeds, in both the axial and perpendicular directions to the main axis. This data supports the direct correlation of fibre mat strength with target rotation speed. Furthermore, the Young's modulus in the fibre direction increases compared with that in the perpendicular direction. Increasing the target rotation speeds is a facile method to control the mechanical anisotropy. This result is consistent with the work of Kharaziha [100], which shows in **Fig 2.20(b)** that the aligned fibre mats demonstrated an increased strength and reduced elongation when compared with randomly oriented fibre mats.

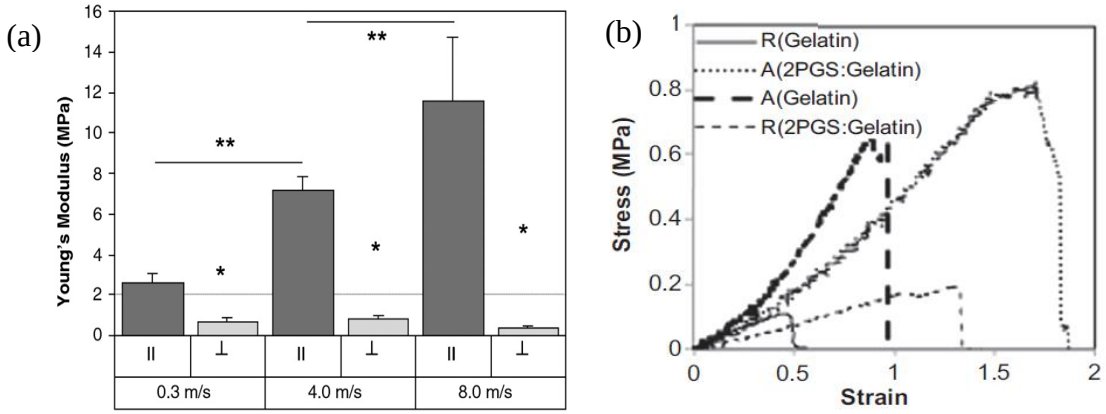

Figure 2.19 (a) The Young's modulus tested in parallel and perpendicular directions from PCL fibre-aligned scaffolds produced at varying speeds (*p<0.05 vs. parallel at the same speed, **p<0.05 vs. parallel fibres produced a t different speeds) [101], and (b) the stress strain curves of randomly collected (indicated as R) and aligned (indicated as A) gelatin fibre mats. Reproduced with permission from Elsevier [14]

2.3.5 Summary

Electrospinning is a simple, low-cost technique for fabricating nanofibres from thermoplastics. The newly developed core/shell electrospinning method makes it possible to fabricate nanofibres containing elastomers; however, many parameters still need to be optimised. The nanofibre bundles exhibit non-linear stress-strain curves resembling those of natural soft tissues. The large number of fabrication variables in this technique, including the selection of other elastomer-forming prepolymers, the elastomer/thermoplastic ratio, the surface tension, the feeding speed, the solution concentration, the moisture in the chamber, the rotation rate of the collecting mandrel, and the subsequent cross-linking treatment conditions, is likely to provide a wide range of possible mechanical properties for tissue and organ engineering of all soft types.

2.4 Project Goal

The immediate availability of functional tissue replacements for clinical use is of great importance to human healthcare. Huge efforts have been invested in developing man-made biomaterials that mimic the physical and chemical properties of natural tissues [34]. Despite some early successes, there are few synthetic tissue engineering products available for clinical use [5], especially for the repair of soft, mechanically functional tissues such as the heart, lung and intestine. The precise reasons for graft failure in experimental animal studies and preclinical trials are not fully understood, but they include the mechanical dissimilarities between the synthetic biomaterial and the native tissue that it is replacing [6]. Current

synthetic biomaterials are primarily made from thermoplastics, whereas living tissues are elastic. Hence, elastomeric polymers, specifically poly(glycerol sebacate), were chosen for this thesis research project.

Synthetic elastomers exhibit linear elasticity at low strains, while soft tissues are non-linearly elastic [4]. The different mechanical properties of an elastomer are determined by the polymers' intrinsic structure. The polymer chains are randomly tangled in a synthetic elastomer, whereas native protein nanofibres are aligned in the muscular tissue. We believe that producing aligned nanofibrous structures is the key to achieving nonlinear elasticity in a synthetic polymer to better mimic a biological soft tissue. Hence, we have chosen to investigate core/shell electrospinning as the fabrication technique.

Therefore, the goal of this research project is to develop elastomeric biomaterials that closely mimic the properties of natural tissues (e.g., heart muscle) using the core/shell electrospinning technique. The biological tissue-like biomaterials will be able to help regenerate injured soft tissue by delivering functional cells and providing mechanical support to a dysfunctional organ. The specific objectives include:

(1) To establish the feasibility and conditions for core/shell electrospinning PGS and thermoplastics (PLA and PVA).
(2) To fabricate nonlinearly elastic, fibrous biomaterials from PGS pre-polymers using core/shell electrospinning. The nonlinear elasticity can be tuned so that the new biomaterials have wide applicability for soft tissue engineering.
(3) To evaluate the fibrous biomaterials cytocompatibility and degradation kinetics *in vitro*.
(4) To fabricate aligned PGS/PLLA core/shell fibrous mats and identify the variation of the mechanical properties with fibre alignment.
(5) To apply these fibrous materials in cell culture with an ultimate applications for the treatment of myocardial infarction. Most of this work is ongoing and is not presented in this thesis.

Chapter 3

Materials and Experiments

3.1 Materials

Glycerol (purity 99%), sebacic acid (purity 99%), L(+)-lactic acid (LA), esterase from porcine liver (suspension in 3.2 M ammonium sulfate solution, ~130 U/mg protein, Fluka) were purchased from Sigma-Aldrich (Castle Hill, NSW, AU). Chloroform, dimethylformamide (DMF) and tetrahydrofuran (THF) were purchased from Merck (Kilsyth, VIC, AU). The PLLA, also known as RESOMER® L 206 S, was purchased from Sigma-Aldrich (Castle Hill, NSW, AU) and is reported to be ester-terminated with an inherent viscosity of 0.8-1.2 dl/g for a 0.1% solution in $CHCl_3$ at 25ºC, a glass transition temperature of 60-65°C and a melting point of 180-185°C. Poly (vinyl alcohol) (PVA) with different average molecular weights (M_W), varying from 13,000-23,000 (87-89% hydrolyzed), 31,000-50,000 (98-99% hydrolyzed), 89,000-98,000 (99+% hydrolyzed) and 146,000-186,000 (99+% hydrolyzed) g/mol were purchased from Sigma-Aldrich (Castle Hill, NSW, AU). The melting point of PVA is reported by the supplier as being 200°C. These PLLA and PVA were chosen as the shell materials because their melting points should be sufficient to retain the nano-fibre shape during the cross-linking of PGS, at temperatures which range from 120-150°C [108-110].

3.2 Solution miscibility

In the core/shell electrospinning process, the core (PGS) and shell (PLLA or PVA) solutions are extruded from two concentric syringe needles and are spun together, thus remaining in intimate contact during the process. An essential requirement for a successful core-shell spinning process is that these two solutions are not particularly miscible when they are in contact, so that the shell structure can be maintained during the spinning processes and during the subsequent thermal curing treatment. Therefore studies were undertaken of the miscibility of the solutions.

3.2.1 PGS/PLLA solution miscibility

The PLLA solution was added to the PGS pre-polymer solution at four different PLLA/(PLLA+PGS) percentages of 2, 5, 10 and 30 wt%. The miscibility was then

determined by visually examining the precipitation of PLLA upon mixing. Conversely, the PGS pre-polymer solution was added to the PLLA solution at four different PGS/(PLLA+PGS) weight percentages of 2, 5, 10 and 30 wt%. The miscibility was then determined by visually examining the development of a layer of separate PGS solution on top of the PLLA solution.

3.2.2 $PGS_{2:3}$/PVA solution miscibility

The solvent for PVA was water, which is a non-solvent for PGS, whereas the solvents for PGS include ethanol, DMF, THF which cannot dissolve PVA. So PGS and PVA solutions should largely remain in their separate phases during core/shell spinning. To choose the best solvent for PGS, the ethanol, DMF and THF solvents were mixed with 10% PVA in water solution to study their suitability.

3.3 Polymer synthesis

3.3.1 Synthesis of PGS polymers sheets

The synthesis of PGS solid sheets followed procedures that have used previously at Monash University [111]. Glycerol and sebacic acid were thoroughly mixed in glass beakers at a glycerol: sebacate (G: S) molar ratio of 1:1 or 2:3. These mixtures were then heat-treated under a nitrogen atmosphere at 130°C for 24 h, and after removal of the water of esterification, the formed PGS prepolymer was cooled to room temperature under nitrogen. A previous study [111] of the polymerization of PGS 1:1 shows that the loss of glycerol under these conditions is about 1.4% and so the loss for the PGS 2:3 would be expected to be even less and thus negligible. The pre-polymer was then dissolved in THF, cast onto glass slides, dried under ambient conditions overnight, and then dried a second time under a vacuum overnight at room temperature. The dried slides were then heated at 130°C under a vacuum for 72 h to cause crosslinking of the PGS. After cooling to room temperature in the vacuum, the polymer sheets were peeled off the glass slides after soaking in water for 15 mins, and were thoroughly dried under a vacuum for 4 days at room temperature.

3.3.2. Synthesis of PGS-co-LA polymer and PGS-PLLA blends

During the cross-linking treatment of core/shell spun fibres, it is possible for physical mixing (via diffusion) and a chemical reaction (via copolymerisation or transesterification) to occur between the PGS pre-polymer and PLLA at the interface of their solutions. Therefore, it is

important to examine the effects that polymer blending and copolymerisation/ transesterification exert on the elastic properties of the newly synthesised material.

To investigate the effect of copolymerization/transesterification, a series of PGS-co-LA polymers were synthesised for investigation. Glycerol and sebacic acid were thoroughly mixed in glass beakers at a glycerol: sebacate (G: S) molar ratio of either 1:1 or 2:3. These mixtures were then heat-treated at 130°C under a nitrogen atmosphere for 24 h, as described previously [111], and a PGS pre-polymer was formed after cooling under nitrogen. PGS pre-polymers were then thoroughly mixed with lactic acid (LA) at a G: S: L molar ratio of 1:1:(0.25, 0.5 or 1) or 2:3:(0.25, 0.5 or 1). These mixtures were then dissolved in THF, cast onto glass slides, dried under ambient conditions overnight, and then dried a second time under a vacuum overnight. The dried slides were then heated at 130°C under a vacuum for 72 h to stimulate copolymerisation/transesterification, followed by cooling to room temperature under a vacuum. Finally, the polymer sheets formed in this manner were peeled off after soaking in water, and thoroughly dried under a vacuum for 96 h at room temperature and then mechanically tested.

To synthesise the PGS-PLLA blends, the PGS pre-polymer (100g/100ml THF solvent), and PLLA (20g/100ml solvent consisting of 4:1 chloroform/DMF) were again prepared as above, then mixed to give four different mixtures in which the weight percentage of PLLA in the polymer blends were 2%, 5%, 10% and 30%. After vigorous mixing, the mixture phase-separated into a clear PGS-rich THF top layer and a clear PLLA-rich chloroform/DMF bottom layer. In each case, the clear PGS-rich top layer was then cast onto a glass slide and dried overnight at room temperature and then cured under the same conditions as used for PGS (130°C under a vacuum for 72 h). After curing, the polymer-blend layer was peeled from the substrate as discussed above and mechanically tested. Since the PLLA solution was not completely miscible with the PGS solution, the weight percentages are termed “nominal”.

3.3. Electrospinning

3.3.1 PLLA electrospinning

PLLA has been successfully spun from a mixture of dichloromethane and DMF at volume ratios of 9:1 by Ou et al. [63] but this was not successful in the current work; the rapid evaporation of the dichloromethane always resulted in blockage of the needle tip. Substitution of dichloromethane by the higher boiling chloroform at differing solvent ratios

revealed that the 4:1 v/v ratio of chloroform to DMF provided the most successful electrospinning of PLLA.

A PLLA solution 20g/100ml solvent (a 4:1 v/v ratio of chloroform to DMF) was spun using a Y-flow 2.2D-350 electrospinner (Y-flow Nanotechnology Solution, Spain). A spinneret with the inner diameter 1.4 mm was used and the flow rate was 1ml/h. The voltage used was between positive 10-13 kV at the tip of the spinneret and -2 kV at the collector. The collection distance between the spinneret tip and the aluminium foil collector was 15 cm – this distance ensured that most of the solvent had evaporated and leaving a solid fibre.

3.3.2 PVA electrospinning

PVA polymers of four different weight average molecular weight ranges: 13,000-23,000, 31,000-50,000, 89,000-98,000, and 146,000-186,000 g/mol, were dissolved in hot water (95°C) at various concentrations of 35, 20, 12 and 8 g/100ml solvent, respectively. These particular concentrations were chosen because their steady shear viscosities were very close (within a factor of two). One of the factors that affects electrospinning is the solution viscosity [112, 113]. Because preliminary experiments with the intermediate molecular weight polymers indicated that fibres could be spun readily at the concentrations of 20 and 12 g/100ml solvent, for the PVA of 31,000-50,000 and 89,000-98,000 g/mole polymers, respectively, their viscosity was used as a guide for the selection of the concentrations of the other PVA materials.

The solutions were then spun using a Y-flow 2.2D-350 electrospinner (Y-flow Nanotechnology Solution, Spain) with a spinneret, the inner diameter of which was 1.4 mm with a flow rate of 1 ml/h. Based on previous successful electrospinning experiments, the voltage used was between positive 10-17 kV at the tip of the spinneret and -2kV at the collector. The collection distance between the spinneret tip and the aluminium foil collector was 18 cm – this distance ensured that most of the solvent had evaporated and so left a solid fibre.

3.3.3. PGS/PLLA core shell electrospinning

A Y-Flow 2.2D-350 electrospinner (Yflow Nanotechnology Solutions, Spain) was set up with a two-fluid coaxial spinneret, and the inner tube had inner and outer diameters of 0.6 mm and 0.9 mm respectively while the outer tube had an inner diameter of 1.4 mm. Thus the cross-sectional areas of the two flows were 0.283 and 0.903 mm^2. A voltage potential ranging

from 10-13 kV, but usually 12 kV, was applied between the tip of the spinneret and the collector plate located 200 mm below. PGS prepolymer with G:S 1:1 was prepared using the same method mentioned in Section 3.3.1.The feed flow rates of the core (PGS 100g/100ml solvent in THF) and the shell (PLLA solution 20g/100ml of a solvent mixture of 4:1 chloroform/DMF) solutions ranged from 0.1 ml/h versus 1 ml/h to 0.5 ml/h versus 1ml/h, respectively. The spun fibres were collected on a static plate.

To fabricate PGS/PLLA fibre mats with different alignments, the core and shell feeding rate at 0.3:0.9 ml/h was used and the fibre was collected by a rotation drum (with circumference 16 cm) at different rotation speeds 0, 500, 1000, 1500 and 2000 rpm, corresponding to surface velocities of 0, 80, 160, 240 and 320 m/min, respectively.

The spun fibre mats were optionally placed in a vacuum oven purged with nitrogen and were then heated at 130°C under vacuum in a vacuum oven for 72h to cross-link the PGS. {Alternatively the spun fibre mats were first purged with nitrogen in the vacuum oven then heated at 130°C under vacuum for 3 days to cross-link the PGS.

3.3.4 Fabrication of $PGS_{2:3}$ fibre mats using core/shell electrospinning

The Y-Flow 2.2D-350 electrospinner was set up as described above. A voltage potential of either 12 kV or 15kV was applied at the tip of the spinneret and -2 kV at the collector. The collection distance between the tip and collector was 18 cm – this distance ensured that most of the water in the PVA solution had evaporated and so left a solid fibre.

PGS prepolymer with a G:S ratio of 2:3 was prepared using the same method mentioned in Section 3.3.1. The core solution used a concentration of 100g of $PGS_{2:3}$ in 100 ml of THF, while 20 g/100ml solvent PVA (M_W 31,000-50,000) and 12 g/100ml solvent PVA (M_W 89,000-98,000) in water solution was used as the shell solution. The feed/flow rates of the core and shell solutions were initially set at 0.1 and 1 ml/h, respectively. The spun fibre mats collected on the aluminium foil were heated at 130 °C under vacuum for 72 h to crosslink the $PGS_{2:3}$. After the heat treatment, each $PGS_{2:3}$/PVA core/shell fibrous mat was soaked in hot water (95 °C) for 4 hours until most of the PVA shell had been removed, leaving a $PGS_{2:3}$ mat behind. The mat was then dried at ambient temperature and pressure for 24 h, followed by drying under a vacuum for 24 h.

To prepare water saturated $PGS_{2:3}$ fibre mats, the mats were soaked in water for 2 h at room temperature until fully saturated.

3.4 Characterization

3.4.1 Scanning electron microscopy (SEM)

The surfaces of the samples were sputter-coated with platinum with a thickness of ≈1 nm, and a JEOL 7001F field emission gun scanning electron microscope (SEM) or a FEI NovaNano 430 field emission gun scanning electron microscope (FEGSEM) were used to take secondary electron images of specimens. To observe the core/shell structure of PGS/PLLA core/shell fibre mats, fibre mats were cut crosswise using an Ultracut S Cryo-Microtome at -120 °C. The cross-sections were also coated with platinum with ≈1 nm and then analysed by SEM. The fibre diameter and alignment of each specimen were determined using ImageJ 1.47v software developed by Wayne Rasband, National Institutes of Health, USA.

3.4.2. Determination of the degree of esterification in PGS

The degree of esterification was determined by acid group titration of the remaining carboxyl groups in the PGS. In the acid group titration method [111, 114], 1 g of sample was dissolved (prepolymer) or swelled (crosslinked polymer) in an ethanol (25%)/toluene (75%) mixture in a flask sealed with Parafilm^{TM} film. The crosslinked polymers were ground in to a powder and soaked in the solvent mixture for 24 h to achieve high degrees of swelling. The carboxyl groups were then titrated with a standardized 0.1 mol/L solution of potassium hydroxide (KOH) in ethanol, keeping the flask sealed from atmospheric CO_2 when standing. Bromothymol blue solution (10 drops) was used as a pH indicator, and the end-point of the titration was taken when the solution changed from yellow to bluish green. For the crosslinked samples, the end point was taken to have been reached when the colour of the indicator remained bluish green for 1 h after the last titration addition. The percentage of the reaction of the carboxylic acid groups was calculated using the following equation:

$$\text{Percentage reaction (\%)} = \left(1 - \frac{Moles\ unreacted\ carboxylic\ acid\ groups}{moles\ original\ carboxylic\ acid\ groups}\right) \times 100$$

$$= \frac{(V_1 - V_0) \times {C}/{m_0}}{2/(M_{SA} + M_{Gly} \times {n_{Gly}}/{n_{SA}})} \times 100 \qquad \text{(Eq 3.1)}$$

Where V_1 is the volume in liters of 0.1 mol/L KOH used for the sample titration, V_0 is the volume for the blank test (without sample), C is the concentration of KOH (0.1 mol/L), m_0 is the mass of the sample, M_{SA} and M_{Gly} are the molecular weights of sebacic acid and glycerol,

respectively, and n_{SA} and n_{Gly} are the number of moles of sebacic acid and glycerol, respectively in the sample.

3.4.3. Rheology of PVA and $PGS_{2:3}$ solutions

The steady shear viscosity of the PVA (with different M_W 13,000-23,000, 31,000-50,000, 89,000-98,000, and 146,000-186,000 g/mol,) solutions in water and $PGS_{2:3}$ prepolymer in THF were measured with a MCR501 Physica rheometer (Anton Paar) in parallel plate (50 mm diameter) mode with 0.5 mm gap and operated at 23°C with shear rates varying from 1 to 1000 s^{-1}.

3.4.4. Fourier Transform Infrared (FTIR) spectroscopy

Attenuated Total Internal Reflectance-Fourier Transform Infrared spectroscopy (ATR-FTIR) analysis using a Nicolet 6700 spectrometer and a Smart Orbit single-bounce diamond ATR accessory was conducted for $PGS_{2:3}$, PVA (M_W 8,9000-9,8000), $PGS_{2:3}$/PVA fibre mat and $PGS_{2:3}$ fibre mat. To enhance the physical contact between the PVA powder or fibre mats and the ATR crystal, the samples were compressed between two smooth, flat glass plates, thus giving smooth and shiny surfaces before they were mounted in the ATR unit.

3.4.6 Differential Scanning Calorimetry (DSC)

The thermal properties of the PVA powder, $PGS_{2:3}$/PVA core/shell fibre mat and $PGS_{2:3}$ fibre mats were evaluated with a Perkin Elmer, Pyris 1 differential scanning calorimeter (DSC). The samples for DSC measurements were approximately 7 mg while the heating rate was set at 20 °C/min. The melting (T_m) temperatures were measured at the peak of the process, the glass transition (T_g) was defined by the mid-point inflection in the heat capacity curve.

3.5 Tensile testing

Tensile test specimens were punched out using a standard dog-bone-shaped mould, with a gauge length of 12.5 mm and a width of 3.25 mm. The thickness of each specimen was measured using a micrometer. Cyclic and tensile testing were conducted for each specimen at the ambient conditions, using an Instron 5860 mechanical tester equipped with a 100 N load cell. The cyclic test specimens were stretched to a strain of 15 %, which is typical of the dynamic loading strain of soft tissues, such as cardiac muscle, under normal physiological conditions [115]. The crosshead speed for cyclic testing (performed once per polymer type) was chosen to be 25 mm/min to enable comparison with previous studies [116]. The strain was then released and then reapplied nine more times at the same rate to provide the

hysteresis curve for one cycle and for numerous cycles. For the tensile tests (repeated at least 5 times), the crosshead speed was selected to be 10 mm/min which was also consistent with the rates used previously [109]. To mimic the application status of the materials *in vivo*, the tensile and cyclic tests also carried out on the $PGS_{2:3}$ mat and $PGS_{2:3}$/PVA mat after they had been soaked in water until saturated with water.

The tensile stress (σ)-strain (ε) behaviour of elastomeric polymers can be readily described by the equation of rubber elasticity [117]:

$$\sigma = \nu RT(\lambda - \frac{1}{\lambda^2}) \approx 3\nu RT\varepsilon = E\varepsilon, \qquad \text{(Eq 3.2)}$$

Where σ is the engineering stress, $\lambda = 1 + \varepsilon$ is the extension ratio, ε is the engineering tensile strain, E is the Young's modulus, ν is the network strand density (the concentration of crosslinked chains in the polymer), R is the universal gas constant, and T is the absolute temperature. At low strain values, this equation can be linearised with an error of 8.8 % when ε = 10 %. Therefore, the Young's modulus of $PGS_{2:3}$ solid sheet specimens was determined by taking the value of σ/ε when ε = 10 %.

For the porous electrospun mats, Eq (3.2) does not adequately describe the stress-strain curves due to the combination of fibre orientation, slipping and stretching, however, the stress-strain curves of spun sheets could be considered roughly linear at small strains (see Section 3.5). In order to compare the stiffness of $PGS_{2:3}$ solid sheets and $PGS_{2:3}$ fibrous mats, we used the slopes of stress-strain curves of each sample at a small strain (ε = 10 %) as an approximation. The ultimate tensile strength (UTS) and the elongation at the breaking values were read directly at the breaking point of the tensile test.

Resilience describes the capability of a material to deform reversibly without a loss of energy [116], and was calculated from the stress-strain data of the first cyclic stress-strain test and also from the average values of the subsequent 9 cycles. The resilience of a material is expressed as the following ratio, for a strain of 15 % [118]:

$$\text{Resilience} = \frac{\text{Area under unloading curve}}{\text{Area under loading curve}} \qquad \text{(Eq 3.3)}$$

It should be noted that subsequent cycling of the strain did not follow the same curve for the $PGS_{2:3}$/PVA fibre mats and dry $PGS_{2:3}$ fibre mats, suggesting that morphological changes had occurred in the fibres.

Biological tissues are usually found to exhibit a non-linear elasticity and several constitutive equations have been proposed for this behaviour [107, 119-121]. These functions predict that stress increases near-exponentially with strain. The Young's modulus is often replaced by the tangent modulus (also known as "stiffness" in medical science), defined as the slope at any point of a stress-strain curve. According to the equation of Mirsky and co-worker [3, 107, 122], the tangent modulus, *E*, is proportional to the stress exerted on it, as in the following Equation:

$$E = \frac{d\sigma}{d\varepsilon} = k\sigma + \alpha, \qquad \text{(Eq 3.4)}$$

or

$$\sigma = \frac{\alpha}{k}(e^{k\varepsilon} - 1) \qquad \text{(Eq 3.5)}$$

Where the slope *k* (dimensionless) is defined as the stiffness constant. Several other workers [123, 124] have also found that Eqs (3.4) and (3.5) provide a good model for biological tissues. If the stress is very low, Equations 3.4 and 3.5 show that E is equal to the constant α and is the Young's modulus. The data was fitted to Equation 3.4 using the Matlab R2013a software (The Math works, Inc. US).

3.6 Cytocompatibility assay

Cytocompatibility assays were performed according to the standard cytotoxicity assessment set by the International Standardization Organization (ISO 10993). Prior to culture, 48-well plates (Falcon, BD Bioscience, North Ryde, Australia) were coated with a 0.1% w/v gelatin solution and washed using phosphate-buffered saline to remove any residual solvent. SNL Mouse fibroblasts (STO-Neo-LIF, University of California, Davis) were then seeded to each well, which contained 1 ml of Dulbecco's modified Eagle's medium (DMEM) (Gibco®, Australia) supplemented with 10.0% foetal bovine serum, 1.0% Glutamax (Gibco®, Australia), and 0.5% penicillin/streptomycin, at a target density of 5000 cells/well. The negative control for the test was 1 ml of the cell culture media with no additives. The PLLA-only fibre mats were used as a positive control, and the cell culture medium (1 ml) containing inoculated cells without scaffolds was used as a negative control. The plate was then cultured under standard incubation conditions of 37 °C and 5% CO_2 in humid air, with medium changed every second day. When the cell monolayer had reached a confluence of 80% on day 4, electrospun PGS/PLLA core/shell fibre mats, PGS solid sheets, $PGS_{2:3}$ fibrous mats,

$PGS_{2:3}$ solid sheets and control PLLA fibre mats (sterilised by treatment with 70% ethanol in deionised water, and dried overnight in a cell culture hood) were placed in contact with the cell monolayer covered with cell culture medium in the 48-well plate. Cultures were then allowed to grow for a further 2 days, following a previous Monash University study [125]. Then cell images were obtained using EVOS® Imaging system (Life Technologies, Australia) at 40× magnification.

At the end of the incubation period, the spent culture media samples were collected and the degree of cytotoxicity was determined using a commercial assay kit (TOX-7, Sigma-Aldrich) [109, 126] to measure the quantity of lactate dehydrogenase (LDH) released into the culture media by dead or dying cells ('RELEASED LDH'). Wells with live cells were then filled with 0.5 ml of fresh cell culture medium containing TOX-7 lysis buffer, and cellular LDH was then extracted from these lysates ('TOTAL LDH'). The overall LDH level per well was then determined by measuring the absorbance of the supernatant from the centrifuged medium at 490 nm (after subtracting the background absorbance at 690 nm), using a multi-well plate UV-vis spectrophotometer (Thermo Scientific). The LDH absorbances were converted to a cell count based on a linear standard curve. Therefore, the cytotoxicity can be expressed as follows:

$$\text{Percentage of dead cells} = \frac{\text{released LDH}}{\text{released LDH} + \text{total LDH}} \times 100. \qquad \text{(Eq 3.6)}$$

3.7 Cell proliferation

Cell proliferation was assessed using a commercial AlamarBlue™ assay kit (Life Technologies). AlamarBlue™ is non-toxic to cells and does not interrupt cell culture growth, but AlamarBlue is reduced by living cells to the reduced form which has a different absorption spectrum in the visible region, allowing quantitative measurement of the cell activity and a continuous measurement of cell proliferation kinetics. Therefore, the AlamarBlue™ assay is appropriate for evaluating the long-term cytotoxicity of biomaterials that undergo biodegradation under physiological conditions [127]. For this assay, culture media wells were seeded with SNL fibroblasts (2000 cells per ml) into each well of a 48-well plate and cultured as described above, in the presence of sterilised PGS/PLLA fibre mats (test material) or sterilised PLLA fibre mats (material control). Material-free media with cells

(positive controls) and the cell culture medium alone (negative control) were also included in independent wells on the same plate.

After culture for 48 h, 0.1 ml of the AlamarBlue™ indicator was added to each well (with the exception of the background controls) and incubated under standard culture conditions for a further 5 h. The medium was then transferred to a new plate, after which the UV-vis absorbance of the medium at wavelengths of 570 and 600 nm was measured. This procedure was repeated every 48 h until confluence was reached, which was typically after 6 days. Cell proliferation was quantified by the percentage reduction of AlamarBlue™ from its normal oxidized form to the reduced from using the following equation [126]:

$$\%\,\text{Reduced} = \frac{\varepsilon_{OX}(\lambda_2)A(\lambda_1) - \varepsilon_{OX}(\lambda_1)A(\lambda_2)}{\varepsilon_{RED}(\lambda_1)A'(\lambda_2) - \varepsilon_{RED}(\lambda_2)A'(\lambda_1)} \times 100 \quad , \qquad \text{(Eq 3.7)}$$

where $A(\lambda_1)$ and $A(\lambda_2)$ are the absorbance values of test wells measured at wavelengths λ_1=570 nm and λ_2=600 nm, respectively, and $A'(\lambda_1)$ and $A'(\lambda_2)$ are the values of absorbance at the same wavelengths for negative control wells containing only culture medium and AlamarBlue™. All values were blanked based on the readings of background controls. The remaining parameters were the molar extinction coefficients (in $Lmol^{-1}cm^{-1}$): $\varepsilon_{OX}(\lambda_1)$=80.586, $\varepsilon_{OX}(\lambda_2)$=117.216 for the oxidized form and $\varepsilon_{RED}(\lambda_1)$=155.677 and $\varepsilon_{RED}(\lambda_2)$=14.652 for the reduced form.

3.8. Cell culture work

3.8.1 Viability of human embryonic stem cell (hESC)-derived cardiomyocytes

Cardiomyocytes derived from the human embryonic stem cell (hESC) line H7 (University of California, Davis) were grown in Matrigel-coated six-well plates (Falcon, BD Bioscience, North Ryde, Australia), with daily changes of mouse embryonic fibroblast - conditioned medium supplemented with 8 ng/mL of recombinant human basic fibroblast growth factor and antibiotics (50 U/mL penicillin (Gibco®， Australia) and 50 mg/mL streptomycin (Gibco®， Australia) [126]. For differentiation of cardiomyocytes, H7 embryoid bodies (EBs) were cultured in low adherence plates for 4 days in differentiation medium. The EBs were plated out onto plastic dishes coated with 0.5% gelatin and spontaneously beating areas,

which appeared from day 9 after EB formation, were micro-dissected from EB outgrowths at day 30 [126].

The contractile motion of the cells was studied through a Nikon Eclipse TS100 inverted microscope with Hoffman modulation contrast optics, coupled to a Basler (model A602f) camera and captured using Quick Caliper (SDR Clinical Technologies) software at 80 frames s^{-1}. The video captures were analysed using the Metamorph® Imaging software suite. The rationale for this approach is that (a) ESC-derived cardiomyocytes (ESC-CMs) have a strong tendency to aggregate so techniques to assessing cell viability and cytotoxicity based on the homogenous seeding density of cells cannot accurately be achieved; and (b) overgrowth with more rapidly proliferating fibroblasts may bias these methods. Therefore, we used the intrinsic contractile activity of cardiomyocytes and scored the beating rates of hESC-CMs by videomicroscopy.

3.8.2 Isolation and culture of enteric neural crest (ENC) cells

To obtain ENC cells for growth on the PGS/PLLA fibrous mat, intestinal tissue was collected from embryonic day 14½ EDNRB-Kikume mice (carrying a Kikume reporter under the control of the EDNRB locus, a kind gift from Hideki Enomoto, Japan) [128]. The intestinal tissue was digested for 35 min at 37 °C in F12 media (Gibco-Invitrogen, USA) supplemented with 0.5% w/v dispase II (Roche, USA) and 0.1% w/v CLSAFA collagenase (Worthington, USA). 1 mM EDTA was added for a further 10 min to disrupt cadherin-based cell adhesions. The digested tissue was then mechanically triturated and the cell suspension washed in F12 media supplemented with 5% FCS and filtered through a 40 mm cell-strainer (BD Falcon, USA). 10 mg/ml propidium iodide (Sigma, USA) was added and Kikume expressing live cells were sorted using a MoFlo cell sorter (MoFlo, USA). These cells were plated onto the PGS/PLLA fibrous mat at an approximate density of 3500 cells/mm^2 and grown in a 1:1 mixture of DMEM (Thermo-Fisher, USA) and F12 (Gibco-Invitrogen, USA) with L-glutamine, B27 and N2 (Gibco-Invitrogen, USA), and 20 ng/ml of hFGF and hEGF (R&D systems, USA) and penicillin and streptomycin (SigmaeAldrich, USA).

3.9 Enzymatic degradation *in vitro*

The enzymatic degradation processes were based on previous published works [129-131]. Samples with 2 cm^2 surface area cast PGS and PGS/PLLA fibre mats were cut using standard mould, weighted and sterilised with 70% alcohol for 15 min followed by drying in a tissue

culture hood for overnight. The samples were placed in a 24-well tissue culture plate filled with 2 mL of Dulbecco's modified Eagle's medium (DMEM) (Gibco®, Australia) and esterase (0.3 unit esterase per mg polymer were added to each well as defined in previous experiments [129]).

The above culture plates were then placed in a 37 °C culture incubator. The culture mediums with solutions of enzymes were changed every day. After incubation for 7, 14, 21, 28 and 35 days, specimens were removed from the culture plated, wiped and washed with water and dried in a vacuum oven at room temperature until no further change in weight was detected (giving a mass m_t). Four specimens from each experiment were measured. The precentage of weight loss was given by equation:

$$\text{Weight loss } (\%) = \frac{m_t - m_0}{m_0} \times 100 \qquad \text{(Eq. 3.8)}$$

Where m_0 is the initial dried mass and m_t is the vacuum dried weight measured after incubation. The thickness of each specimen was also measured before and after 35 days of degradation.

Culture media from each well (containing degradation products form the specimens and enzyme) were collected after 1 day of incubation for pH measurement to provide the degree of acidification of degradation environments. The pH of each solution was measured by insertion of a pH glass electrode (Hanna® Instruments, HI 1230B) attached to a pH meter (Hanna® Instruments, HI 1230B) into the solution and recording of the reading after the electrode was stabilised. These data were recorded as the difference in pH value of the solution in which the samples were immersed and incubated for 1 day compared with the culture medium with enzyme incubated at the same condition, pH_{biomat} - $pH_{biomat\text{-}free}$.

3.10 Statistical analysis

In most cases (identified in the text), experiments were performed with five samples per experimental group, and the statistical outputs are shown in the form of a mean with standard error (± SE). A one-way analysis of variance (ANOVA) with Turkey's *post hoc* test was performed to analyse the significant differences, and significance levels were set at a *p*-value of less than 0.05.

Chapter 4

Mechanically tissue-like elastomeric PGS/PLLA core/shell fibres and their potential applications

4.1 Introduction

The stress-strain nature of biological tissues has been observed to be quite unlike most materials [107]. They undergo elastic (i.e, reversible) stretching to high levels of extensibility but they also exhibit non-linear deformation behaviour in which the stress rises at an increasing rate as the strain is raised. In contrast, thermoplastic polymers proposed for tissue replacement, such as polylactic acid (PLA), polyglycolic acid (PGA) and their copolymers, show a decreasing rate of rise in stress prior to plastic deformation (i.e. non-reversible deformation) at low strains. Therefore, one of the major problems encountered by biomaterials scientists in repairing the majority of soft tissue types is the need to replicate their innate and complex elasticity[4]. Despite some previous success [34], there are few synthetic tissue engineering products available for clinical use in the repair of soft, mechanically functional tissues, such as heart, lung and intestine [5]. These mechanical dissimilarities between synthetic biomaterials and tissue for repair are believed to be the major cause of graft failure in experimental animal studies and preclinical trials [6].

Research activity focusing on the development and clinical application of synthetic biodegradable soft elastomers as transplantable biomaterials for tissue engineering has increased over the past decade [4]. For example, poly (polyol sebacate), or PPS, is a new family of cross-linked, biodegradable elastomers that has recently been developed for soft tissue repair and regeneration applications [7, 132]. Chen et al. (2008) have reported that the Young's modulus of a PPS family member, poly(glycerol sebacate), or PGS, ranges between 0.05 and 1.5 MPa, which is similar to the stiffness of muscle tissues [9].

In an animal study using a rat model, PGS sheets were grafted as heart patches and performed the intended mechanical function in terms of inhibiting scar formation in infarcted heart muscles [11]. However, this study also revealed two critical drawbacks of using PGS patches. Firstly, the grafted patches were completely absorbed in 6 weeks. This time frame is too rapid

for the recovery of a diseased heart, a process which takes approximately 6 to 12 months [11]. Secondly, and perhaps more significantly, an arrhythmia (irregular heartbeat), attributable to the mechanical property mismatch between the PGS patch and the heart muscle, was observed. The stress-strain curves of synthetic elastomers are relatively *linear* at low strains, particularly at 15% which is the maximal strain of living tissues, but biological tissues, such as heart muscles, exhibit *non-linear* stress-strain curves [4] which we call here "J-shaped" as discussed above. The primary reason for these different elastic behaviours may be that the polymer chains form random coils between the crosslink points within the synthetic elastomer network, while protein nanofibres tend to be straighter and aligned within muscle fibres. Therefore, the production of an aligned, or partially aligned, nanofibrous structure within a synthetic polymeric material may be ideal for matching the non-linear elasticity of biological tissues.

The production of nanofibres from cross-linked elastomers is technically challenging. The first challenge of producing synthetic core-shell nanofibres has been recently solved by electrospinning [133-135]. A second problem is that a crosslinked elastomer cannot be dissolved in a solvent for the electrospinning process. While the literature reports investigations on photopolymerization of monomers and oligomers during the electrospinning process [136], such a technique is not possible with the PPS materials of interest here because they do not contain photopolymerizable groups. If the material is not photopolymerized during electrospinning, it must be capable of forming a rigid, relatively non-adhesive fibre once the solvent has evaporated in the electrospining process. However before PPS is thermally crosslinked, it is a viscous polymer which cannot retain a nano-fibrous form after spinning. In fact the PPS oligomer needs to be thermally cured at elevated temperatures to form an elastomer. Fortunately, the recent development of a core/shell electrospinning technique could offer an opportunity to address these problems [13, 63]. Core/shell electro-spun fibres with elastomeric cores can be formed when a pre-polymer that is not cross-linked is ensheathed by a suitable thermoplastic in solution, with both materials being fed into the electrospinner simultaneously but via separate core and annulus flows. Following collection of the core-shell nano-fibre, thermal crosslinking process of the prepolymer can be undertaken *in situ* if the solid thermoplastic shell can maintain its tubular shape at the curing temperature. Yi and LaVan [13] have reported the production of core-shell PGS/poly-L-lactic acid (PLLA) nanofibres using this method. In addition, they claimed that they could remove the thermoplastic shell from the final product by dissolution in

chloroform but did not provide SEM evidence for this. However, we believe that, when used as a biomaterial scaffold, the addition of a thermoplastic shell would be beneficial in controlling the degradation rate of the final product. Therefore, the objective of the present study was to systematically explore the fabrication procedures of PGS/ PLLA fibrous materials using the core/shell electrospinning technique, to investigate the mechanical behaviour of these mats, evaluate their *in vitro* biocompatibility and potential in application as biomaterial scaffolds.

4.2. Results and Discussion

4.2.1 PLLA electrospinning

The establishment of a stable condition for PLLA electrospinning was the precondition for PGS/PLLA core/shell electrospinning. Dichloromethane and chloroform have previously been successful in electrospinning PLLA [63, 65]. However, we found that electrospinning with dichloromethane as a solvent was not successful due to rapid evaporation, causing blockage at the needle tip and preventing fibre spinning. Instead, chloroform, which has a lower evaporation rate, was chosen as the main solvent for PLLA. Following the work of Ou [63], DMF was added to the chloroform to further reduce the solvent evaporation rate and make the spinning more stable. After preliminary experiments, chloroform and DMF with volume ratio 4:1 was finally used as the solvent for PLLA.

PLLA solution with a concentration less than 12.5 g/100 ml solvent resulted in spray formation. As shown in F**igure 4.1a** spun PLLA solution with a concentration of 12.5 g/100 ml solvent produced thin fibres with large beads, and the beads were eliminated when the concentration increased to 20 g/100 ml solvent (**Figure 4.1b**).

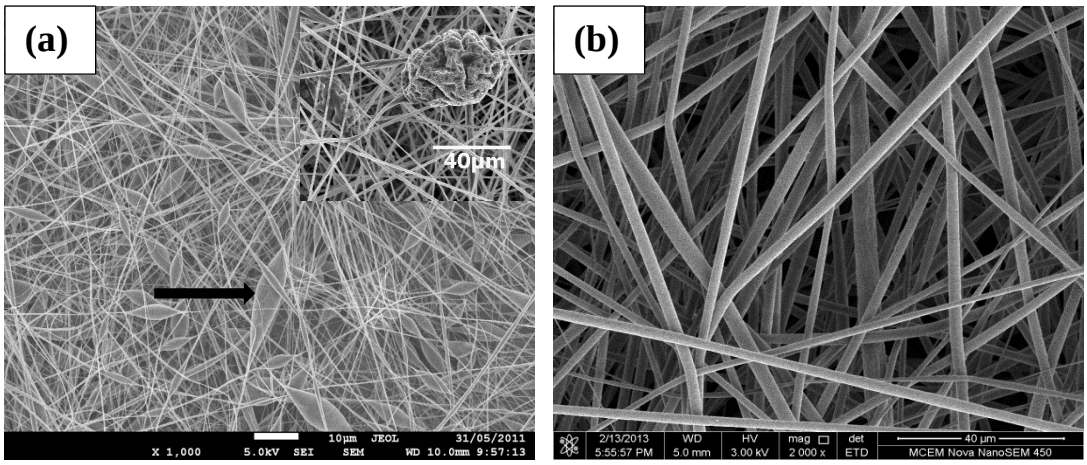

Figure 4.1 SEM image of PLLA with different concentrations (a) 12.5 g/100 ml solvent and (b) 20 g/100 ml solvent (spun at +12 and -2 kV, feeding rate 1 ml/h and collection distance 200 mm). The arrow in (a) points at a droplet or bead on the fibre.

The optimised fabrication parameters for PLLA fibres was 20 g/100 ml solvent PLLA in chloroform and DMF with a volume ratio 4:1, the voltage applied on the needle and collector were +12 and -2 kV, and the collection distance was 200 mm.

4.2.1. Miscibility of the PLLA and the PGS solutions

When the PLLA 20 g/100 ml solution in chloroform/DMF was added to the PGS 100 g/100 ml solution in THF, phase separation was observed in mixtures containing between 2 and 5 wt% of the PLLA in the PGS/PLLA blend. Therefore, the miscibility of the PLLA with the PGS is between 2 and 5 wt%. After small amounts of the PGS 100g/100ml solution in THF was added to the PLLA 20 g/100 ml solution in chloroform/DMF, phase separation was observed, indicating that the miscibility of the PGS solution in the PLLA solution is lower than 2 wt% of PGS in the PGS/PLLA blend. These results indicate that the PLLA and PGS solutions should largely remain as separate phases during core/shell spinning. However, small amounts of the PLLA shell material will dissolve in the PGS core material and this may compromise the elastomer's properties. This small amount of PLLA may exist as an intimate solution with the PGS polymer chains, or it may also react with the PGS during cross-linking to form a PGS/PLA graft or copolymer. Therefore, the effects of the presence of PLLA and LA on the mechanical properties of the PGS/PLLA grafts/blends and PGA-LA copolymers were investigated.

4.2.2. Mechanical properties of PGS/PLLA blends

The PGS/PLLA mixtures (either grafts or blends or both) were prepared by adding PLLA to a PGS pre-polymer, casting into sheets and solvent evaporation followed by heat treatment to cross-link the pre-polymer chains (**Table 4.1**). With an increase in the nominal wt% of PLLA, the Young's modulus, UTS, elongation at break and resilience do not markedly change and addition of the PLLA to the blend does not compromise the elasticity of the PGS matrix **(Table 4.1)**. It is interesting to note that the elongations at the break point of the PGS/PLLA blends are, on average, higher than pure PGS, although the increments are not statistically significant.

Table 4.1 Mechanical properties of PGS/PLLA blends/copolymers after heat treatment in vacuum at 130°C for three days to crosslink the PGS component.

Nominal percentage of PLLA in blends (wt%)	Young's modulus (MPa)	UTS (MPa)	Elongation at Break (%)	Resilience
0	1.23 ± 0.06	0.70 ± 0.04	88 ± 8	0.98 ± 0.01
5	1.27 ± 0.05	1.04 ± 0.15	124 ± 18	0.98 ± 0.01
10	1.17 ± 0.27	0.77 ± 0.07	101± 36	0.97 ± 0.01
20	1.23 ± 0.09	0.73 ± 0.10	83 ± 19	0.97 ± 0.01

4.2.3. Mechanical properties of PGS-co-LA copolymers

The mechanical properties of the PGS-co-LA polymers with a 1:1 or 2:3 molar ratio of glycerol to sebacic acid are shown in **Figure 4.2**. The mechanical properties of the PGS(1:1)-co-LA polymer are similar to those of the pure PGS counterpart, and no significant differences were detected between any pair of the four polymer groups compared with each other. Two counteracting mechanisms could likely be responsible for the lack of significant changes. Lactic acid contains both hydroxyl and carboxyl groups and can therefore react with both glycerol and sebacic acid. Therefore lactate units in the network chains will increase the physical distance between the cross-link points, lowering the cross-link density and reducing the rubbery modulus and strength [117] in comparison with a pure PGS polymer that is treated under identical conditions. Furthermore, lactic acid should significantly reduce the polymerisation kinetics in comparison with the polymerization of pure PGS. This observation was in accordance with experiments which show that the polycondensation reaction of lactic acid is much slower than that of glycerol and sebacate and requires a higher reaction

temperature [137, 138]. Therefore, the incorporation of lactic acid into the PGS network has a tendency to soften the polymer product because it reduces the extent of polyesterification compared with that in neat PGS. Conversely, the side $–CH_3$ chains on lactic acid molecules could stiffen the copolymer network by increasing its T_g, since PLLA has a T_g of 60-65°C compared with -23°C for PGS [125]. In this manner, these counteracting mechanisms could result in relatively insignificant changes to the mechanical properties of the PGS-co-LA polymers, compared with pure PGS or PLLA.

The results of **Figure 4.2** also partly concur with those of Sun *et al.* [138] in their study of poly(glycerol-sebacate-lactic acid), where the copolymers were synthesised at 140°C for 30 h and the elastic moduli of the copolymers were measured using nano-indentation. This study showed no significant increments in the elastic moduli of the copolymers synthesised at a G:S:L molar ratio of 1:1:(0-0.5), as conducted in the present study. However, the elastic modulus of the copolymer increased abruptly at a molar ratio of 1:1:1 [138], which is inconsistent with our result for the same ratio. This discrepancy is likely caused by the different synthesis conditions used in forming the copolymer, or in the different testing methods used (surface versus bulk). Further research is required to enable an in-depth understanding of the effects of treatment temperature on the cross-linking kinetics and surface structure of the PGS-co-LA system.

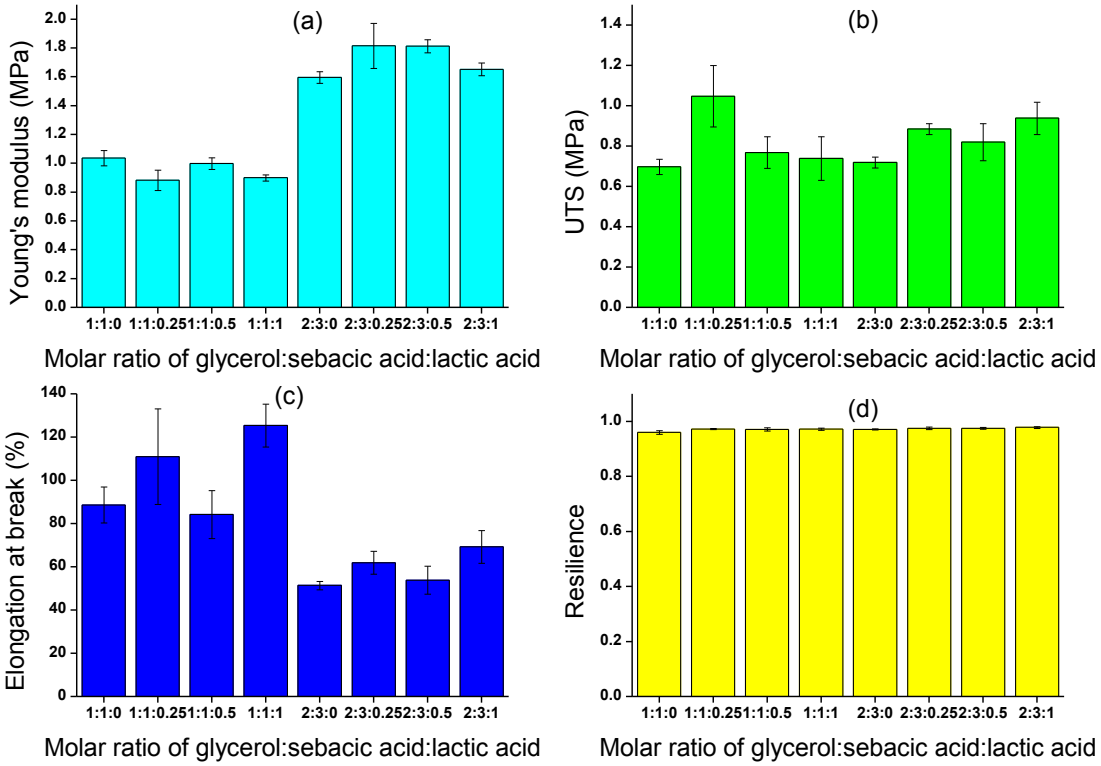

Figure 4.2 The Young's modulus (a), UTS (b), elongation at break point (c) and the resilience (d) of the PGS-co-LA polymer with a 1:1 or 2:3 G:S molar ratio and synthesised in a vacuum at 130°C for three days.

Thus, even if a PGS-co-LA copolymer can form at the interface of the electrospun core and shell fibre, the elastic properties of the core PGS fibres would not be compromised.

A comparison of the PGS-based polymers at a 1:1 and 2:3 molar ratio of G:S shows that the former had approximately two thirds of the Young's moduli (approximately 1 MPa), and almost double the elongation at rupture (80-120 %) compared to the PGS-based materials containing 2:3 G:S molar ratio (1.5 MPa and 50-70 %, respectively). There are three hydroxyl groups in a glycerol monomer and two carboxyl groups in a sebacic acid monomer. The reaction kinetics of the primary –OH groups, which is found at both terminals of the glycerol molecule, are faster than those of the secondary –OH groups found in the middle of the glycerol molecule [111, 139, 140], such that the polymerisation is dominated by the formation of PGS polymer chains. The cross-linking process through reaction of the secondary –OH groups, becomes the dominant kinetic process only when the free primary –OH groups in the reactant system have been consumed. At a 1:1 G:S molar ratio, esterification is dominated by the reaction of the primary hydroxyl groups with sebacic acid,

leaving a large fraction of the secondary –OH groups on the glycerol units unreacted, thus lowering the cross-link density of the PGS network. At a 2:3 G:S molar ratio, which is the theoretical stoichiometric molar ratio required for a complete reaction between the hydroxyl and the carboxyl groups, most of the secondary –OH groups are reacted, resulting in a highly cross-linked network. As a result of the higher crosslink density of the systems with the 2:3 G:S molar ratio, the modulus is higher and the elongation to break lower which in agreement with the theory of rubber elasticity [117].

Figure 4.2d shows high resilience of these polymers and no significant effect of crosslinking on the UTS. Depending on the crosslink density, the UTS can either increase or decrease as the crosslink density rises [141] as a result of competing factors. Thus it appears that for the systems with 1:1 and 2:3 G:S molar ratios, the crosslink densities are close to the maximum in the dependence of UTS on crosslinking.

Based on the desirable elongation to break, the PGS formed by a 1:1 G:S molar ratio was considered to be the best choice for use in this section of the present study.

4.2.4. Optimisation of the core/shell electrospinning conditions

The parameters that affect electrospinning and the resultant PLLA polymer fibres that are spun have been extensively described in the relevant literature [62, 64, 65], and include PLLA solution parameters (such as the molecular weight and the surface tension) and the processing conditions, including the electrical potential, operating temperature and feed flow rates. The most important processing factor affecting the core/shell spinning process in the present study was found to be the ratio of the feed flow rate of the core solution to that of the shell solution. Polymer globules were formed in the fibre mats (**Figure 4.3a**) when the feed flow rate of the PGS core solution (0.1 mL/h) was 20 times lower than that of the shell solution (2.0 mL/h). The globules formed in the present core/shell spun mats, as shown in **Figure 4.3a**, were approximately 10 μm in diameter and these were larger and more spherical than the 1 μm globules which have been observed by other researchers [31] in the electrospinning of fibrous PLLA mats. Li and Xia [31] have suggested that globules or beads are formed on the electrospun fibres as a competition between the entanglement-controlled viscoelastic properties of the polymer solution(s) which tends to form fibres, and with the surface tension effect which tends to form droplets, and with the electrostatic forces which tend to increase the surface area and thus form fibres. These workers [31] also suggested that the formation of beads can be eliminated by increasing the polymer concentration, however

in our work variation of the concentrations of the core and the shell solutions failed to prevent the formation of the globules. Thus polymer concentration may not be the only factor affecting bead formation. When the feed flow rate of the core PGS solution was increased, the formation of the large beads was effectively eliminated, and uniform diameter fibres were produced **(Figure 4.3b, c).** Thus when low feed flow rates of the core are used (e.g. 0.10 mL/h for core and 2 ml/h for shell as in **Figure 4.3a** the core solution may not be able to maintain a continuous flow, therefore causing an accumulation of the core solution around the inner needle tip, which periodically collapses into the shell after the core accumulation had reached a certain level. The morphology in **Figure 4.3b** resulted from slower core versus shell solution feed rates (0.2 ml/h versus 0.80 ml/h), similar to **Figure 4.3c** (0.30 versus 0.90 ml/h). However, when these were increased (0.50 versus 1.0 ml/h), the fibres became fused to each other (**Figure 4.3d**). It appears that at the latter high feed rates (0.50 versus 1.0 ml/h), the amount of shell material being fed into the spinneret was insufficient to fully cover the core, leading to the leakage of the PGS pre-polymer, which resulted in a fusion of the fibres when they were heat-treated for cross-linking.

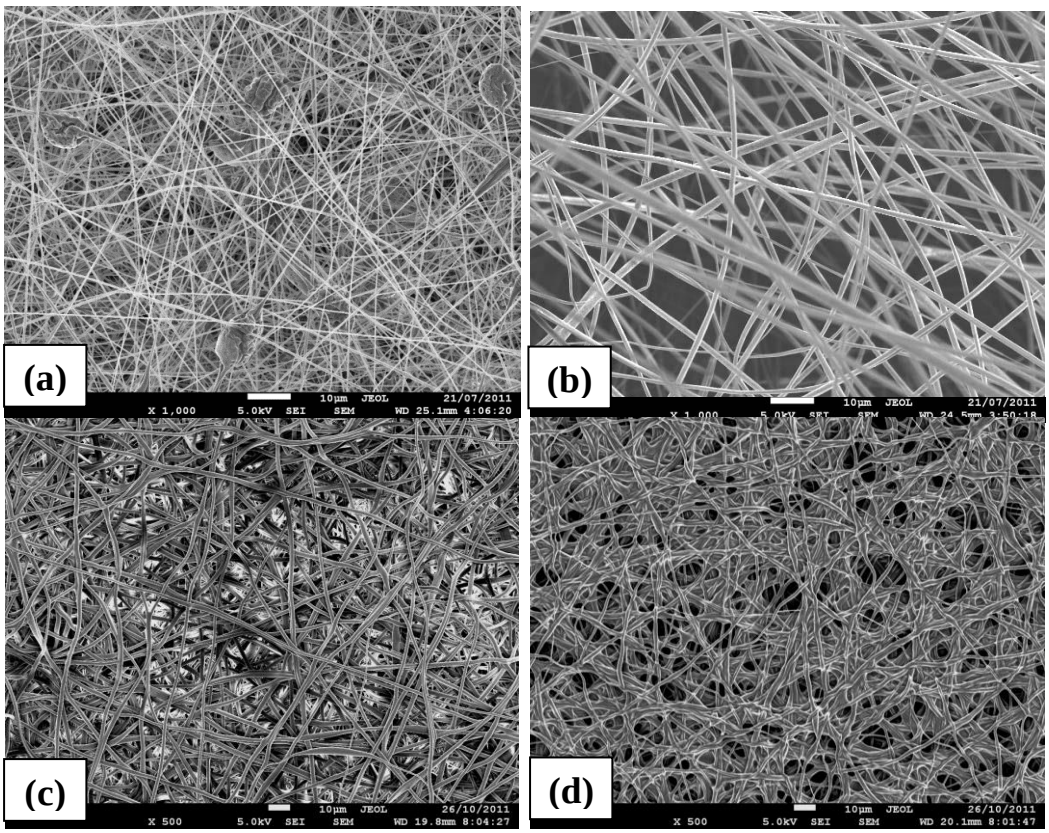

Figure 4.3 SEM images of PGS/PLLA core/shell fibres fabricated at different core to shell feed flow rates: 0.10 ml/h vs. 2 ml/h at 10 kV (a), 0.20 ml/h vs. 0.80 ml/h at 12kV (b), 0.30 ml/h vs. 0.90 ml/h at 12kV (c) and 0.50 ml/h vs. 1.0 ml/h at 13kV (d). The material was

heat treated for crosslinking at 130 °C for 72 h. The optimal conditions are shown in (b) and (c). The ratios of core solution radius and shell solution thickness in spinning (calculated from concentrations and relative flow rates) for (a)-(d) are 0.28, 0.81, 1.00 and 1.37, respectively.

For the examination of the core/shell structure, a fibre mat was sectioned in liquid nitrogen at -120°C, using the cryogenic microtome sectioning technique, and the cross section was examined by SEM. **Figure 4.4** shows an example of the PGS/PLLA core/shell fibrous mats produced at one of the optimal conditions **(**see **Table 4.2)**, while **Figure 4.5** shows that a nano-porous structure was observed in the PLLA shell throughout the fibrous sample, which is in accordance with the results of previous studies [62, 64, 65]. The formation of porosity is probably the result of the evaporation of THF from the spun PGS/THF core solution. An additional benefit of this nanoporous structure is that it softens the rigid PLLA shell and so enhances the elastic match between the core PGS and shell PLLA under mechanical loading.

Table 4.2 Optimal core/shell electrospinning conditions under a voltage potential of 12 kV.

PGS solution (g/100ml THF)	**PLLA solution** (g/100 ml of 4:1 chloroform:DMF solvent)	**Feeding rates of PGS (core):PLLA (shell)**	**Relative flow rate (ml/h)**
100	20	0.30 : 0.90 or 0.20 : 0.80	1:3 or 1:4

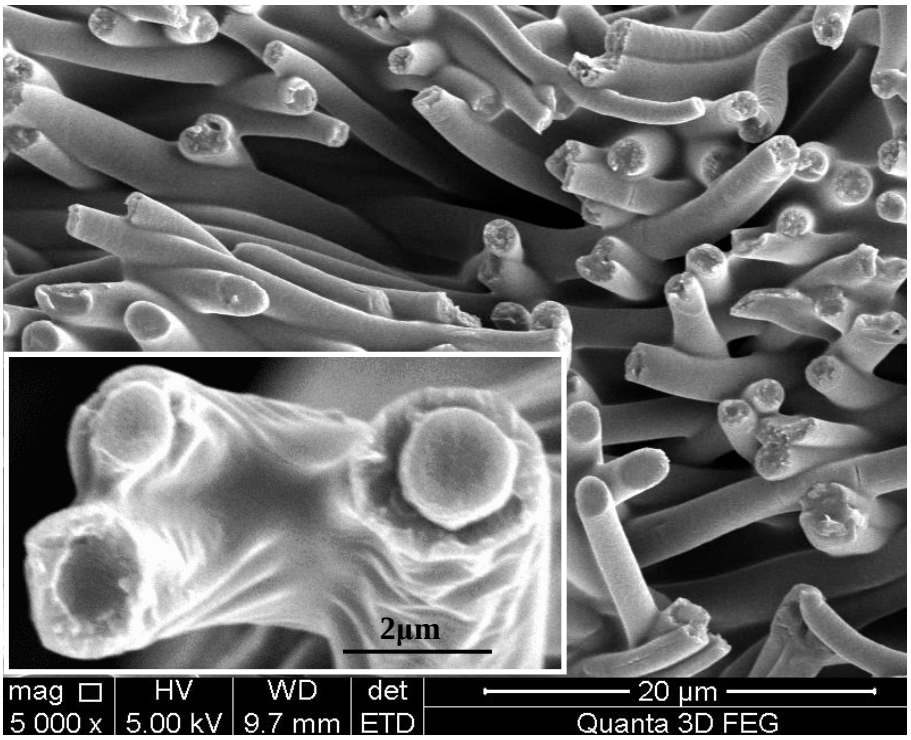

Figure 4.4 Cross-sectional SEM image of a PGS/PLLA core/shell fibrous sheet. The inset shows the core/shell structure at a high magnification. The fibres were spun at a core feed flow rate of 0.20 ml/h and a shell feed flow rate of 0.80 ml/h at 12 kV. The material was crosslinked at 130 °C for 72 h. The specimen was sectioned at -120°C in a cryogenic microtome.

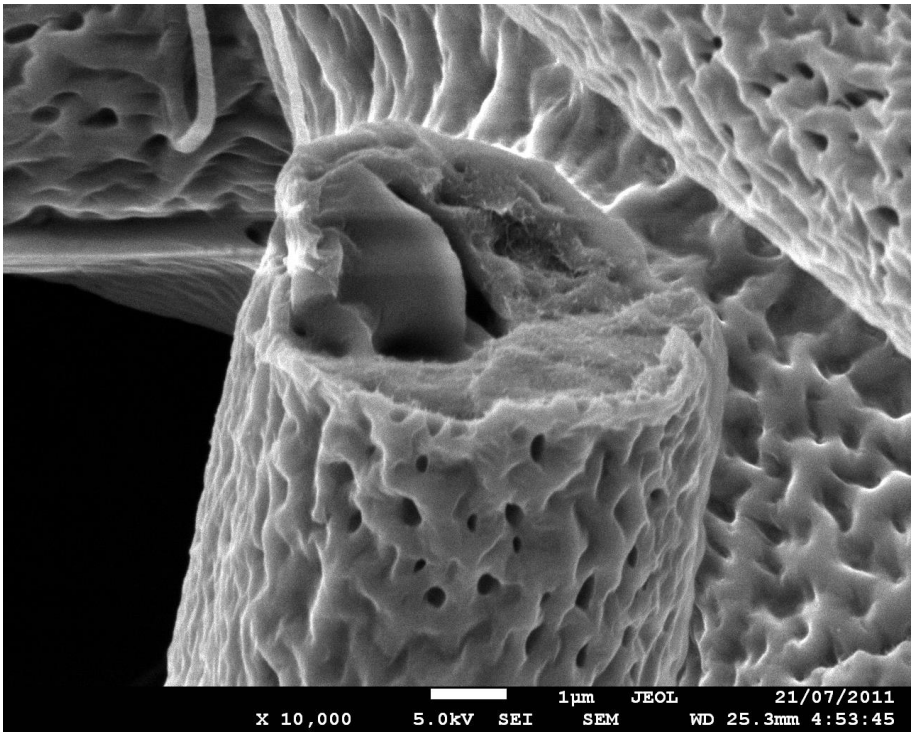

Figure 4.5 SEM image of the porous microstructure within the PLLA shell of a PGS/PLLA core-shell fibre. The fibres were spun at a core feed flow rate of 0.2 ml/h and a

shell feed flow rate of 0.8 ml/h at 12 kV. The material was crosslinked at 130 °C for 72h. The specimen was sectioned at -120°C in a cryogenic microtome.

Table 4.3 shows that the fibre diameter increases as the core feeding rate is raised and the shell feeding rate is reduced. This does not appear to be due to the concentration of polymer in the solvents since these only vary from 25 to 27.5 wt% and so the reason for this variation in fibre diameter is uncertain.

Table 4.3 Mechanical properties of the core/shell mats.

Feeding rates of PGS (core):PLLA (shell) (in ml/h)	Wt% PLLA in the fibres*	Fibre diameter (μm)	Stiffness constant	UTS (MPa)	% Elongation to rupture
0.20:1.00	67	1.3±0.4	6±2	0.8±0.4	15±3
0.20:0.80	62	2.0±0.2	10±3	1.5±0.5	22±2
0.30:0.90	55	2.2±0.2	18±2	1±0.2	25±3

* calculated from the solution concentrations and the feeding rates

In the study by Yi and Lavan [13] of PGS/PLLA core/shell nanofibres, the final PLLA shell was essentially a protective coating, and they claim that it was ultimately removed by solvent washing. However maintenance of the PLLA shell can address the known drawback of overly rapid PGS degradation. Firstly, the more slowly degrading PLLA shell can stabilise the degradation rate of the final product. Therefore, the composite material could be applied to the engineering of many types of soft tissues, which require long recovery periods of several months or years, and variable degradation kinetics. Secondly, the excellent biocompatibility of PLLA may improve the cytocompatibility of the fibrous mats, in comparison with the pure PGS fibres alone. Therefore, the PLLA shell was retained in the final products, and the characterisation and bio-assessment was conducted on the PGS/PLLA core/shell fibrous materials as a composite scaffold.

4.2.5. Mechanical properties of fibrous mat materials

The stress-strain curves of the PGS/PLLA core/shell fibrous sheet materials were J-shaped (**Figure 4.6**), similar to the non-linear profile observed for biological tissue elasticity [107]**.** The volume fractions of the more rigid PLLA and of the softer PGS in the fibres, the porosity of the mats, and the adhesion of the fibres to one another, are expected to have a large effect on the mechanical properties of the mats. **Table 4.3** shows that the PLLA content in the fibres varies from 55 to 67% (see **Table 4.3**) for the mats studied in **Figure 4.6** and **4.7**. The fibrous mats varied in porosity from 73 to 76 % w/v, based on the measurement of weight and

volume (calculated from the dimensions) of the spun mats. In addition, while the extent of fibre adhesion of one to another has not yet been determined, it is expected that this adhesion will significantly affect the stress-strain behaviour of the fibrous materials. However the main variation in behaviour of the mats in **Figs 4.6** and **4.7** appear to be due to the variation in the proportion of the more rigid PLLA shell to the more flexible PGS core. As a result, an increased core feed flow rate and thus a lower content of PLLA results in a more compliant and stretchable mat having a larger elongation to rupture and a lower modulus, as given in **Table 4.3**.

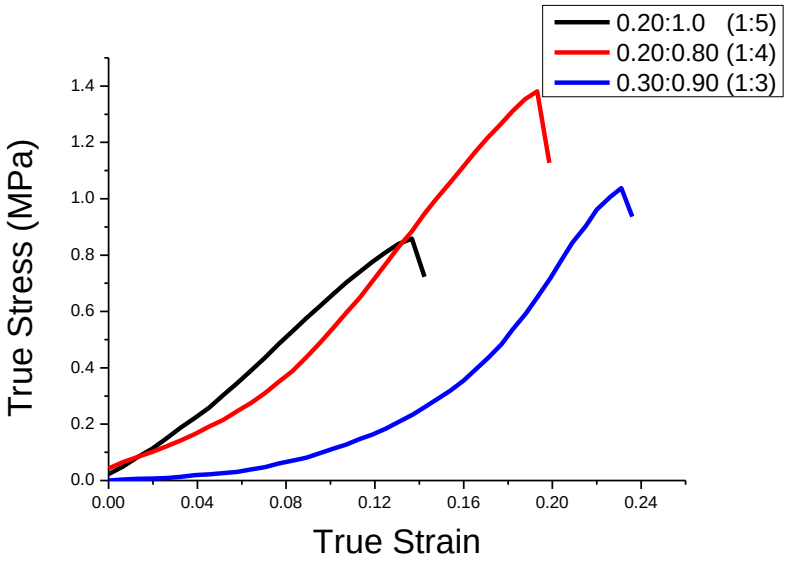

Figure 4.6 Stress-strain curves of the PGS (core)/PLLA (shell) fibre sheets fabricated at three core to shell feed flow conditions: 0.20 ml/h vs. 1.0 ml/h, 0.20 ml/h vs. 0.80 ml/h and 0.30 ml/h vs. 0.90 ml/h, having PLLA contents of 67, 62 and 55 wt% respectively.

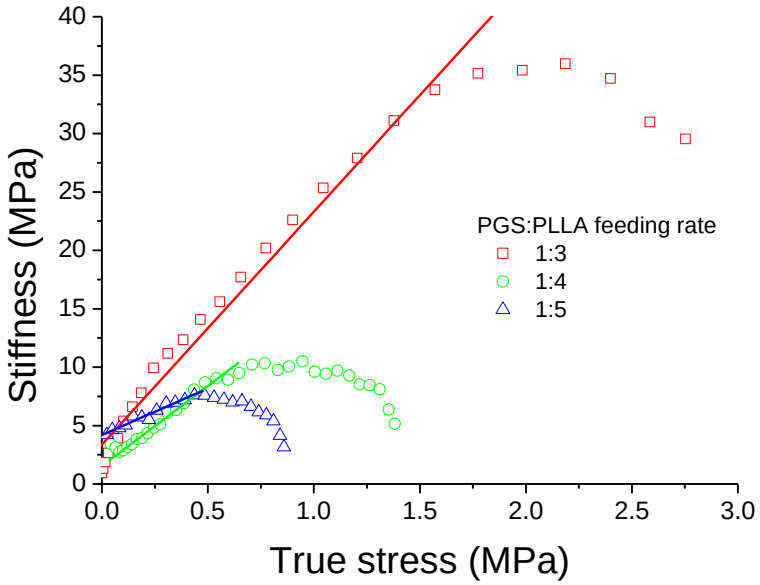

Figure 4.7 Stiffness-stress relationship of the PGS/PLLA fibrous mat material spun at different core/shell feeding rates 1:3 1:4 and 1:5 having PLLA contents of 67, 62 and 55 wt% respectively. The stiffness constant of this stiffness-stress relationship is given in Table 4.3. For the 1:5 specimens, Equation 3.5 (Chapter 3) only fitted the data until a strain of approximately 7±1%, for the 1:4 specimens the fit was reasonable until 11±2%, while for the 1:3 specimens the Equation fitted the data up to 17±3%.

Using the non-linear stress-strain equation proposed by Mirsky, [3, 107, 122] representative linear plots of stiffness (or tangent modulus) versus stress are shown in **Figure 4.7.** The stress-strain data for the system produced with a core feed flow rate of 0.3 ml/h and a shell feed flow rate of 0.9 ml/h were best fitted by Equation 3.5, as indicated by the agreement of the data with the equation. The UTS, elongation to break and stiffness constant of this system is 1.0 ± 0.2 MPa, 25 ± 3 % and 18 ± 2, respectively. The stiffness is comparable to the values 12 to 20 previously exhibited by heart muscular tissues [3, 107, 122] while the UTS and elongation to break are higher than the typical values of 0.02-0.5 MPa and 20% found for heart muscular tissues [9, 12].

The material, produced at a core feed flow rate of 0.3 ml/h and a shell feed flow rate of 0.9 ml/h and containing 55 wt% PLLA, was subjected to cyclic testing over five deformation and recovery cycles. The data demonstrates that although the fibrous mat material exhibited hysteresis and dissipated energy during the cycle, the stress-strain overlapped and were reproducible (**Figure 4.8**). The resilience of these materials was determined to be ~70%, suggesting that they may be similar to elastomeric proteins, which have resilience ranges from 50% for partially hydrated elastin, to 90% for fully hydrated collagen and elastin [54].

The very flat segment at the start of the stress-strain curve is due to very low stress initially borne by the fibrous sheet, which is typical feature of fibrous materials and soft tissue [142]

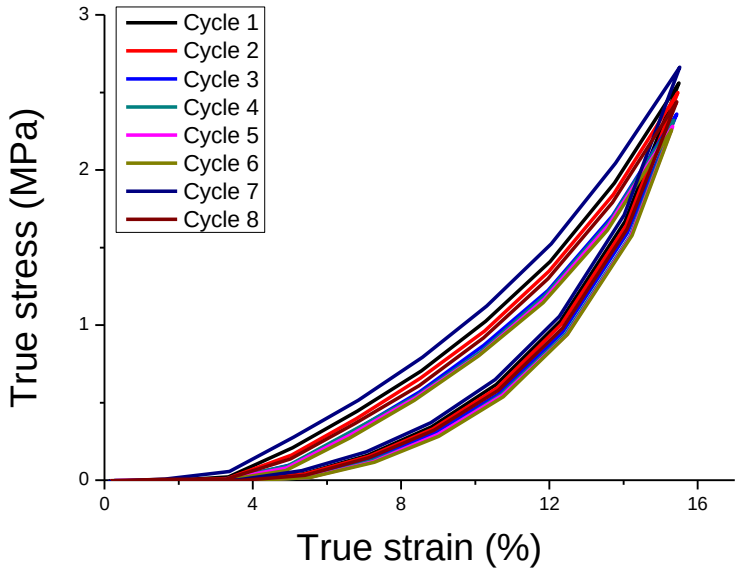

Figure 4.8 A cyclic stress-strain curves of a PGS/PLLA core/shell fibrous mat spun at a core feed flow rate of 0.30 ml/h and a shell feed flow rate of 0.90 ml/h at 12 kV.

4.2.6. *In vitro* evaluation: cellular viability and proliferation

A visual examination of the SNL cell growth did not indicate major cytotoxicity in any of the tested groups, as shown in **Figure 4.9**. SNL cells attached to the bottom well and proliferated in the material-free culture media and media soaked with PGS/PLLA and the PLLA fibrous materials. After 2 days, the number of cells in each well had increased to over 10,000 and almost covered the surfaces, as shown in **Figure 4.9**. Quantitative measurements using the AlamarBlue™ reagent demonstrated that SNL cells proliferated almost linearly with time on the PGS/PLLA fibres soaked in the culture medium, as well as in the two control groups, as shown in **Figure 4.10**. Quantitative LDH measurements, shown in **Figure 4.11**, demonstrated that the cytocompatibility of the PGS/PLA fibrous materials was of the same standard as the two control groups, with no significant differences in cell death between cultures containing the PGS/PLA fibrous mats and material-free control cultures.

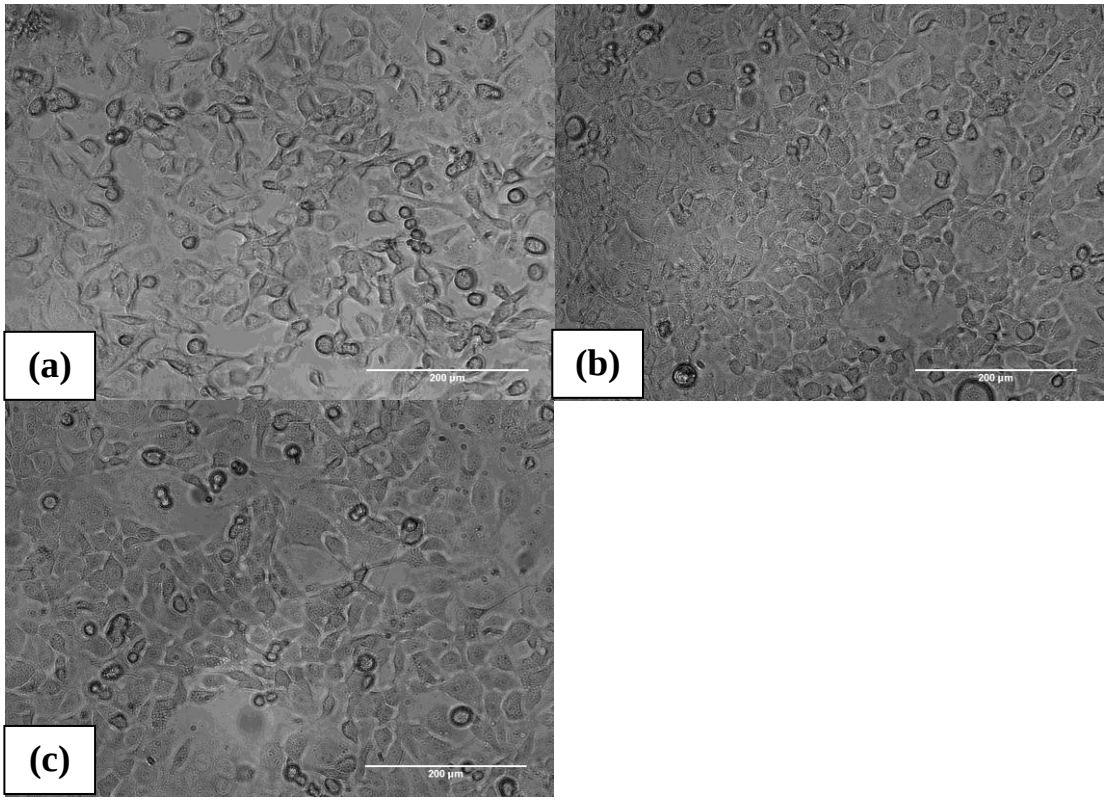

Figure 4.9 SNL cells cultured for 2 days in a material-free culture medium (negative control) (a), PGS/PLLA fibre mat soaked with culture medium, produced from spinning at a core feed flow rate of 0.30 ml/h and a shell feed flow rate of 0.90 ml/h at 12 kV followed by PGS crosslinking at 130 °C for 72 h (b), and PLLA fibre mat soaked with culture medium and used as a positive control (c).

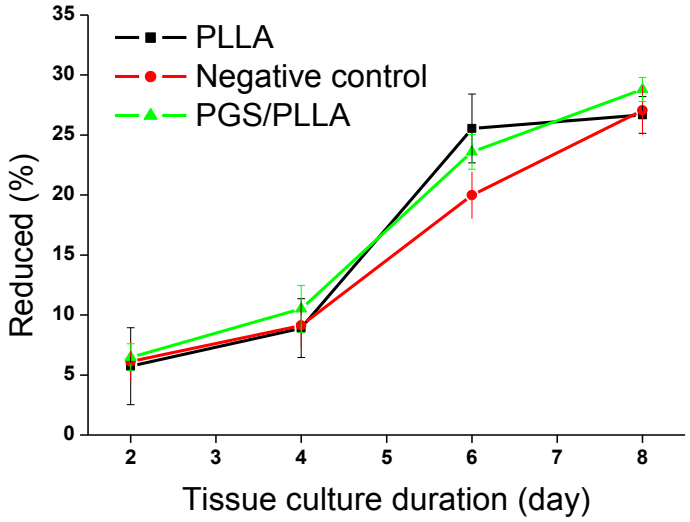

Figure 4.10 SNL cell proliferation kinetics measured by the AlamarBlue™ technique (detecting the chemical reduction of AlamarBlue). The initial plating density was 2000 cells per well in a 48-well plate (n = 5). Overall, there were no significant differences between any two of the three groups that were analysed ($p > 0.05$). The PGS/PLLA fibre mat was spun at a core feed flow rate of 0.30 ml/h and a shell feed flow rate of 0.90 ml/h at 12 kV followed by PGS crosslinking at 130 °C for 72 h.

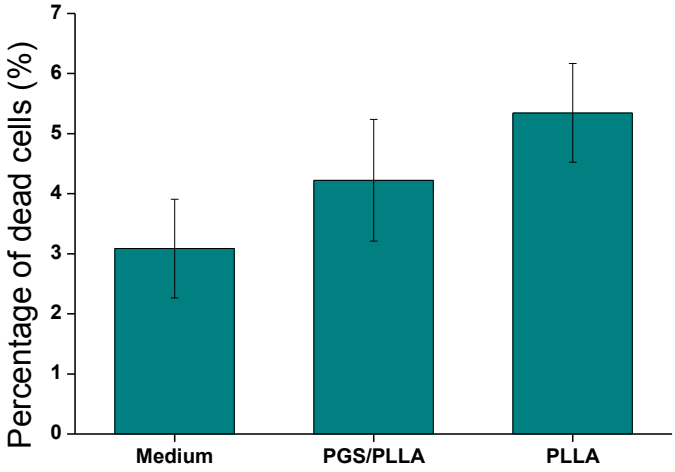

Figure 4.11 Cytotoxicity of PGS/PLLA core/shell spun materials, detected by measuring the release of lactate dehydrogenase (LDH) from the cells after 4 days of cultivation (n = 5). No significant differences existed between any two of the three groups ($p > 0.05$). The PGS/PLLA fibre mat was spun at a core feed flow rate of 0.30 ml/h and a shell feed flow rate of 0.90 ml/h at 12 kV followed by PGS crosslinking at 130 °C for 72 h.

4.2.7. Viability and function of hESC-derived cardiomyocytes

Studies on the viability and function of hESC-derived cardiomyocytes was undertaken in collaboration with D.F. Newgreen from the Murdoch Children's Research Institute, The Royal Children's Hospital. To assess the viability of beating ESC-CMs, beating clusters were directly plated in the medium that had been soaked with PGS/PLLA mat specimens. Visual examination showed beating hESC-CM cardiomyocytes remained a healthy phenotype when cultured in the presence of the PGS/PLLA mat (spun at a core feed flow rate of 0.3 ml/h and a shell feed flow rate of 0.9 ml/h, and treated at 130 °C for 72 h). hESC-CMs were maintained as spontaneously beating colonies for over 1 months until interrupted, with beating rates of hESC-CM clusters in the presence of PGS/PLLA comparable to a larger population on tissue culture plastic (**Figure 4.12**). Values of beating rates for hESC-CM in the presence of PGS/PLLA at various time points lie within the range for hESC-CM in material-free medium, indicating that the PGS/PLLA materials are capable of supporting optimal functional activity of hESC-CM.

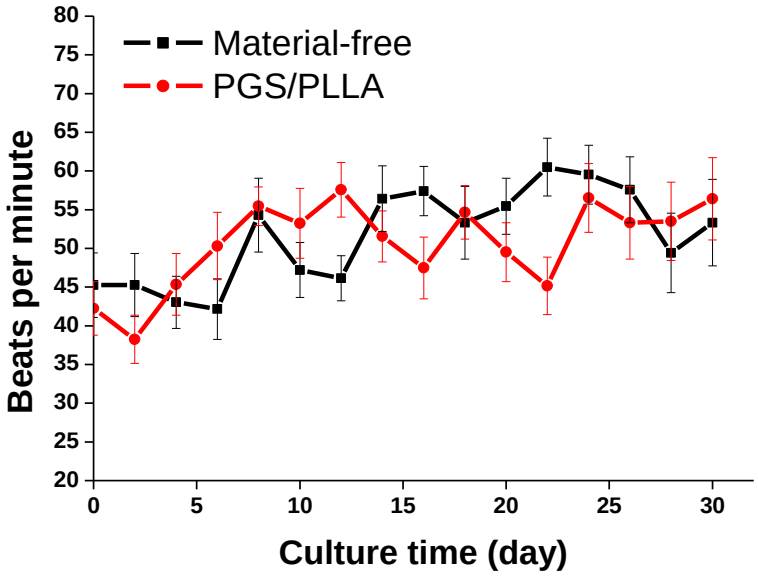

Figure 4.12 Average beating rate of cardiomyocytes in basal media compared with cardiomyocytes cultured in the presence of PGS/PLLA core-shell spun fibrous sheet (n = 5).

4.2.8. ENC cell delivery capabilities *ex vivo*

Studies of the ENC cell delivery capabilities *ex vivo* was undetaken in collaboration with R. Ben from the Department of Anatomy and Neuroscience, University of Melbourne. Under defined media conditions we have shown that the PGS/PLLA fibrous mat is compatible with the growth of mouse ENC cells expressing the ENC lineage marker SOX10 (a marker of ENC glia and progenitor cells) and TUJ1 (which marks neuronal-subtypes) (**Figure 4.13a**). Attachment of the ENC cells to the mat occurred overnight and the maintenance of these ENC cell types did not require preconditioning of the fibrous mat or addition of ECM molecules. After one week of *in vitro* culture, ENC progenitor cells could be identified on the fibrous mat by concomitant uptake of EDU and SOX10 expression (**Figure 4.13b**). An interesting observation was that mouse single-cell seeded ENC cells grown on the PGS/PLLA fibrous mat formed discrete cell clusters resembling ganglia (the functional unit of the ENS) (**Figure 4.13a**). It is likely that the mat is compatible with the self-organising potential of ENS ganglion cells [143].

We then tested the ability of the PGS/PLA fibrous mat to deliver ENC progenitor cells into a recipient avian embryonic gut - during a defined period the recipient gut contains no endogenous ENS and is therefore considered an aganglionic *ex vivo* model that recapitulates the key features of Hirschsprung disease. In this case when the membrane is applied to the

serosal surface of the recipient gut (**Figure 4.13c**), the mouse ENC cells depart from the fibrous mat and re-locate to the interior of colonic wall; a layer where the ENS would be expected to reside (**Figure 4.13d**). Once inside the gut environment the ENC cells formed a chain-like network which is the characteristic behaviour of *de novo* innervation of aganglionic gut by ENC progenitor cells [144]. A chain-like network was never observed in ENC cells cultured alone on the fibrous mat. To our knowledge this is the first demonstration of ENC cell delivery via the serosal surface of the gut wall by direct application of a nontoxic mat. However, under the conditions used here, the embryonic ENS-deficient hindgut would be unlikely to undergo any significant peristaltic contractile forces. Therefore, an *in vivo* test was designed to test the ability of the fibrous mat to remain in contact and deliver ENC cells to a post-natal peristaltic intestine.

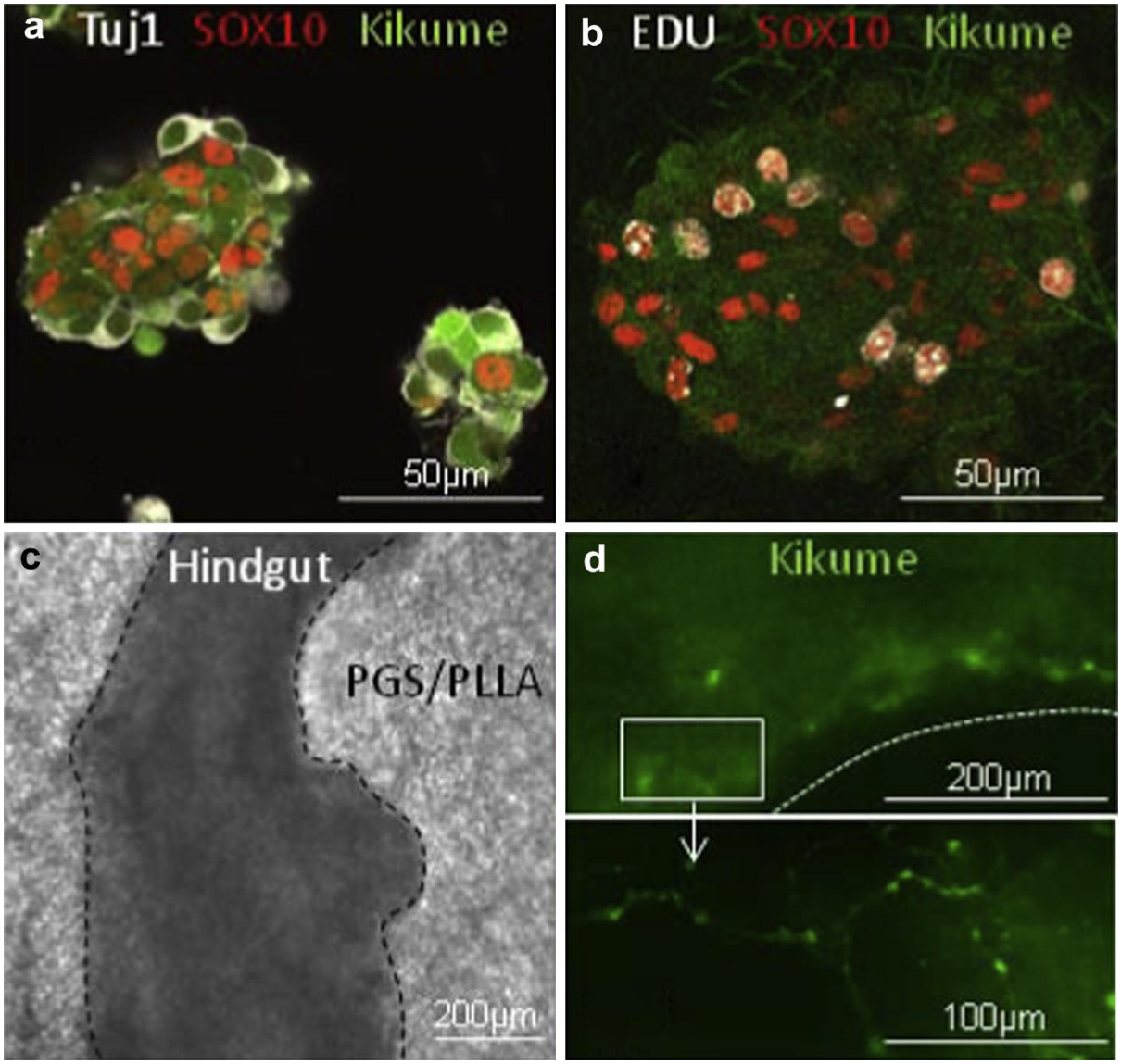

Figure 4.13 An *ex vivo* cell transplant trial using the PGS/PLLA fibrous mat. (a) EDNRB-Kikume mouse ENC cells cultured on PGS/PLLA fibrous mat maintain expression of ENC-lineage antigens SOX10 (glial and progenitor cell marker) and TUJ1 (neuron and neurite marker). (b) On the mat EDNRB-Kikume mouse ENC are able to proliferate as assessed by EDU uptake exclusively in Sox10 expressing cells. (c) Assembly of the ex-vivo trial: ENS-deficient quail hindgut (outlined by the black dotted line) is attached to (i.e. on the top of) the PGS/PLLA fibre mat (the background of the image) seeded with EDNRB-Kikume mouse ENC cells (light grey background). (d) Following removal of the hindgut after 3 days of *ex vivo* growth, the mouse ENC cells have migrated through the serosa (dotted line) and have formed a *de novo* chain-like network in the interior of the embryonic colonic wall (as shown in the enlarged image).

4.3. Conclusions

Non-linearly elastic biomaterials were successfully fabricated from a chemically cross-linked PGS elastomer and a thermoplastic PLLA, using the core/shell electrospinning technique. The optimal fabrication conditions were established for electrospinning, including a critical parameter for spinning, which is the ratio of the feed flow rate of the core solution to the shell solution which ranges from 1:3 to 1:4 (**Table 2**). Under optimal conditions, the electrospun PGS/PLLA core/shell fibrous materials demonstrated muscle-like mechanical properties with J-shaped, elastic stress-strain curves, and the UTS, rupture elongation and stiffness constant of the PGS/PLLA fibrous mats were 1 ± 0.2 MPa, 25 ± 3 % and 18 ± 2, respectively; these findings are as good as those observed in studies of heart muscular tissues. *In vitro* evaluations demonstrated that the PGS/PLLA core/shell fibres are excellent biocompatible materials. Finally, the large number of variables in the core/shell electrospinning process provides a wide range of possible mechanical properties and degradation kinetics, which could broadly be applied to the engineering of many soft tissues, such as tendon, intestines, cardiac muscle and lung epithelium. Further research will focus on the expansion of the mechanical and degradation profiles of this material system, as well as *in vivo* clinical applications.

Chapter 5

Enzymatic degradation of $PGS_{1:1}$/PLLA core/shell fibre mats and comparison with PGS sheets

5.1 Introduction

PGS is a biodegradable crosslinked soft elastomer and is increasingly used in a variety of biomedical applications such as nerve and myocardium tissue engineering [7, 9, 145]. PGS is synthesised by step growth polymerisation of glycerol with sebacic acid [7], and the ester bonds formed during polycondensation can be enzymatically hydrolysed. PGS has minimal toxicity to the host body because its degradation products, glycerol and sebacic acid, are both endogenous molecules found in human metabolites [10, 129]. The PGS used for biomaterials studies is generally composed of a 1:1 or 2:3 molar ratio of glycerol with sebacic acid. In the discussion below, all of the PGS materials were synthesized from a 1:1 molar ratio of glycerol with sebacic acid. The degradation rates of PGS are generally faster than other polyesters, such as polylactide and polyglycolide, so that the rapid degradation kinetics of PGS has become one of the major draw-backs in the application of tissue engineering [12, 129]. Wang and co-workers [7] examined the degradation characteristics of PGS (pre-polymerized at 120 °C for 24 h and then crosslinked at 120 °C for 48 h) *in vitro* and after 60 days in phosphate buffer solution (PBS) at 37 °C with agitation and found that the weight loss was 17±6%. Similar *in vitro* degradation kinetics were also reported by Liang et al. [131], where the weight loss of PGS (pre-polymerized at 125°C for 24 h and then crosslinked at 125 °C for 48 h) was around 10-25% after 60 days in a tissue culture medium DMEM. Li et al. [130] reported an 8% weight loss of PGS (pre-polymerized at 130° for 24 h and crosslinked at 130°C for 48 h) after incubation at 37°C for 5 weeks in standard culture medium. However, the *in vivo* degradation kinetics of PGS (pre-polymerized at 120°C for 24 h and then crosslinked at 120°C for 48 h) was much faster than the *in vitro* degradation rates [7, 10]. According to Wang et al. [7, 10], PGS implants lost over 70 wt% of their mass in the test period of 35 days implantation in rats, and they were completely resorbed after 60 days. Similarly, Stuckey et al. [11] found that the PGS (pre-polymerized at 120°C for 24 h and then crosslinked at 120°C for 48 h) was completely resorbed in 6 weeks when used as a pericardial heart patch. An explanation for the fast *in vivo* degradation of PGS is the

enhanced hydrolysis of PGS via enzymatic action. [12]. Chen *et al.* [129, 131] have researched and established the amount of enzyme usage of an *in vitro* enzymatic degradation protocol that is required to simulate and quantitatively capture the features of *in vivo* degradation of PGS. Hog liver esterase is often used to catalyse the *in vitro* hydrolysis of carboxyl esters, because *in vivo*, esterase has been reported to be the primary enzyme responsible for the degradation of polymeric implants [146-148]. The degradation by hog liver esterase of flat 1mm thick PGS sheets (pre-polymerized at 125°C for 24 h and then crosslinked at 125 °C for 48 h) has been reported to occur at approximately 0.6-0.9 mm of thickness per month[131], which falls within the range of *in vivo* degradation rates (0.2-1.5 mm/month) of PGS crosslinked using similar conditions [10].

The observed rapid degradation of PGS (in several weeks) is believed to limit their application as a scaffold material in engineering tissues that have healing rates of several months or years (e.g., cardiac muscle) [12]. Ideally the degradation kinetics of materials used in tissue engineering should match to the healing rates of injured tissue so that they can promote the regeneration of injured tissue [149-151] before their degradation. Poly (L-lactic acid) (PLLA) degrades significantly more slowly than PGS, and was reported to completely resorb after 2 to 5.6 years *in vivo* [40, 152]. In previous research outlined in Chapter 4, a spun fibrous material containing a PGS core and PLLA shell was successfully fabricated and exhibited excellent mechanical properties and cytocompatibility. However, the degradation kinetics of these composite fibres, which have a high surface area, is unknown. Hence, the objective of this work is to compare the *in vitro* degradation of newly developed PGS/PLLA core/shell fibre mats with solid sheets of PGS in the presence and absence of hog liver esterase enzyme (0.3 units per mg of biomaterial).

5.2 Results and discussion

5.2.1 Improvement in the protocol for measuring mass loss during *in vitro* degradation

In previous PGS enzymatic degradation research [129, 131], removal of enzymes from the biomaterial surface was achieved by wiping and washing the surface in water. However since PGS/PLLA core shell fibre mats are porous structures, this process could not completely remove the hog liver esterase enzyme attached to the fibre surface, resulting in an unexpected increase in the total weight of the mats, especially at the commencement of

exposure of the mats to culture media containing enzyme. As show in **Figure 5.1** after wiping and washing the mat surface in water, there was still a large amount of enzyme (the round particles attached on the fibre surface) remaining on the surface or in the pores of the PGS/PLLA fibre mat. As a result, at the beginning of the enzyme degradation study, the mass of the fibre mats increased, and after 5 weeks degradation the weight change was still positive. Thus, the decrease in weight after week 2 may have been caused by removal of some of the adsorbed enzyme and/or hydrolysis of PGS/PLLA fibres.

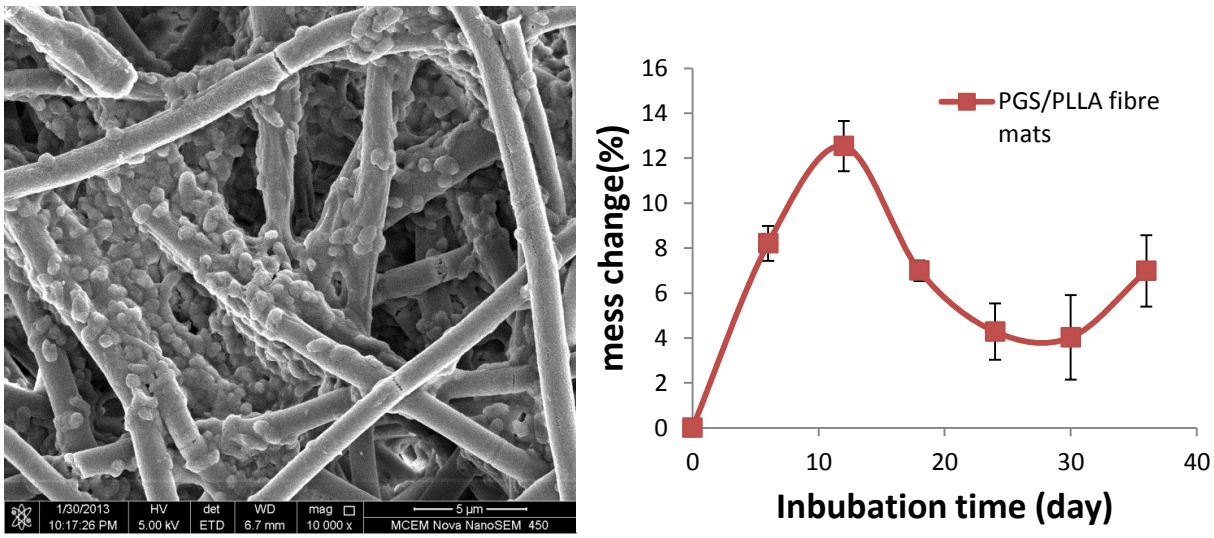

Figure 5.1 SEM of the surface of PGS/PLLA fibre mat cleaned using the methodology of Li et al. [130] and Liang et al. [131] after exposure to hog liver esterase enzyme. The mass change during 35 days of exposure to culture medium is also shown.

A new washing protocol was developed which successfully removed the enzyme adsorbed to the fibre mats during enzyme degradation. The protocol involved removing the fibre mats from the culture medium with enzyme and immersing them in warm water (at 37°C) for 24 hours before drying and weighing. As shown in **Figure 5.2**, this method was able to remove most of the enzyme attached to the fibre surface.

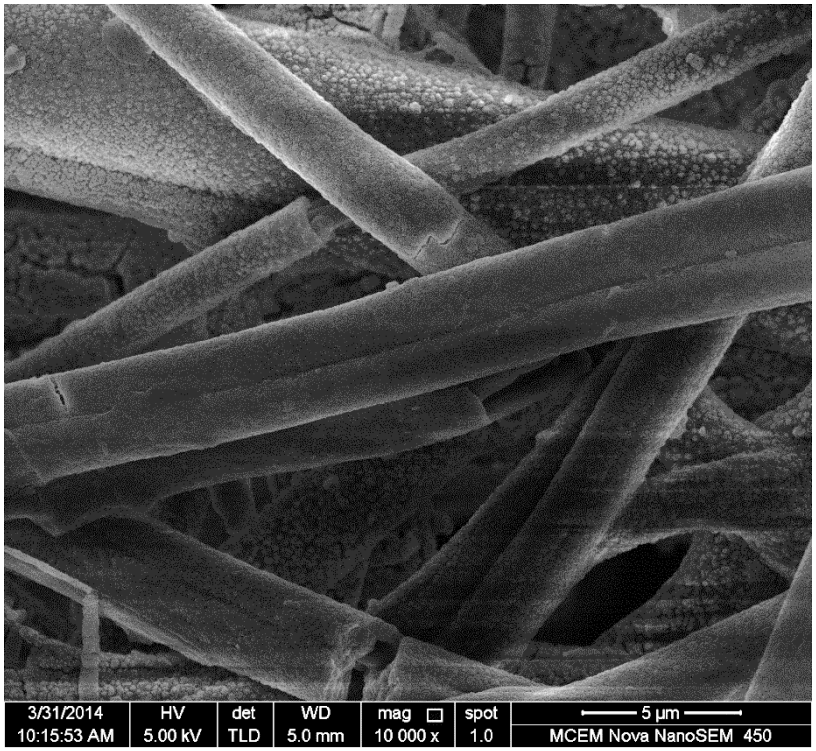

Figure 5.2 PGS/PLLA fibre mat removed from the hog liver esterase enzyme degradation media then washed in floating warm water at 37 °C for 24 hr

5.2.2 Mass loss during *in vitro* degradation

As shown in **Figure 5.3**, the degradation kinetics of the PGS sheet and fibre mats were faster in the culture medium with hog liver esterase enzyme than in the culture medium alone. The mass loss of PGS was 7.7±2.0% after exposure for 35 days to the culture medium, and this was increased to 61.7±8.3% when exposed to the culture medium with enzyme **(Figure 5.3 (b)**. However the effects of the enzyme on the degradation rates of PGS/PLLA fibre mats was quite small, with the mass loss only increasing from 3.9±0.7% to 4.7±1.1% after exposure to culture medium containing the enzyme for 35 days.

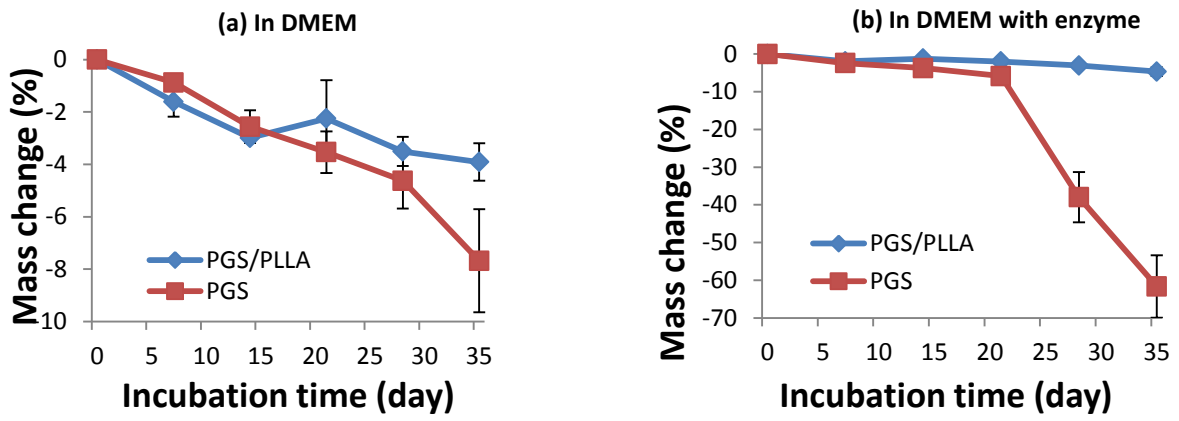

Figure 5.3 Percentage mass of PGS sheet and PGS/PLLA core/shell fibre mats after incubation at 37°C in (a) tissue culture medium DMEM and (b) tissue culture medium DMEM with the addition of hog liver esterase enzyme (0.3 units enzyme per mg biomaterial) for up to 35 days. The PGS sheet and in the mats was pre-polymerised at 130°C for 24 h and cross-linked at 130°C for 3 days.

Enzymatic degradation of biomaterials is limited to the surface, both *in vitro* and *in vivo* [153-155], because large sized enzymes, such as esterase, are primarily immobilised on the surface and cannot diffuse into the bulk [156]. As a result, the overall degradation of PGS is localised to the surface. As shown in **Figure 5.4 (a & b)**, the surfaces of the PGS sheets after 35 days of degradation in culture medium, with or without enzyme, all have micro cracks, but the number of cracks on the PGS in the presence of enzyme are much more frequent. Also the surface of PGS incubated in the medium with enzyme was rougher than the PGS cultured in medium only. The large number of cracks and increased roughness could dramatically increase the contact area between PGS and enzyme culture medium and this might be the reason for the increased mass loss of PGS in the last 3 weeks of exposure to culture medium with enzyme (see **Figure 5.3 b)**.

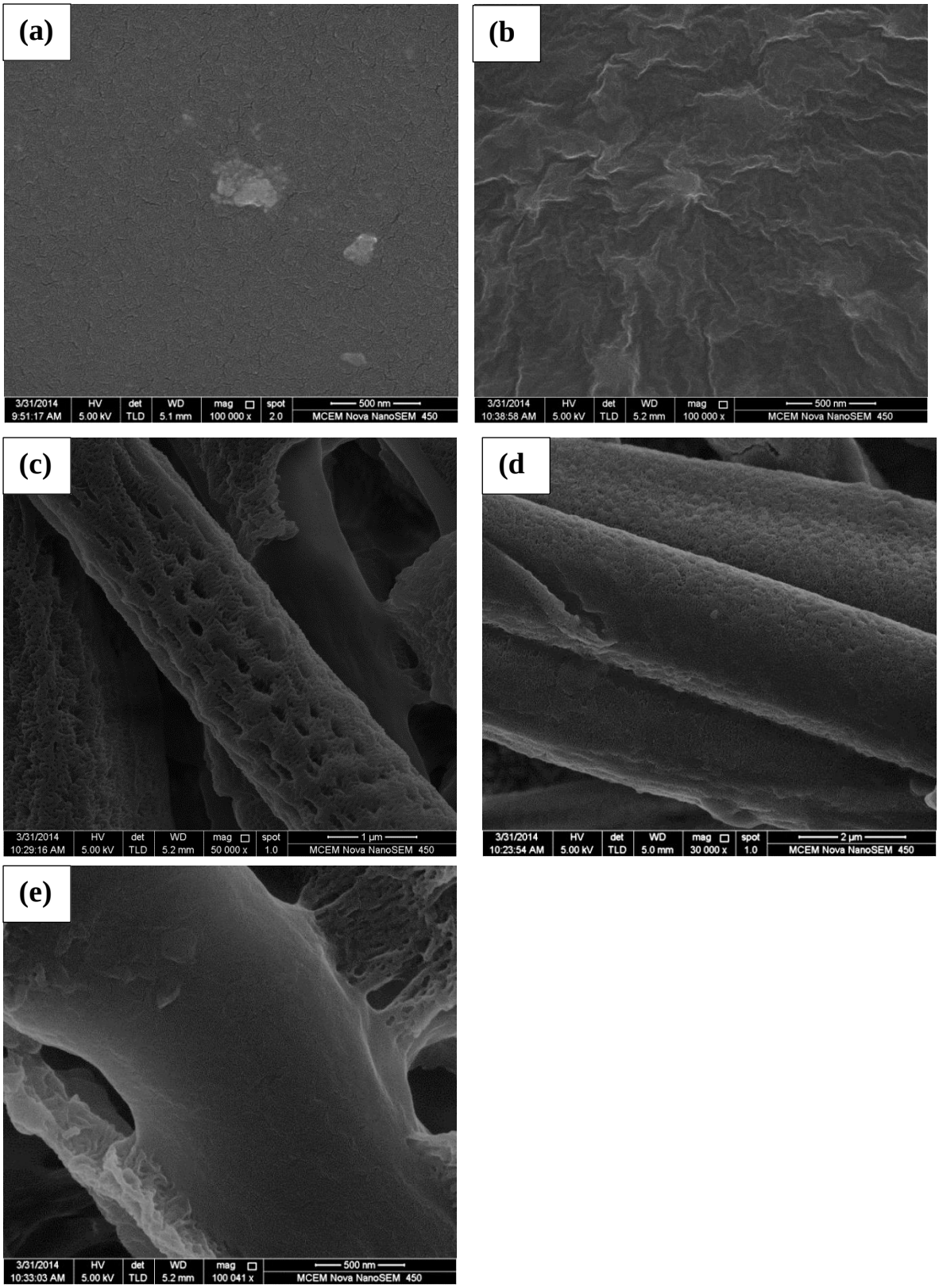

Figure 5.4 SEM of (a) PGS sheet after incubation for 35 days in standard tissue culture media, (b) PGS sheet after incubation for 35 days in media with esterase, (c) PGS/PLLA fibre mat after incubation for 35 days in culture medium (d) PGS/PLLA fibre mat after incubation for 35 days in culture medium with esterase (e) accidentally exposed PGS core from PGS/PLLA fibre mat after incubation for 35 days in standard tissue culture media.

However there were no cracks on the surface of the PLLA shells (**Figure 5.4 c and d)** which indicated the PLLA could effectively protect the PGS core from degradation, and is consistent with the small mass loss up to 20 days (**Figure 5.3 b**). **Figure 5.4 (e)** shows the surface of an exposed PGS core on the fibre mats after some regions of the PLLA shell were mechanically damaged during the cleaning or physically damaged during incubation and washing. This surface exhibited microcracks as found with the PGS incubated in medium with and without enzyme.

5.2.3 Reduction in sheet and fibre mat thickness during *in vitro* degradation

A reduction in PGS sheet thickness was observed both in culture medium alone and in culture medium with hog liver esterase enzyme, and followed a similar trend to the mass loss (**Figure 5.5 a and b)**. The reduction of PGS sheet thickness is about 8.5% and 37% per month (0.02 mm and 0.1 mm for a 0.3 mm thick sheet) in tissue culture medium and culture medium with enzyme, respectively, which is in qualitative agreement with the 7.7% and 62% mass loss of PGS in culture medium and culture medium with enzyme, respectively These results are also consistent with previous research [130, 131] which reported a mass loss of 10% and 60% of PGS after 35 days *in vitro* degradation test with culture medium and culture medium with hog liver esterase enzyme. Enzyme-assisted degradation of PGS sheet is believed to be predominantly through surface erosion and degradation layer-by-layer [21]. The correlation between percent thickness reduction and the percent mass loss shown in **Figure 5.5** for PGS is consistent with this conclusion because a bulk degradation process would not be expected to change the sheet thickness significantly in the early stages.

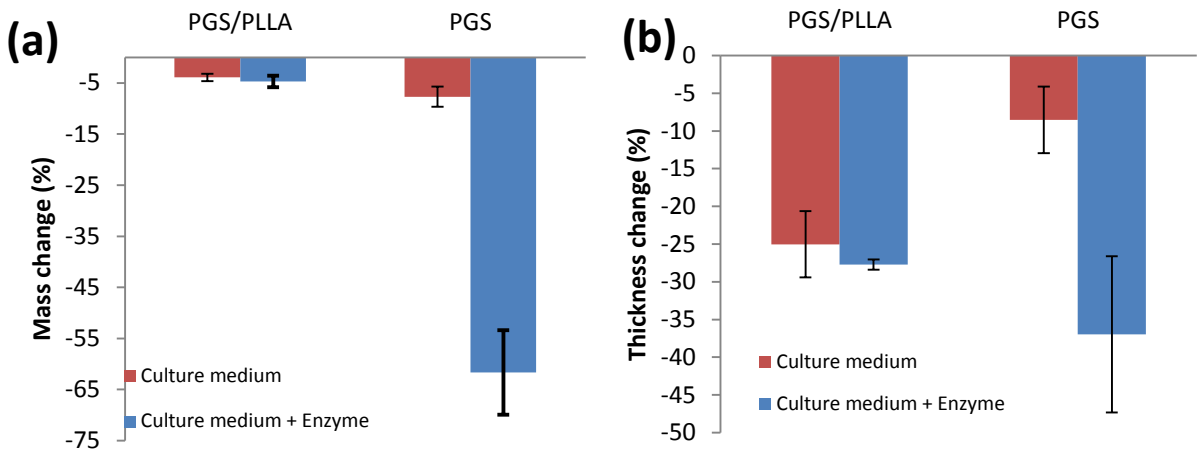

Figure 5.5 Mass change (a) and thickness change (b) of PGS/PLLA fibre mats and PGS sheets after 35 days immersion in culture media or in culture media with enzyme.

Since the enzyme-assisted degradation of PGS is believed to occur through surface erosion [130], the degradation of the bulk material, in terms of mass loss, should be influenced by the surface area. The micro-cracks and surface roughness observed on the PGS sheet may increase the surface area of PGS polymer, leading to very fast degradation rates observed for PGS sheet incubated in the culture medium with enzyme. However the surface area of PGS/PLLA fibre mats is significantly greater than for the solid sheet of PGS. Despite this increase in surface area, the observed slow degradation rate of PGS/PLLA fibre mats, regardless of the culture medium or enzyme, demonstrates that the PLLA shell reduces the degradation rate of the PGS core.

The thickness reduction of the PGS/PLLA fibre mats did not significantly depend on the culture medium and this did not correlate with the mass loss data (see **Figure 5.3**). The reduction in thickness was 25% (0.05mm) after incubated in culture medium and 28% (0.06mm) in culture medium with enzyme for 0.21mm thick fibre mats. Hence the change in thickness was not caused by mass loss. A likely reason for the reduction in thickness of the mats is a re-arrangement and compaction of the non-woven PGS/PLLA core shell fibres during the incubation and washing process.

5.2.4 Change in pH during exposure of materials to culture medium

The pH of the culture medium has a significant influence on both the enzyme's activity and the hydrolytic degradation rate of the polymer [130], and so the pH of the medium was monitored during the degradation studies. The changes in pH of PGS sheets and PGS/PLLA

fibre mats during the 35 days incubation in medium and medium with enzyme are shown in **Figure 5.6**.

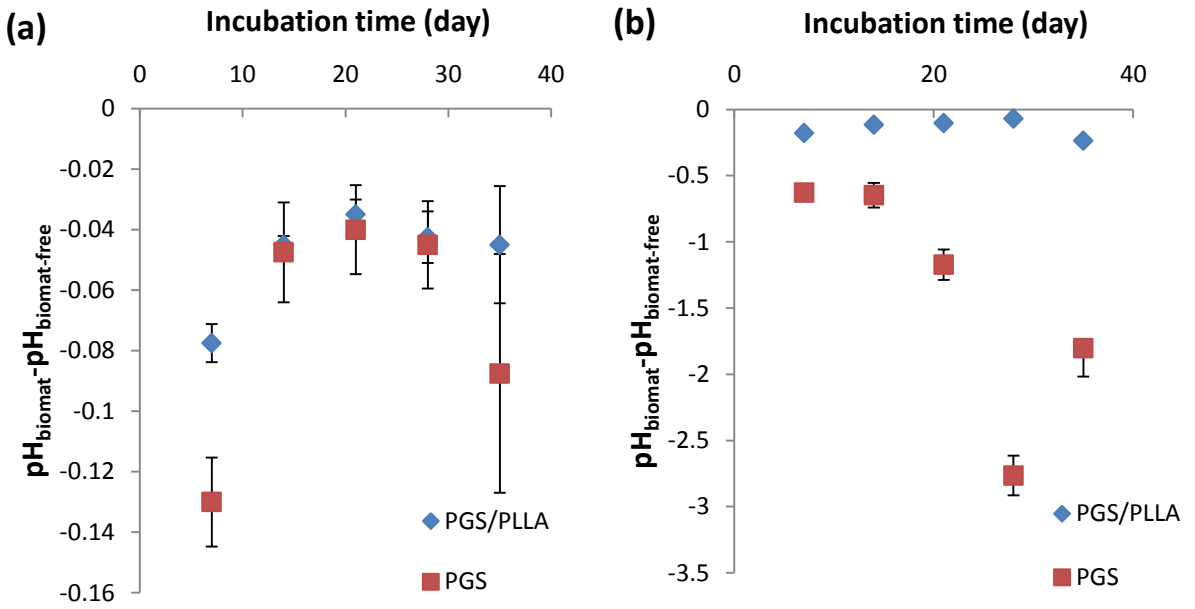

Figure 5.6 pH_{biomat} - $pH_{biomat\text{-}free}$ versus incubation time at 37°C for up to 35 days. pH_{biomat} represents the pH values of the (a) DMEM medium, (b) DMEM medium with enzyme (0.3 units per mg of biomaterial), whereas $pH_{biomat\text{-}free}$ represents those culture media cultured under the same condition but without materials.

Hydrolysis of PGS and PLLA produces sebacic acid and lactic acid, so the degradation of PGS and PLLA will cause acidification in the surrounding culture medium. According to the mass loss data, the PGS cultured in medium with enzyme degraded faster than the samples cultured in medium without enzyme, so the pH drop of PGS sheet cultured in the medium were smaller than that cultured with enzyme. Since the PGS/PLLA fibre mats degraded much slower than PGS sheet in culture medium, with or without enzyme, the pH drop of PGS/PLLA fibre mats was always smaller than for PGS cultured under the same conditions. These observations of the pH values are in agreement with the results of the degradation rates, illustrating the importance of the catalysing effect of the enzyme and indicating that the PGS/PLLA fibre mats have good degradation resistance.

5.3 Conclusions

In this work, the degradation rate of PGS/PLLA fibre mats was found to be much slower than PGS sheets when cultured in medium or in medium with esterase enzyme. The presence of

the enzyme in the medium increased the mass loss of PGS sheets from 7.7% to 61.7% which is similar to the rates of degradation *in vivo* [10] but the enzyme had very limited effects on PGS/PLLA fibre mats, only increasing the mass loss of PGS/PLLA from 3.9% to 4.7%. This indicated the PGS/PLLA fibre mats should have very good *in vivo* degradation resistance and may therefore find potential *in vivo* applications such as for cardiac tissue engineering.

Chapter 6

Aligned core/shell electrospinning of PGS/PLLA with tuneable structural and mechanical properties

6.1 Introduction

Soft tissues exhibit non-linear elastic stress-strain behaviour which is quite different from that observed with the currently widely used thermoplastic polymers and their copolymers [107]. This mechanical dissimilarity between synthetic biomaterials and natural tissue is believed to be the major cause of failure in experimental animal studies and preclinical trials [6]. In the previous study, PGS/PLLA core/shell fibre mats were successfully fabricated which could not only mimic the non-linear elastic properties but also have ultimate tensile strength, rupture elongation and stiffness constants comparable to those of muscle tissue.

The stress-strain curves of synthetic elastomers are comparatively linear (the stress rises at same rate as the strain is raised until elongations over 100% are reached) while biological tissues exhibit non-linear J-shaped (the stress rises at an increasing rate as the strain is raised) at up to 15% strain [9]. The reason for this behaviour is that the molecular chains in synthetic polymers are randomly tangled, but the biological tissues are made of proteins which contain aligned nanofibres [12]. An aligned structure [4] can be produced by electrospinning of synthetic polymers and it has been proved that the aligned fibre scaffolds can mimic natural extracellular matrix better than non-aligned polymers [2]. Electrospun fibres can also enhance cellular alignment and guide the growth of cells, so that the fabrication and mechanical properties of aligned fibre scaffolds have drawn more and more attention recently [1, 2, 100, 103, 157, 158]. In previous studies it has been accepted that alignment can increase the strength of fibre scaffolds [99-101], but the effects of alignment of these non-linear elastic fibre mats, especially the effects on resilience and the stiffness constant, remain an open question.

There are two commonly used methods in electrospinning to fabricate aligned fibre scaffolds. The first method is to use parallel electrodes as collectors and in Kharaziha's work [100], the electrodes were fabricated using aluminium foil. In this way, the electrodes created an electric field so that when highly charged electrospun jets where directed at this electric field,

the spun jets deposited perpendicular to the electrodes and so made aligned fibre scaffolds. However one drawback of this method is that only a certain degree of alignment could be achieved. If, the electric field strength was increased beyond the optimum to produce more aligned fibre scaffolds, the increased instability of the spinning jets caused by the increasing voltage had an effect to decrease the alignment [97]. The second method of fabricating aligned electrospun fibres is to use a rotating mandrel as the collector so that the fibres can be laid in the direction of rotation [1]. This is the method adopted in the present work and fibre mats with different alignments were fabricated by increasing the rotation speed of the mandrel.

In Chapter 4, the electrospinning conditions for PGS/PLLA core/shell electrospinning were optimized, producing PGS/PLLA core/shell fibres which had very good biocompatibility and reduced degradation speed. In this section of the thesis, a tuneable rotation mandrel (16 cm in circumference) with rotation speed from 0 to 2000 rpm, corresponding to surface velocities of 0, 80, 160, 240 and 320 m/min, respectively, was used to fabricate PGS/PLLA core/shell fibre mats with different degrees of alignment.

6.2 Results and discussion

6.2.1 Alignment and diameter measurements

6.2.1.1 PLLA fibre alignment and diameter measurements

Figure 6.1 shows the orientation of the PLLA fibres when electrospun using different mandrel rotational speeds. In previous publications the alignment of the fibres was measured in terms of a statistically calculated "angular deviation", in which a smaller angular deviation indicated a more aligned structure [2, 106]. In the present work, we use a simpler parameter which we term the "angle standard deviation" to indicate the variation in their alignment. This was calculated by measuring the angular orientation of a large number of fibres in the SEM images, relative to the rotational direction and then the determining the standard deviation of these fibre orientations. The angle standard deviation deviation thus calculated ranges from approximately 52° for totally random to 0° for completely aligned fibres.

A comparison of the alignment of the PLLA fibre mats collected at different rotational speeds in **Table 6.1** shows that increasing the speed enhanced the alignment of the fibre mats. The angle standard deviation of PLLA fibre mat collected at 0 rpm was 44.4°, which is close to the theoretical value for random orientation of 52°, while the angle standard deviation of fibre

mats collected at 1000 rpm and 2000 rpm reduced to 30.9° and 22.2° respectively. In addition, the rotational speeds also affect the fibre diameters; fibres collected at 0, 1000, and 2000 rpm had diameters of 2.6±0.1 μm, 2.3±0.1 μm, 2.2±0.1 μm, respectively. The reduction in diameter of fibres with increased rotational speed appeared to be due to the stretching force applied to the unattached fibres by sections of the fibres deposited on the rotating mandrel. This finding is consistent with previous publications [159-161]

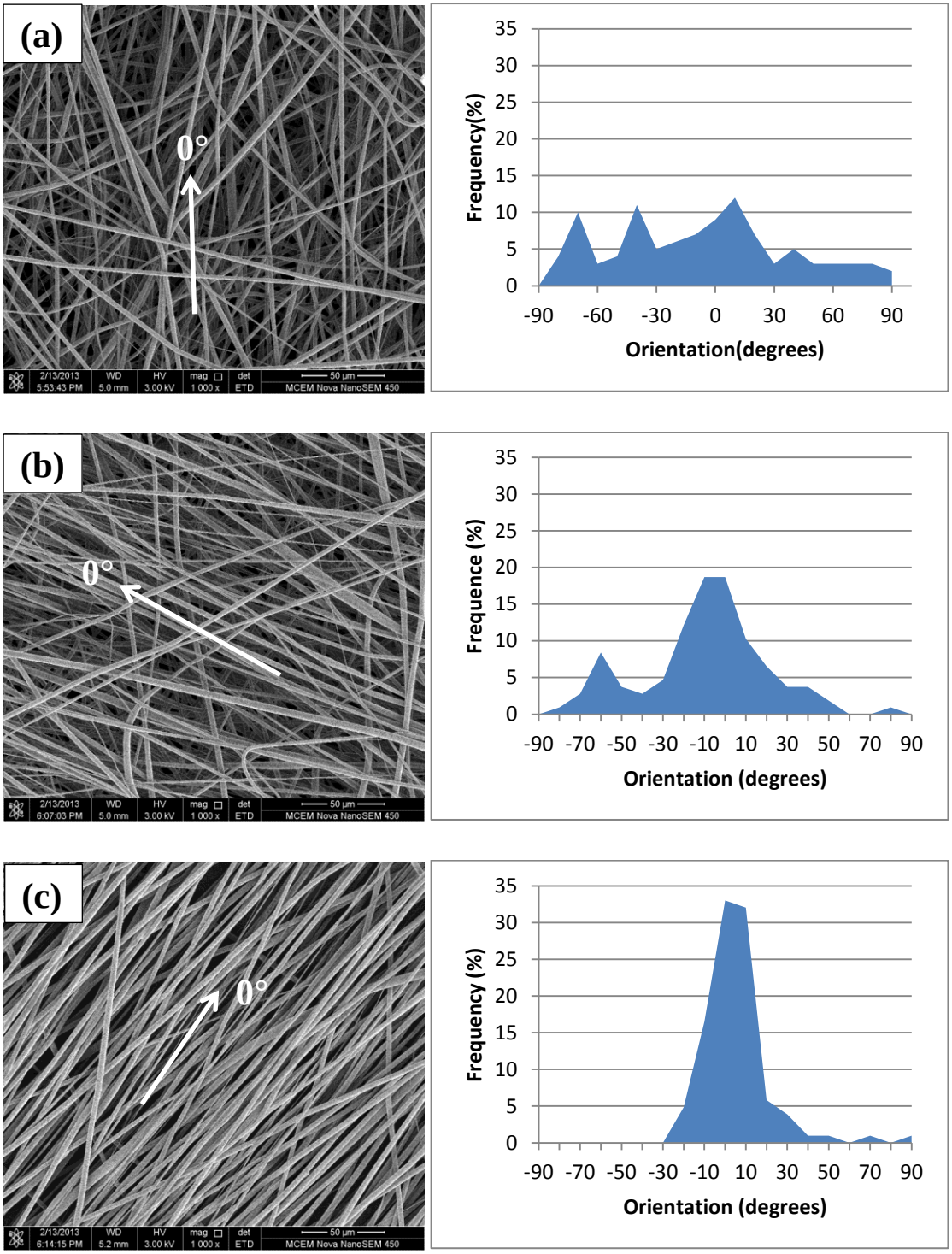

Figure 6.1 SEM and distribution of angular orientation of PLLA fibres collected using a mandrel with 16 cm circumference at different rotation speeds (a) 0 prm, (b) 1000 rpm, and (c) 2000 rpm

Table 6.1 Diameters and angle standard deviation of PLLA and PGS/PLLA fibre mats collected at different speeds

Materials	Collection speeds (rpm)	Diameters (μm)	Angle standard deviation
PLLA	0	2.6±0.1	44.4°
	1000	2.3±0.1	30.9°
	2000	2.2±0.1	22.2°
PGS/PLLA	0	2.5±0.1	49.5°
	1000	2.2±0.1	33.0°
	2000	2.1±0.1	27.0°

6.2.1.2 PGS/PLLA fibre alignment and diameter measurements

Figure 6.2 illustrates the orientation of the PGS/PLLA fibres when electrospun using different mandrel rotational speeds. With increasing rotational speed, the angle standard deviation of the fibre mats decreased from 49.5° to 33.0° and even further to 27.0° (see **Table 6.1**) for rotational speeds of 0, 1000 and 2000 rpm, respectively. These angle standard deviations are larger than those found for the PLLA fibres collected at the same rotational speed, indicating that the PGS/PLLA core-shell electrospinning produced a less aligned fibre structure. The fibre diameters of PGS/PLLA also decreased with increasing rotational speeds, and gave average diameters of 2.5±0.1μm, 2.2±0.1μm and 2.1±0.1μm (see **Table 6.1**) when collected at 0, 1000, 2000 rpm, respectively, due to the stretching forces caused by the rotation of the mandrel surface. Although the overall polymer solution feeding rate of PGS/PLLA core/shell fibre (1.2 ml/h) was more than that for the PLLA fibre (1ml/h), the average diameters of PGS/PLLA fibres were slightly smaller than the diameters of the PLLA fibres (2.6±0.1μm, 2.3±0.1 μm, 2.2±0.1μm at 0, 1000 and 2000 rpm, respectively). One reason for this might be due to the difference in jet stability of the PGS/PLLA solution compared with the PLLA solution. Fibres can be produced at lower critical voltages for solutions with higher conductivity because greater repulsive forces are generated at the jet surface, increasing the drawing force and producing fibres with smaller diameter.

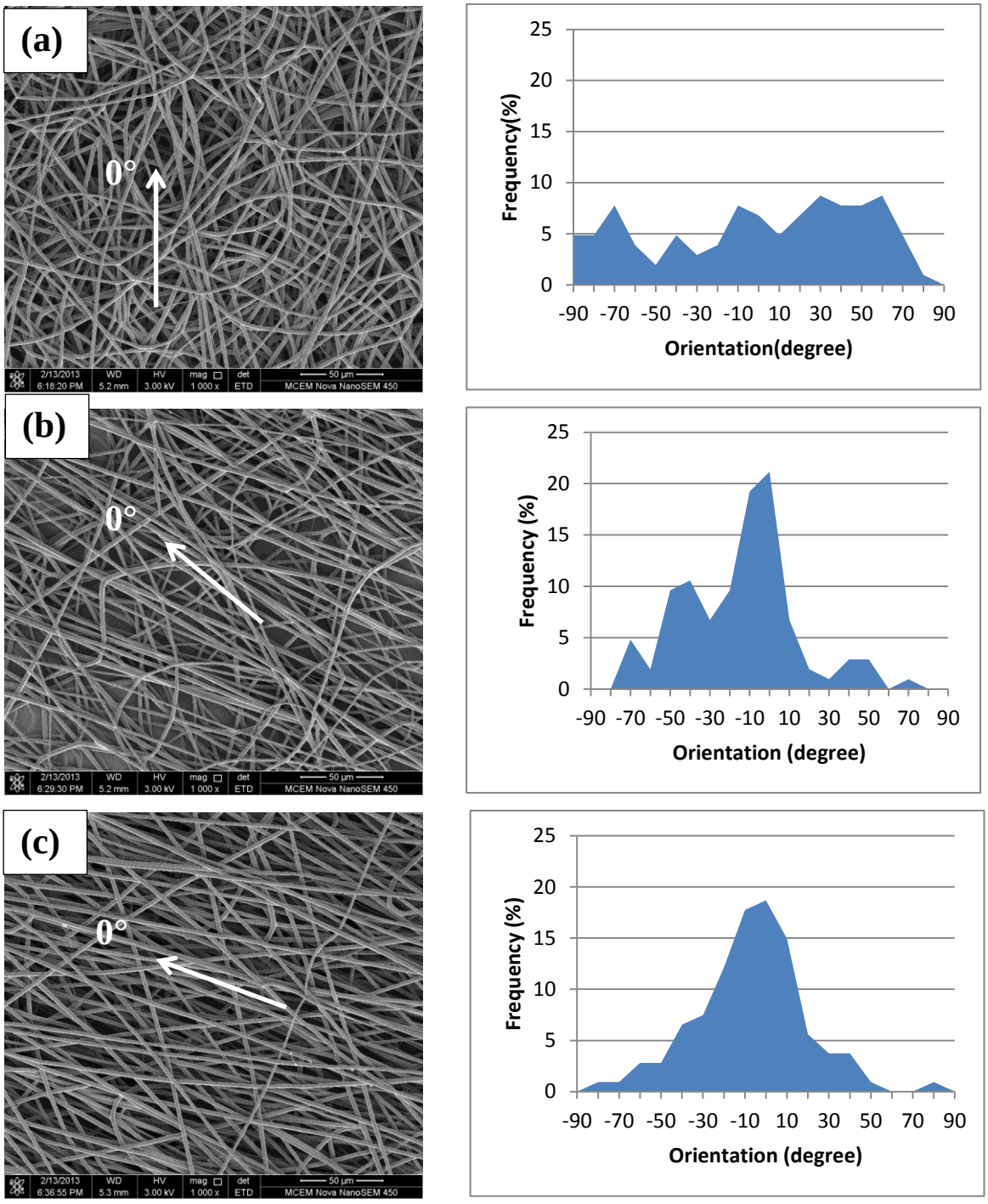

Figure 6.2 SEM and angle distribution of PGS/PLLA fibres collected using a mandrel with 16 cm circumference at different rotational speeds (a) 0prm, (b) 1000 rpm, and (c) 2000 rpm.

6.2.2 Mechanical properties

6.2.2.1 Tensile tests of PLLA alignment fibre mats

The tensile stress-strain behaviour of the electrospun PLLA fibre mats is shown in **Figure 6.3** and the data summarized in **Table 6.2**. The curves are concave to the strain axis which is typical of a rigid thermoplastic which undergoes yielding. However, the mechanical properties of the PLLA fibre mats are quite different compared with cast PLLA sheet. PLLA sheet is quite rigid and has a yield stress over 46MPa and breaking strain around 10% according to our measurement and these results are consistent with previous finding[162]. However the electrospun PLLA fibre mats are much softer with UTS of 1MPa, probably due to the porous nature of the mats, while the breaking strain was increased to about 75%, perhaps due to the additional strain in the mat caused by fibre movement and realignment. Previous publications have observed that an increase of fibre alignment can raise the strength of fibre mats [100, 101]and this is consistent with the data in **Figure 6.3**. However, it is interesting to observe that the failure strain of PLLA fibre mats did not decrease with increasing strength as observed in other studies, [100, 101].

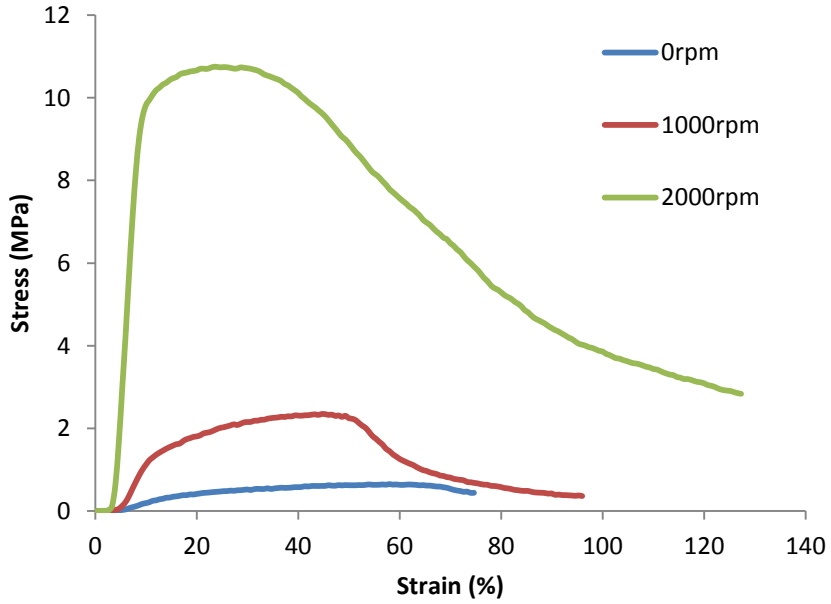

Figure 6.3 Stress-strain curves of PLLA fibre mats collected at different rotational speeds using a mandrel with 16 cm circumference.

Table 6.2 Mechanical properties of PLLA fibre mats collected at different rotation speed (using a mandrel with 16 cm circumference).

Rotational speed	**PLLA fibre mats**	
(rpm)	**UTS (MPa)**	**Elongation to rupture (%)**
0rpm	0.8±0.2	75±4
1000rpm	2.6±0.3	96±7
2000rpm	8.5±1.7	126±9

6.2.2.1 Tensile tests of PGS/PLLA fibre mats

The stress-strain behaviour of PGS/PLLA fibre mats with varying mandrel rotational speeds and thus differing levels of orientation are presented in **Figure 6.4** and **Table 6.3**. In contrast to the behaviour of the PLLA fibre mats, the stress-strain behaviour of the PGS/PLLA fibre mats is convex to the strain axis (or "J-shaped") and this behaviour is typical of natural soft tissues [4]. This behaviour is believed to be associated with the elastomeric nature of the core of the fibres. **Figure 6.4** also shows that the strength and elongation to break rise with increasing orientation and then pass through a maximum (see also **Table 6.3**), but the resilience is virtually unchanged. One reason for the better mechanical properties of aligned PGS/PLLA fibre mats, especially those collected up to 1000 rpm, is the turbulence caused by the rotation of the mandrel which could increase the speed of solvent evaporation in the spun fibres. As indicated in **Figure 6.5**, the surfaces of the spun fibres are not always smooth but, depending on the spinning conditions, can contain pores. The degree of porosity of the PGS/PLLA fibres collected at 1000 rpm was much greater than those collected at 0 rpm. The formation of a porous surface is probably due to the evaporation of solvent from the polymer solution, as suggested by other workers [62]. As a result, when the fibres land on the collector the chance of fusing to other fibres would be greatly reduced. So the aligned fibres in aligned PGS/PLLA fibre mats could move more freely under the application of a tensile stress unaffected by fused fibres and this would increase their elongation to break and UTS.

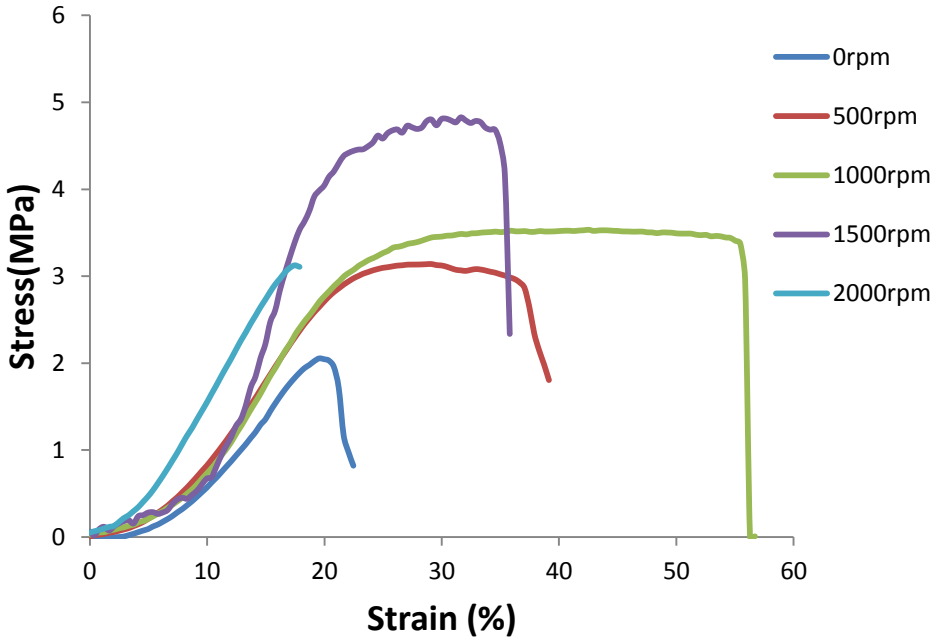

Figure 6.4 Stress-strain curves of PGS/PLLA fibre mats collected using a mandrel with a 16 cm circumference at different rotation speeds at and heat treated after purging the vacuum oven with nitrogen.

Table 6.3 Mechanical properties of PGS/PLLA mats with different alignments

Rotational speed (rpm)	**Fit to Equation 3.5 (%Elongation)**	**Resilience %**	**Stiffness constant**	**UTS (MPa)**	**Elongation to rupture (%)**
0	17.2±0.7	64.1±0.5	9.3±2.5	2.2±0.2	25.1±1.1
500	17.8±0.6	64.6±0.1	11.1±1.9	3.0±0.2	35.9±2.8
1000	19.0±1.8	67.7±0.2	12.5±1.3	3.5±0.1	53.4±7.0
1500	20.6±3.6	62.3±0.7	14.1±0.9	4.5±0.3	35.8±7.0
2000	15.0±5.3	60.0±0.2	15.9±1.6	3.8±0.1	18.6±5.7

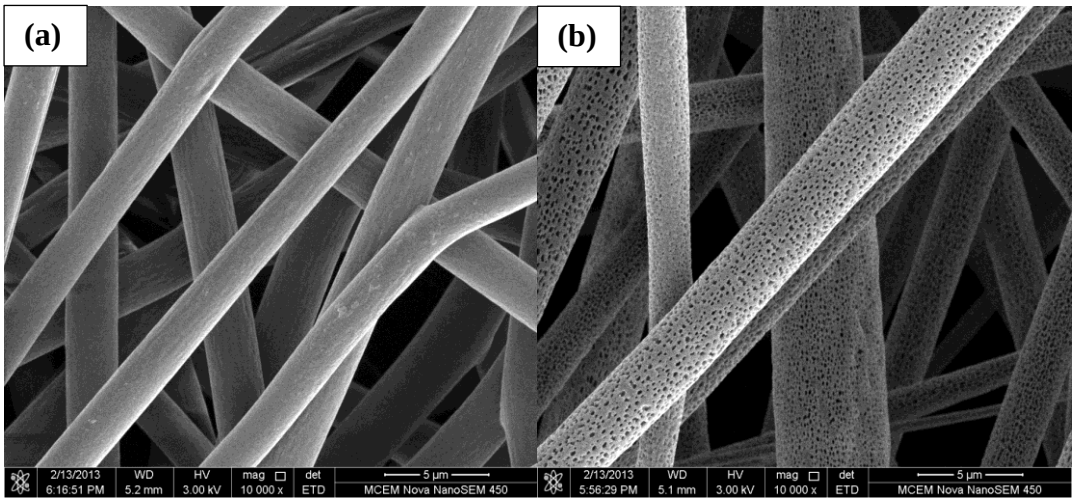

Figure 6.5 Surface SEM of PGS/PLLA fibre mats collected at (a) 0 rpm and (b) 1000 rpm using a mandrel with a 16cm circumference

The UTS and elongation to break of the PGS/PLLA fibre mats are higher than the typical values of 0.02–0.5 MPa and 20% found for heart muscular tissues [12] which bodes well for the application of these fibre mats to a soft-tissue biomedical application of soft tissues [33]. The stiffness constant of PGS/PLLA fibre mat varied from 9 to 16 for mandrel rotational speeds increasing from 0 to 2000 rpm, respectively. These stiffness constants are comparable to the values 12 to 20 previously found for heart muscular tissues [3, 107, 122].

6.3 Conclusions

Using a rotational mandrel collection method, PLLA and PGS/PLLA fibre mats were fabricated with different alignments. An increase of the rotational speed of the mandrel collection plate increased the alignments of the fibre mats and generally improved the mechanical properties. Increased fibre alignments of the PGS/PLLA fibre mats caused a continuous increase in stiffness constant but UTS and elongation first rose with increasing alignment and then decreased for highly aligned fibre mats. All of the PGS/PLLA fibre mats exhibited muscle-like mechanical properties such as a J-shaped stress-strain curve and excellent elasticity within the biologically relevant 15% strain range.

Thus, in this work, PGS/PLLA fibre mats were fabricated with a variation of the fibre alignment which resulted in a wide range of mechanical properties (resilience from 60% to 68%, stiffness constant from 9 to 16, UTS from 2 to 5 MPa, elongation from 19% to 53%) which we believe could greatly extend the application of PGS/PLLA fibre mats in soft tissue engineering.

Chapter 7

Fabrication, mechanical properties and cytocompatibility of elastomeric nanofibrous mats of $PGS_{2:3}$

7.1. Introduction

Soft biological tissues typically undergo elastic deformation with high extensibility and they exhibit a unique behaviour in that stress rises at an increasing rate with increasing strain, i.e. a J-shaped stress-strain curve or convex to the strain axis. As such, a biomaterial serving to replace damaged tissues (perhaps as scaffolds) should be nonlinearly elastic and have similar mechanical properties as the biological tissues. However, it is often difficult to achieve a satisfactory balance of compliance and biocompatibility simultaneously in a pure elastomeric material [12]. With poly(glycerol sebacate) (PGS), for example, the PGS synthesized with a stoichiometric 2:3 mole ratio of glycerol (trifunctional) to sebacic acid (difunctional) has much better biocompatibility than the PGS synthesized with a 1:1 mole ratio, but the polymer is mechanically rigid and less extensible [125]. A version of PGS material that is as soft as muscle and yet has a satisfactory cytocompatibility is still not available. Since the stiffness of a material can be greatly reduced when fabricated into a fibrous mat, in this Chapter, it is hypothesised that a fibrous network of PGS synthesised at the 2:3 mole ratio may offer an opportunity to achieve a satisfactory balance of flexibility and compatibility simultaneously in an elastomeric material.

Electrospinning is a widely used process to produce a fibrous network. Studies have demonstrated that the electrospun nanofibrous scaffolds are good at supporting cellular attachment and proliferation [163]. Electrospinning of thermoplastics, such as polylactic acid, polyglycolic acid, poly(ε-caprolactone) and their copolymers, is a well-established process. However, thermoplastic materials are generally unsuitable for use in the repair of organs/tissues working under dynamic mechanical conditions, such as heart and lung, because they lack the ability to recover their shape after deformation [5]. Hence, there is a need of electrospinning of elastomeric biomaterials, such as PGS [7, 12].

The production of nanofibres from chemically crosslinked elastomers is technically challenging. A major hurdle is that these polymers cannot dissolve in any solvents once cross-linked, and that fibres spun from uncrosslinked prepolymers would flow when they undergo the crosslinking esterification treatment at elevated temperatures. This problem could be addressed by core/shell electrospinning [13, 14]. In the core/shell electrospinning process, a non-crosslinked prepolymer, e.g. poly(glycerol sebacate) [9, 111], can be sheathed by a rigid thermoplastic, such as poly (L-lactic acid) (PLLA), when both materials are fed to the electrospinner simultaneously but via separate flow streams; in this case, the uncrosslinked PGS solution can be directed through an inner tube to form a core, while the PLLA solution flows through the outer tube to form a shell . During the spinning process, much of the solvent can evaporate from the shell, leaving a semi-solid casing around the liquid PGS core. In the subsequent thermal crosslinking treatment, the solid thermoplastic PLLA shell should maintain the tube shape and contain the core PGS material which loses the solvent via evaporation through the thin shell and undergoes the cross-linking reaction. As described in Chapter 4, PGS/PLLA core/shell fibres have been fabricated using the above procedures [13, 14]. The drawback with the use of PLLA as the shell polymer is that this thermoplastic can only be dissolved in solvents such as chloroform, tetrahydrofuran, and dioxane, which is not only environmentally unfriendly, but more seriously, can cause the swelling of PGS core polymer leading to a very fragile fibre. As such, we have found it to be impossible to retain elastic PGS fibres after removing the PLLA shell.

To eliminate the above drawback, in this Chapter the PLLA shell was replaced by polyvinyl alcohol (PVA), an inexpensive and biocompatible polymer. Unlike PLLA, which must be dissolved in an organic solvent [13], PVA is water soluble. PVA has been electrospun by a number of research groups [164-166], and PVA hydrogels have been utilised in regenerating artificial articular cartilage [167] and tendon regeneration [168]. Therefore, the primary objective of this chapter was to produce elastomeric fibres from PGS with a 2:3 monomer mole ratio, using the core/shell electrospinning technique with PVA used as a temporary shell. In addition, the ultimate goal of this work was to produce elastomeric materials that are biocompatible, degradable and mechanically as soft as biological soft tissues.

7.2. Results and discussion

7.2.1. Rheology

The shear rate dependence of the PVA and PGS solutions is shown in **Figure 7.1**. All PVA systems show some degree of shear rate thinning, as expected of polymer solutions with chain entanglement [169], however the extent of entanglements for the PVA with M_w of 13,000-23,000 g/mol must be low because a 25 g/100 ml solvent was found to be almost Newtonian and with a viscosity at least three times smaller than a solution of the same polymer with a concentration of 35 g/100 ml solvent. The maximum shear rates used in the electrospinning were calculated from a standard rheology text [170] and these were found to be 1 s^{-1} for the electrospinning of the PVA fibres, and 3 s^{-1} and 31 s^{-1} for the electrospinning of the $PGS_{2:3}$ core and PVA shell, respectively. These shear rates are overlapped by the shear rates used to measure the shear viscosities. The viscosities of the systems shown in **Figure 7.1** are approximately the same and this was the reason why the particular concentrations were selected. The viscosity of the $PGS_{2:3}$ prepolymer solution also shows pseudoplastic behaviour.

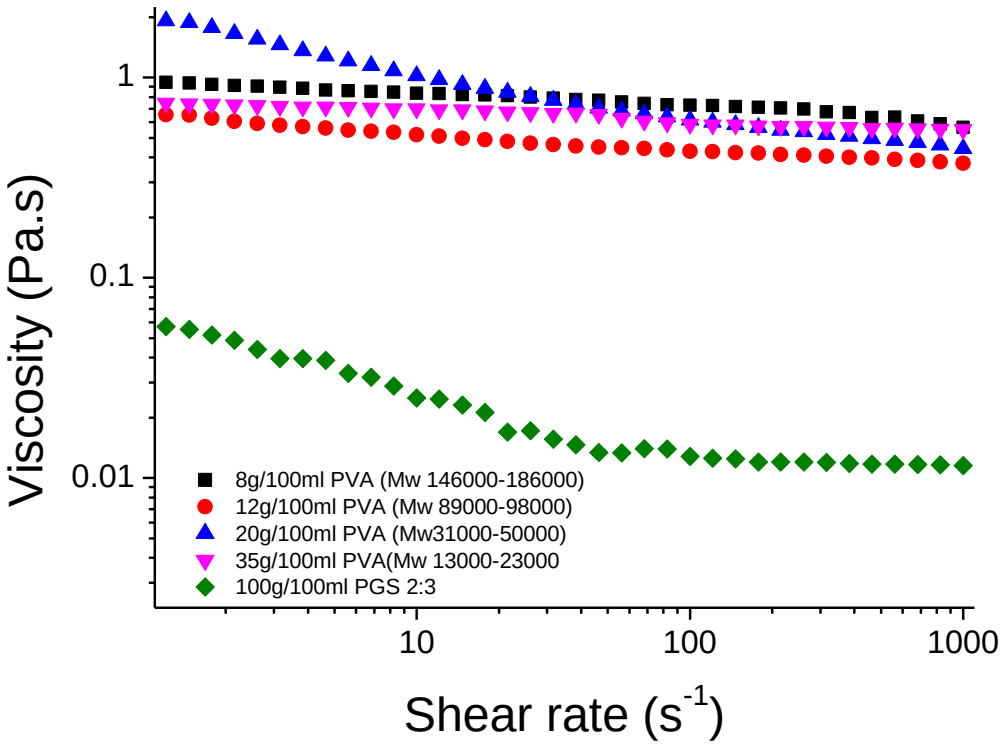

Figure 7.1 Shear rate dependence of the viscosity of the aqueous PVA solutions and $PGS_{2:3}$ prepolymer solution.

7.2.2. Optimisation of PVA fibre fabrication conditions

Electrospinning of PVA with varying molecular weights was attempted under various conditions. **Table 7.1** summarises the optimised conditions when PVA fibres were stably spun and the morphologies of the yielded fibres are illustrated in **Figure 7.2**. Polymer chain entanglement is critical for the formation of a continuous strand [163]. This entanglement is influenced by the extent of chain branching, average molecular weight of the polymer chains and the length distribution of the chains. The solution with 35 g PVA per 100 ml of water and using the lowest molecular weight (Mw=13,000-23,000 g/mol) polymer could not be spun as fibres, irrespective of the spinning conditions, presumably because insufficient entanglements could form. However uniform PVA fibres could be produced from the PVA polymers of both M_W 31,000-50,000 and 89,000-98,000 g/mol, as shown in **Figure 7.2a** and **b.** On the other hand, when a high molecular weight PVA (e.g. 146,000-186,000 g/mol) was spun, the solution was very viscous and caused blockage at the tip of the needle, producing fibres that were not uniform in size, as shown in **Figure 7.2c**. With lower concentrations of PVA of this molecular weight, the jets coalesced on the collection plate and formed a film rather than

fibres because insufficient solvent had evaporated from the jet. In addition, it should be noted that in all cases the PVA fibres were fused at their contact points, as observed at high magnification (**Figure 7.2 a′-c′**). This characteristic should have a significant influence on the mechanical properties of the fibrous network.

Table 7.1 Optimal electrosinning conditions that produced stable PVA fibres, and diameters of spun PVA fibres*. The positive voltage was the minimum to form fibres and neither drops (at low voltages) nor spray (high voltages).

M_w (g/mol) of PVA as-purchased	**Concentration of PVA solution (g/100ml solvent)**	**Minimum positive/negative voltage (kV)**	**Diameters (μm)**
13,000-23,000	35	<+13/-2 (drops) >+13/-2 (spray)	No fibres
31,000-50,000	20	+12/-2	0.22±0.01
89,000-98,000	12	+15/-2	0.40±0.02
146,000-186,000	8	+17/-2	0.66±0.03

*The feeding rate and collection distance were 1 ml/h and 18 cm, respectively

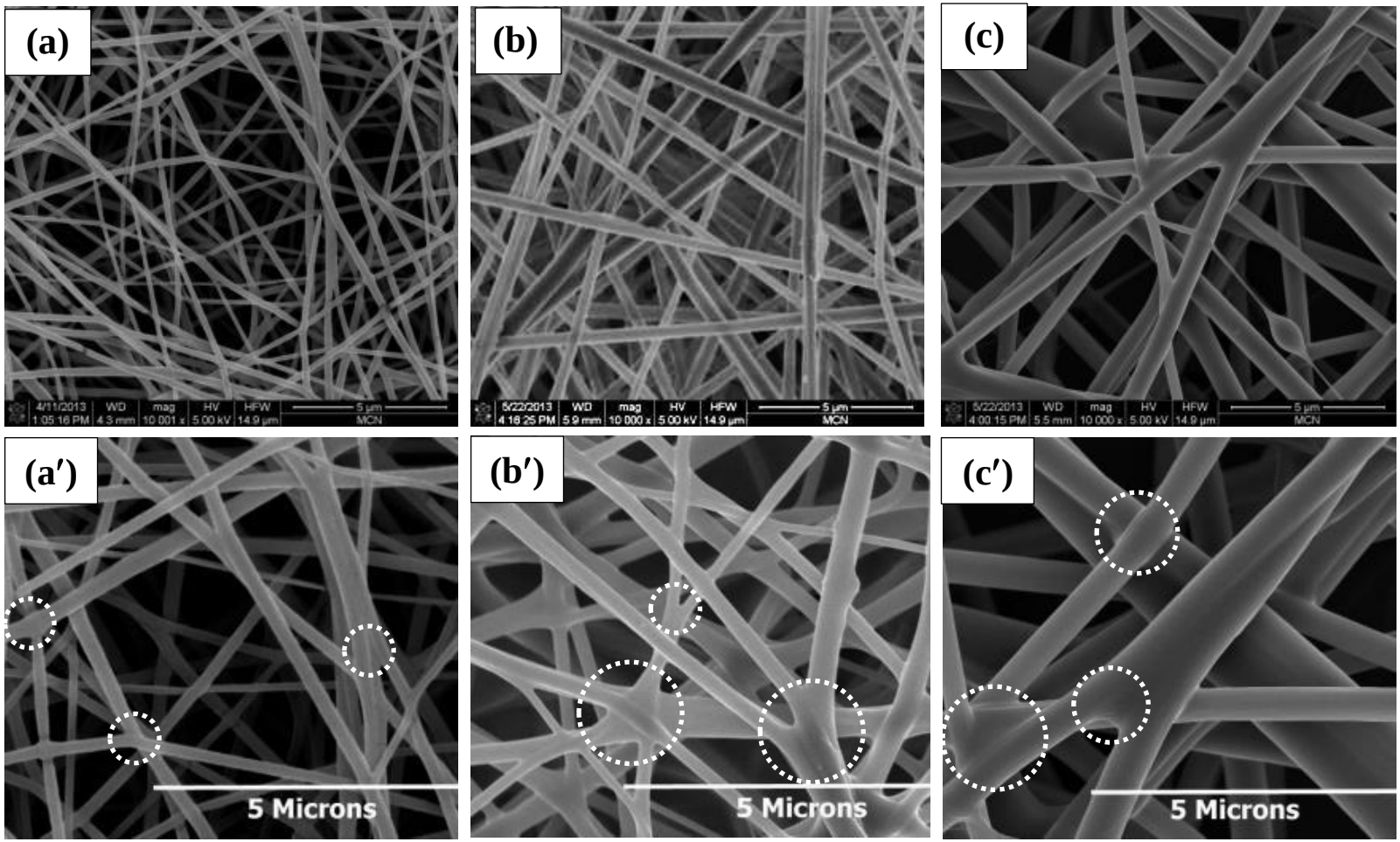

Figure 7.2 SEM images of electrospun fibres from PVA of M_w (a) and (a′) 31,000-50,000 g/mol (20g/100ml PVA in water, voltages: +12 and -2 kV). (b) and (b′) 89,000-98,000 g/mol (12 g/100ml PVA in water, voltages: +15 and -2 kV), (c) and (c′) 146,000-186,000 g/mol (8 g/100ml PVA in water, voltages: +17 and -2 kV). Feeding rate: 1ml/h, collection distance: 18cm for (a)-(c). The fused regions of the fibres shown by the dotted circles in (a′)-(c′) are close-up views of (a)-(c)

The average values of the fibre diameters are given in **Table 7.1**. PVA grades of high molecular weight yielded larger diameter fibres than the low molecular weight PVA grades, as observed by Koski *et al.* [171] Although the voltage and solution concentration also varied during the electrospinning of these polymers, it is unlikely that these other factors caused the observed trend in fibre diameter because a higher voltage or a more dilute polymer solution would be expected to produce a thinner fibre whereas the reverse trend was observed. Thus it appears that the trend in fibre diameter is due to the effect of molecular weight which determines the resistance of the relaxation of polymer chains during electrospinning [56, 172]. Lower molecular weight chains can disentangle and relax more easily under the stretching flow than large polymer chains [171], and so this is the reason why the diameters of fibres fabricated with low molecular weight PVA are smaller than those with high molecular weight PVA.

7.2.3. Optimisation of $PGS_{2:3}$/PVA core/shell fibre fabrication conditions

PVA is soluble in water, which is a non-solvent for $PGS_{2:3}$, whereas the solvents for $PGS_{2:3}$ include ethanol, DMF and THF, which cannot dissolve PVA. Thus $PGS_{2:3}$ and PVA solutions should largely remain in their separate phases during core/shell spinning.

Core and shell feeding rates are one of the most important parameters for core/shell electrospinning [66]. Because the elastomeric core material is the final product and the shell is a temporary support, the feeding rate of a core solution should be set as high as possible so as to maximise the core fibre volume in the final products. On the other hand, the feeding rate of a shell solution should be set to the minimal value which ensures the formation and physical integrity of the shell structure.

In this Chapter, different combinations of core: shell feed flow rates, from 1:10 to 1:5, were trialled and the processing parameters for successful core-shell spinning are given in **Table 7.2**. Uniform $PGS_{2:3}$/PVA core/shell fibres were produced successfully from the PVA polymers with M_w 31,000-50,000, and 89,000-98,000 g/mol at an optimal feed/flow rates and feed rate ratios, as shown in **Figure 7.3**. **Figure 7.1** shows that the viscosity of the $PGS_{2:3}$ prepolymer solution is between 3 and 30 times smaller than the PVA solution This is contrary to the study of Tiwari and Venkatraman [113] which found for a PVA/poly(lactic-co-glycolic acid) electrospun system, the ratio of the viscosities of the core and shell should be less than 2 for efficient spinning. The reason for this disagreement in behaviours is not understood. At

high magnification (**Figure 7.3a′** and **b′**) the $PGS_{2:3}$/PVA core/shell fibres were observed to be fused at their contacting points and this characteristic should have a significant influence on the mechanical properties of the $PGS_{2:3}$/PVA fibrous network .

Table 7.2 Optimal electrospinning conditions that produced stable $PGS_{2:3}$/PVA core/shell fibres

M_w of PVA (g/mol)	**Concentration of PVA solution (g/100ml solvent)**	**Core/shell feeding rates (ml/h)**	**Positive/negative voltage (kV)**	**Diameters (μm)**
31,000-50,000	20	0.1:1	+12/-2	0.26±0.01
89,000-98,000	12	0.2:1.2	+15/-2	0.41±0.02

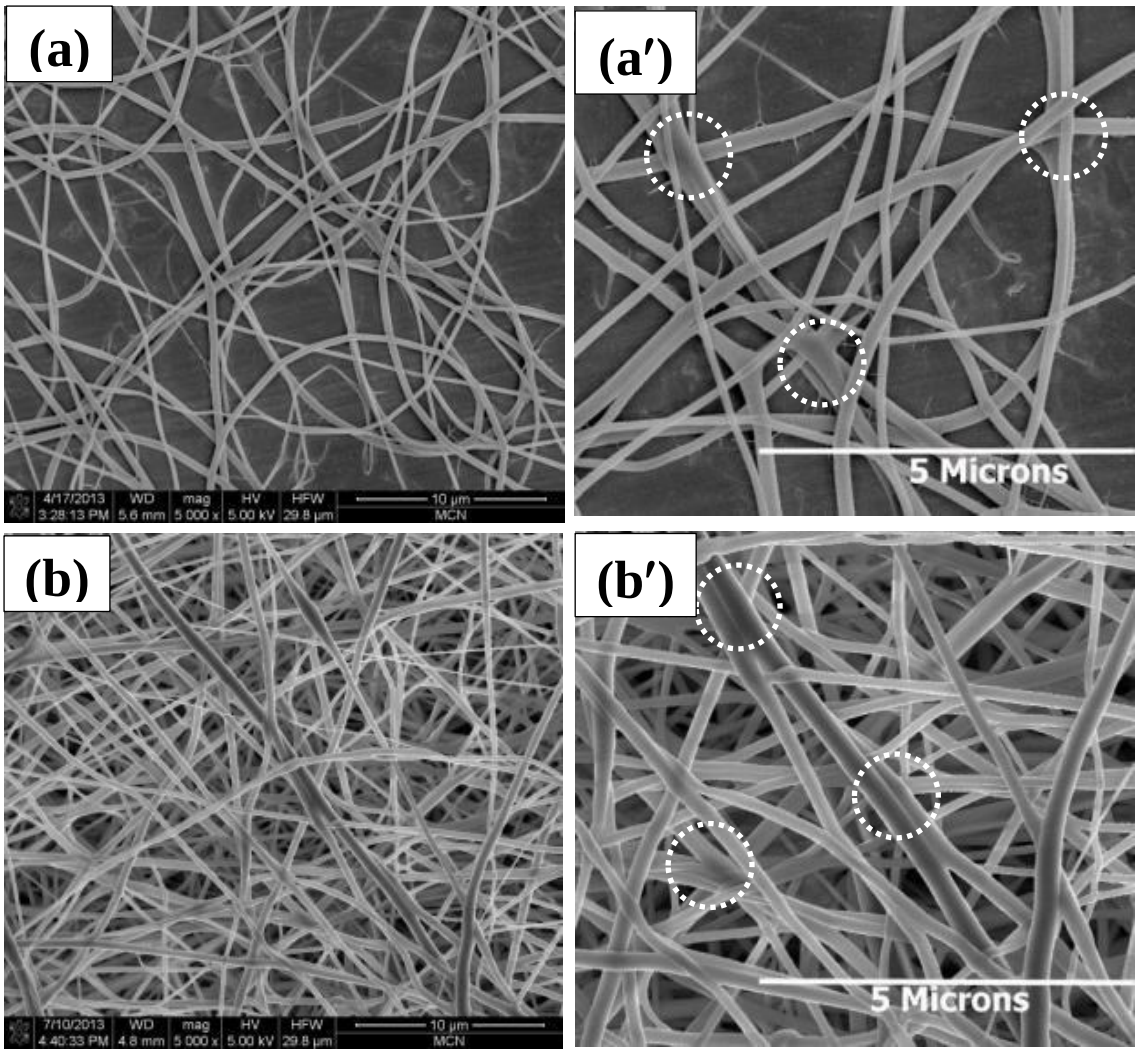

Figure 7.3 SEM images of $PGS_{2:3}$/PVA core/shell electrospun mat after heat treatment at 130°C for 3 days under vacuum. The core solution was 50% v/v $PGS_{2:3}$ in DMF, and collection distance was 18cm.(a) and (a′) PVA of M_w 31,000-50,000 g/mol. The shell solution was 20g PVA in 100ml water: positive/negative voltages were +12/-2 kV, and the

core/shell feeding rates were 0.1:1ml/h. (b) and (b′) PVA of M_w 89,000-98,000 g/mol. The shell solution was 12g PVA in 100ml water, positive/negative voltages were +15/-2 kV, and the core/shell feeding rates were 0.2:1.2ml/h. (a′) and (b′) are close-up views of (a) and (b), respectively which reveal fused regions of the fibres shown by the dotted circles.

For PVA with a molecular weight of 31,000-50,000 g/mol, when the $PGS_{2:3}$/PVA solution feed rate ratio was higher (e.g. 0.1:0.8 = 1:8 in **Figure 7.4a**) than the optimal feed ratios (i.e. 0.1:1.0 = 1:10 in **Figure 7.3a**), the PVA shell was insufficient to cover the core, which led to the leakage of the liquid $PGS_{2:3}$ core prepolymer out of the PVA shell during the subsequent curing treatment, as shown in **Figure 7.4**. Similarly for PVA with a molecular weight of 89,000-98,000 g/mol, it was found that the core-shell feed rate ratio of 0.2:1.2 = 1:6 was the maximal ratio that could produce core/shell fibres with thin and yet intact PVA shells after the crosslinking treatment process, as shown in **Figure 7.3b**, whereas the same PVA shell spun at a higher rate (e.g. 0.2:1.0 = 1:5) did not form coherent fibres.

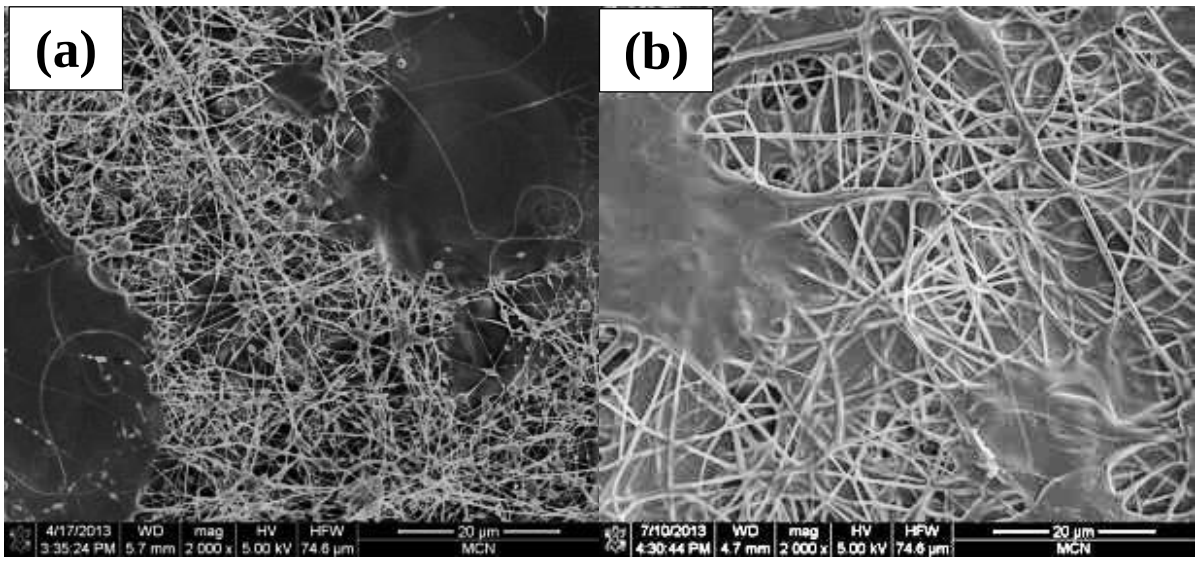

Figure 7.4 SEM images of $PGS_{2:3}$/PVA core/shell electrospun mat after heat treatment at 130°C for 72 h. The core solution was $PGS_{2:3}$100g/100ml THF and collection distance was 18 cm. Note that regions to the left and right of the micrographs appear blurry and this was caused by leaking of PGS from the fibres which is shown in the SEM as a featureless surface. (a) PVA of M_w 31,000-50,000 g/mol. The shell solution was 20g PVA in 100 ml water, positive/negative voltages were +12/-2 kV, and the core/shell feeding rates were 0.1:0.8 ml/h. (b) PVA of M_w 89,000-98,000 g/mol. The shell solution was 12g PVA in 100ml water, positive/negative voltages were +15/-2 kV, and the core/shell feeding rates were 0.2:1.0 ml/h.

Comparing the two groups of $PGS_{2:3}$/PVA core/shell fibrous mats (**Figure 7.3a** and **b**), the core/shell fibres produced with the highest molecular weight PVA (89,000-98,000 g/mol) were more satisfactory due to the following reasons. First, although uniform fibres could be

produced from the lower molecular weight PVA (31,000-50,000 g/mol) as shown in **Figure 7.3a**, the overall $PGS_{2:3}$/PVA fibres produced from this PVA were very thin (see **Table 7.2**). Second, the concentration of the PVA polymer solution with the lower molecular weight PVA had to be much higher than with the higher molecular weight PVA to enable fibre formation, so that the PVA shell using the lower molecular weight PVA was much thicker than with the PVA of M_w 89,000-98,000 g/mol. As a result, the $PGS_{2:3}$/PVA fibres spun from the PVA of M_W 31,000-50,000 g/mol had small diameters and also had a very thin core of $PGS_{2:3}$. As such, it was much more difficult to remove PVA from the core/shell fibres spun from the PVA of 31,000-50,000 g/mol than those made spun with the PVA of M_w 89,000-98,000 g/mol, and the residual $PGS_{2:3}$ fibres remaining after dissolution of the low molecular weight PVA (31,000-50,000 g/mol) was very fragile. Therefore, the subsequent studies on mechanical properties and bio-evaluation were focused on the core/shell fibres spun with the PVA of M_w 89,000-98,000 g/mol at the feed/flow rates of 0.2(core)/1.2 (shell) ml/h. Based on the feed rates and concentrations of the core and shell solutions, the composition of this core/shell polymer was approximately 50:50 wt% $PGS_{2:3}$/PVA.

7.2.4. Fabrication of $PGS_{2:3}$ fibre mats

After the crosslinking the $PGS_{2:3}$ core, the core/shell fibrous mat were soaked in hot water at 95°C for 2 hours to remove the PVA shell. This treatment partially dissolved the PVA shell and formed snow flake-like crystallites around the $PGS_{2:3}$ cores when dried, as shown in **Figure 7.5a** and **b**. This presence of crystallites may seem surprising because PVA is generally atactic, but it can crystallize due to the small size of the hydroxyl group [173]. After an additional 2 hours rinsing in hot water, the snow flake-like morphology was no longer observed under SEM (**Figure 7.5c and d)**, indicating that most of the PVA shells had been removed from the fibre, and $PGS_{2:3}$ fibres or porous mats were left behind. Around the $PGS_{2:3}$ fibres there appears to be a thin polymer film containing many pores. The formation of such a film may be caused by the adhesion of $PGS_{2:3}$ fibres or may be due to the transesterification reaction between the PVA and $PGS_{2:3}$ prepolymer when the fibre mats were cured at 130°C.

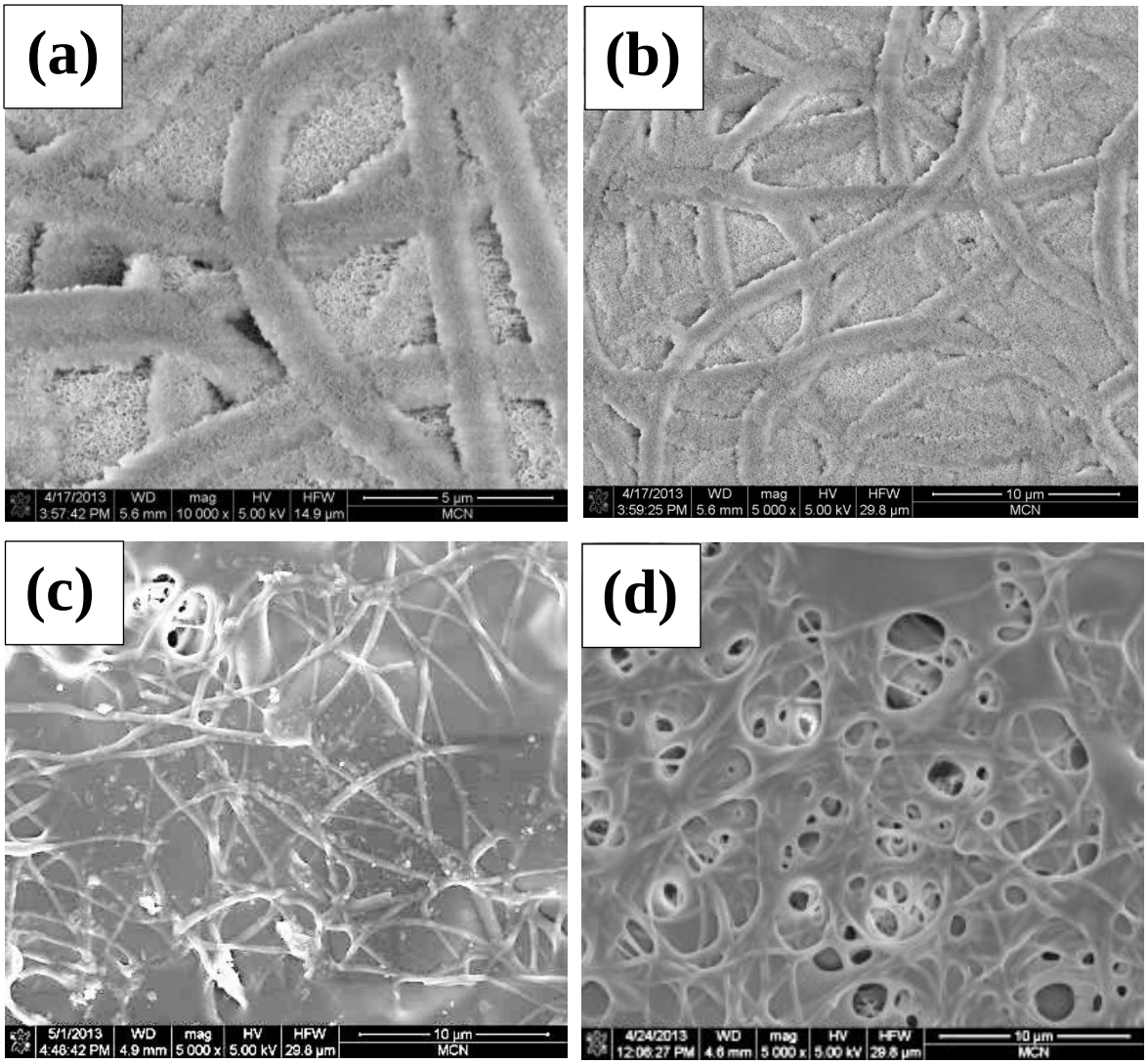

Figure 7.5 $PGS_{2:3}$/PVA fibres spun using PVA M_w 89,000-98,000 g/mol, after PGS curing and following removal of the shell. The shell solution was 12g PVA in 100ml water, the core solution was $PGS_{2:3}$ 50g/100ml THF, and core/shell feed/flow rates were 0.3 and 1.2ml/h, respectively, using positive/negative voltages of +15 and -2 kV, respectively, and with a collection distance of 18 cm. After rinsing the spun mat in hot water at 95 °C for (a) 2 hours or (b) 4 hours, to wash off most of the PVA, the above SEM images were obtained.

7.2.5. Characterisation results of FTIR and DSC

The ATR-FTIR spectra for PVA powder (M_W 89,000-98,000 g/mol), $PGS_{2:3}$/PVA core-shell fibre mat, $PGS_{2:3}$ fibre mat (formed from the $PGS_{2:3}$/PVA fibre mat by soaking in hot water for 4h) are plotted in **Figure 7.6**. The peaks at 2940, 2900 and 2855 cm^{-1} are attributable to the methylene (-CH_2-) group and the methine (C-H) group present in PVA and $PGS_{2:3}$, while the intense stretch at 1155 cm^{-1} was associated with the C-O-C bond in the ester group of PGS [174]. The intensity of the 1155 cm^{-1} peak was strong for the $PGS_{2:3}$ sheet and the

washed $PGS_{2:3}$/PVA, weaker for the virgin $PGS_{2:3}$/PVA and absent in PVA, suggesting that much of the PVA had been washed off the $PGS_{2:3}$/PVA fibres - the overlapping of peaks in this region prevented quantitative analysis. The intense peak at 1733 cm^{-1} due to the carbonyl double bond [174] confirmed the presence of ester groups in $PGS_{2:3}$; no such peak was found in the PVA spectra. The intensity of the ester peak in the spectra of the washed $PGS_{2:3}$/PVA fibre mat is approximately half of that in the virgin $PGS_{2:3}$/PVA fibre mat, which is consistent with the 50:50 wt% composition of the original core-shell fibre. In addition, the intensity of the ester peak of the washed $PGS_{2:3}$/PVA is about 90% of that of the pure $PGS_{2:3}$ confirming that most of the PVA had been removed by washing with hot water. The broad peak area between 3500-3000cm^{-1} in PVA is due to hydrogen-bonded hydroxyl groups [174]. Contrary to that previously observed [109, 175] for $PGS_{1:1}$ (which has excess hydroxyl groups), this peak is not observed in $PGS_{2:3}$ which indicates that almost all hydroxyl groups in the glycerol have been reacted and $PGS_{2:3}$. The intensity of the hydroxyl group's peak in the virgin $PGS_{2:3}$/PVA fibre mat is approximately 70% of that in PVA, whereas the peak in the washed $PGS_{2:3}$/PVA fibre mat is approximately 40% of the PVA peak which indicates that some PVA is still attached to the fibres.

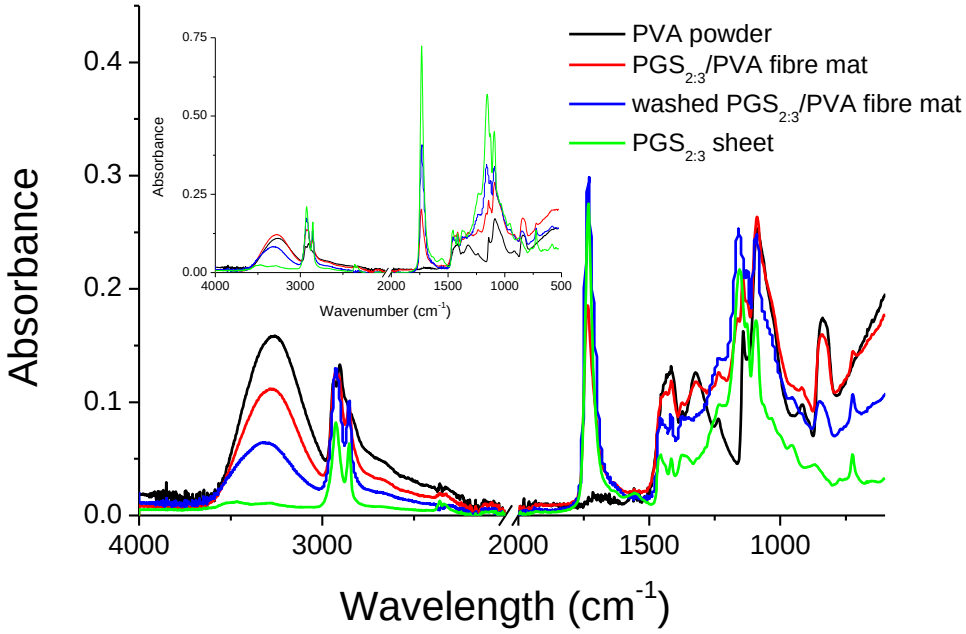

Figure 7. 6 ATR-FTIR absorbance spectra for PVA (M_w 89,000-98,000 g/mol), $PGS_{2:3}$/PVA core-shell fibre mat, $PGS_{2:3}$ fibre mat (formed from the $PGS_{2:3}$/PVA fibre mat by soaking in hot water for 4h) and $PGS_{2:3}$ sheet. The spectra have been normalized by the area under the CH peaks near 2900 cm^{-1} but the same trends in the intensity of ester, hydroxyl and C-O-C peaks is observed as in the un-normalized spectrum (see inset for comparison).

The DSC thermograms for the polymers are shown in **Figure 7.7** The T_g for $PGS_{2:3}$ sheet was -24 °C which is very close to the previously published [125] T_g of $PGS_{1:1}$ (-23 °C) but the heat capacity step was reduced from 0.92 to 0.55 $Jg^{-1}K^{-1}$. The difference between the crosslinked $PGS_{1:1}$ and $PGS_{2:3}$ polymers is that the former has a lower crosslink density since it contains excess hydroxyl groups, but it also has fewer flexible sebacate units. Thus the effect of crosslinking and chain flexibility may counteract one another in their effect on the T_g, but the higher crosslinking degree should decrease the heat capacity step [176]. For the electrospun fibres, the presence of PVA in the fibres would dilute the heat capacity step at the $PGS_{2:3}$ glass transition and so the heat capacity step of $PGS_{2:3}$ fibre mat (i.e., the mat remaining after soaking the $PGS_{2:3}$/PVA fibre mat in hot water for 4h) was lower than in the $PGS_{2:3}$ sheet and higher than in the $PGS_{2:3}$/PVA fibre mat indicating that approximately half of the PVA was washed off the mat, which is in general agreement with the ATR-FTIR results.

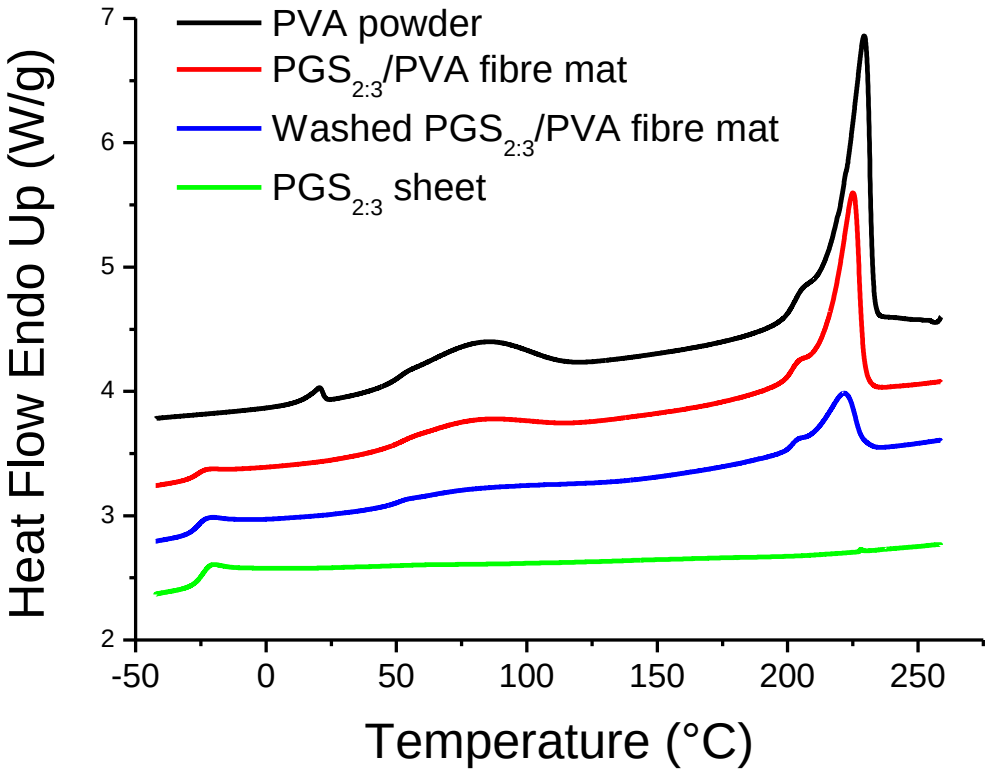

Figure 7.7 DSC curve for PVA (M_w 89,000-98,000 g/mol), $PGS_{2:3}$/PVA core-shell fibre mat, $PGS_{2:3}$ fibre mat (formed from the $PGS_{2:3}$/PVA fibre mat by soaking in hot water for 4h) and $PGS_{2:3}$ sheet

The melting endotherm for PVA has a peak at 229°C which is in good agreement with the value of 230°C quoted by Assendert and Windle [173] but the melting point decreases slightly for the $PGS_{2:3}$/PVA mats (as shown in **Table 7.3**) perhaps due to plasticization by low molecular weight $PGS_{2:3}$ or by transesterification between the ester groups of $PGS_{2:3}$ and the hydroxyl groups of PVA. The heat of fusion of the PVA (per gram of sample) was approximately twice as high as that in the $PGS_{2:3}$/PVA fibre mat and this agrees with the 50:50 wt% composition expected from the feed ratios used in the spinning. The heat of fusion of PVA in the $PGS_{2:3}$ fibre mat was around 20% was around 20% of that in the $PGS_{2:3}$/PVA fibre mat and this is consistent with the successful removal of at least half of the PVA from the $PGS_{2:3}$/PVA fibre mat. This conclusion is also in general agreement with the ATR-FTIR results.

7.2.6 Mechanical properties of fibrous mats

7.2.6.1. Static tensile testing

Figure 7.8 demonstrates typical stress-strain curves of $PGS_{2:3}$ solid sheets, $PGS_{2:3}$/PVA core-shell fibrous mats and $PGS_{2:3}$ fibrous mats in dry or wet conditions. **Figure 7.9** summarizes the average values of Young's modulus, UTS, elongation at break and the resilience of these materials. The dry $PGS_{2:3}$ solid sheet exhibited almost linear stress-strain curves and low moduli, consistent with elastomeric behaviour, and the wet $PGS_{2:3}$ fibrous mat exhibited slightly non-linear J-shaped (i.e., concave to the strain axis) curvature. In contrast the dry $PGS_{2:3}$/PVA core-shell fibre mats and $PGS_{2:3}$ fibre mats showed markedly non-linear (i.e. convex to the strain abscissa). Dry PVA is a rigid thermoplastic polymer [177] and this resulted in $PGS_{2:3}$/PVA mat possessing a higher modulus and UTS but lower resilience than the $PGS_{2:3}$ solid sheets. In addition, the elongation to break of the $PGS_{2:3}$/PVA mat was higher than the $PGS_{2:3}$ solid sheets due to the ability of the $PGS_{2:3}$/PVA fibres to reorient themselves in the tensile direction which added to the total strain. Similarly, the UTS value of dry $PGS_{2:3}$ fibrous mats (i.e., after soaking the $PGS_{2:3}$/PVA fibre mat in hot water for 4h) was lower than that of the $PGS_{2:3}$/PVA counterpart due to the partial loss of the dry PVA shell. Surprisingly, the stress-strain behaviours of the dry and wet $PGS_{2:3}$ fibre mats (i.e., the mats remaining after soaking the $PGS_{2:3}$/PVA fibre mat in hot water for 4h) were very different, and the modulus and UTS were higher for the dry $PGS_{2:3}$/PVA fibre mats but the elongation to break was lower. This behaviour can not result from plasticization of PGS by water because the equilibrium uptake of water is very low, but appears to be due to residual PVA remaining on the surface of the $PGS_{2:3}$ core, perhaps due to a esterification or trans-esterification grafting reaction between the PVA alcohol groups and the $PGS_{2:3}$ carboxylic or ester groups, respectively, during the $PGS_{2:3}$ crosslinking process, as suggested above. The result of this is that in the wet state the residual PVA in the water-soaked $PGS_{2:3}$/PVA fibre mat would be plasticized by the water [178] thus transferring most of the stress to the $PGS_{2:3}$. However, in the dry state the residual PVA would be rigid, conveying thermoplastic behaviour on the mat.

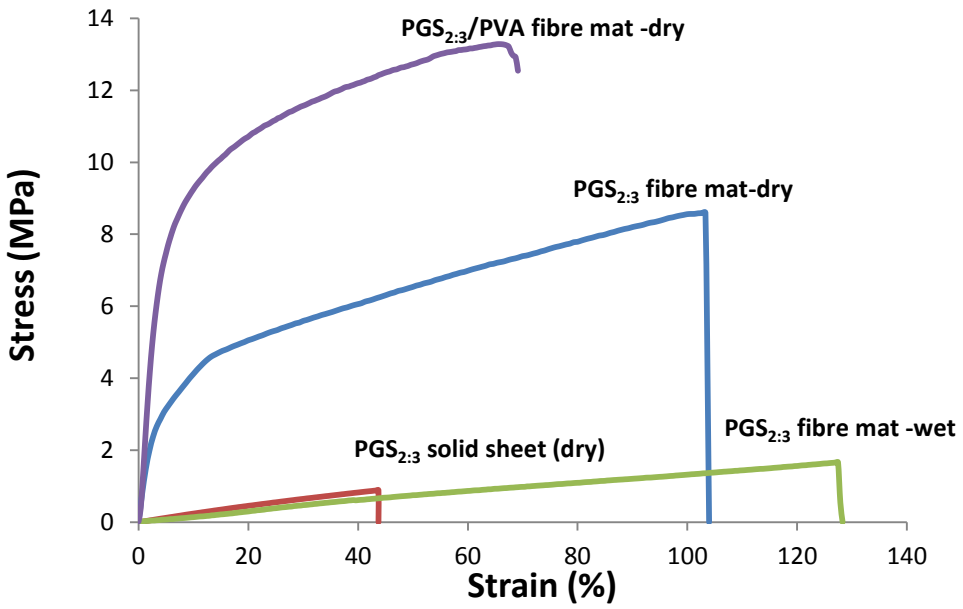

Figure 7.8 Stress-strain curves of $PGS_{2:3}$ solid sheet and of spun $PGS_{2:3}$ fibrous mat (spun at feed rates of 0.2(core)/1.2 (shell) ml/h) , after PGS curing and after the PVA shell (PVA M_w 89,000-98,000 g/mol) had been removed by washing in 95°C water for 4h , tested in dry and wet conditions.

In wet conditions, the $PGS_{2:3}$ fibrous (i.e., the mat that remained after soaking the $PGS_{2:3}$/PVA fibre mat in hot water for 4h) was slightly softer than the $PGS_{2:3}$ solid sheets, and had significantly enhanced rupture elongation (**Figure 7.9c**) because the water played two roles in improving resilience of the $PGS_{2:3}$ fibres mats. Firstly, as mentioned above, the residual rigid PVA shell was plasticized in water. As a result, this softened PVA played little role in the mechanical performance of the $PGS_{2:3}$ fibres mats. Secondly, the water between the $PGS_{2:3}$ fibres acted as a lubricant and reduced the friction between the surfaces of the $PGS_{2:3}$ fibres. Hence, the $PGS_{2:3}$ fibres could move easily when deformed under wet conditions, with much improved extensibility compared with that under dry conditions.

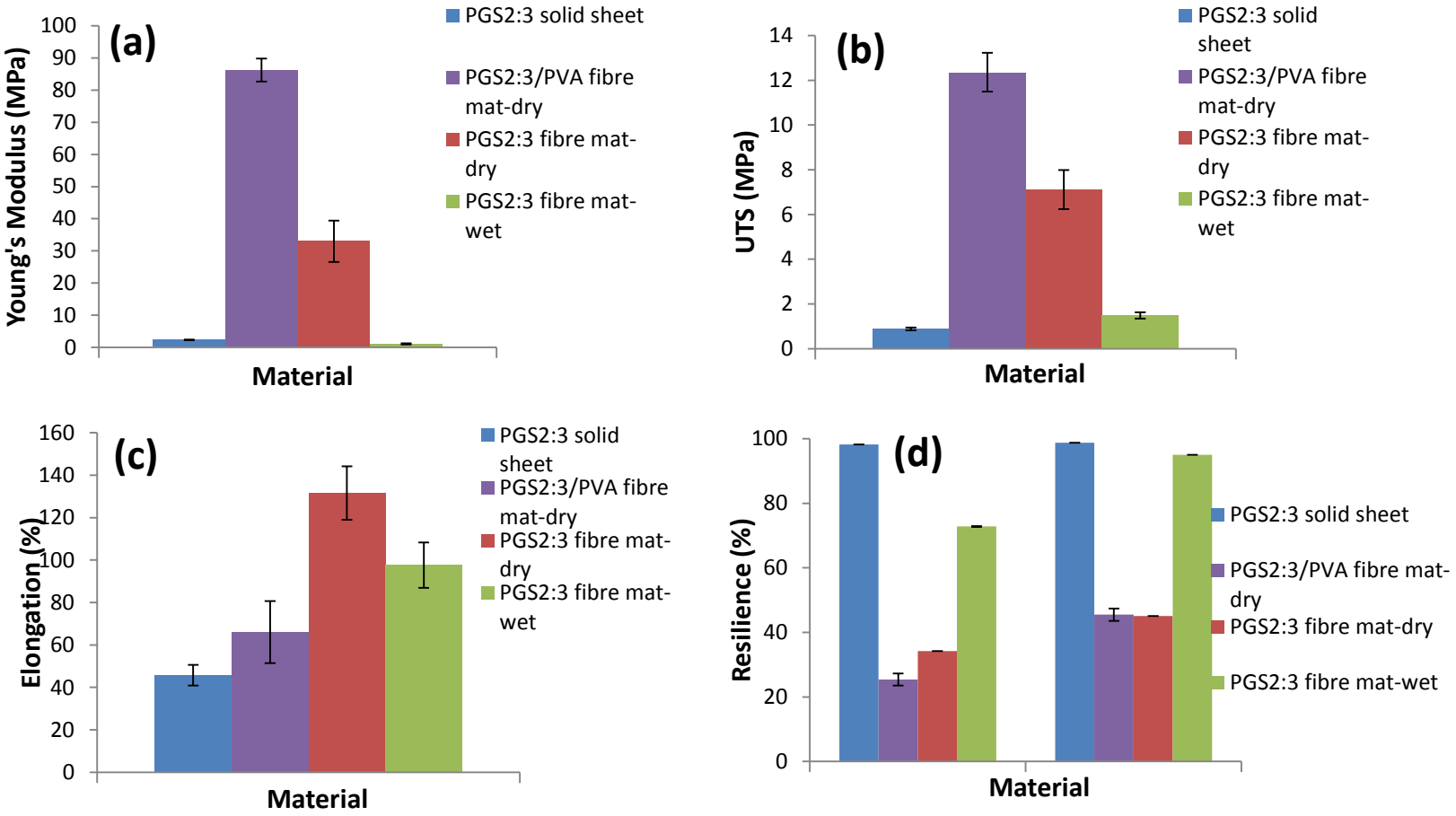

Figure 7.9 The Young's modulus (a), UTS (b), elongation (c) and resilience (d) comparison of $PGS_{2:3}$ solid sheet, dry $PGS_{2:3}$/PVA fibre mat (after PGS curing), dry $PGS_{2:3}$ fibre mat (after PGS curing) and water-saturated $PGS_{2:3}$ fibre mat (after PGS curing) saturated with water . The PGS/PVA fibres were spun at feed rates of 0.2(core)/1.2 (shell) ml/h using PVA with a M_w of 89,000-98,000 g/mol. With the exception of Chart (d), the error bars show the standard deviations; for Chart (d) the bars give the variation in resilience obtained after the first cyclic (left part) and the average of the following cyclic (right part) loadings and unloadings.

The wet $PGS_{2:3}$/PVA and $PGS_{2:3}$ fibrous mats (i.e., the $PGS_{2:3}$/PVA fibre mat after partial removal of PVA) showed J-shaped stress-strain curves at small strains (5% and 40%, respectively), as shown in **Figure 7.10**. J-shaped stress-strain curves are typical for fibre mats. Using the non-linear stress-strain equation proposed by Mirsky [3, 122], the J-shape stress-strain curve can be fitted with **Eq 3.5 (Chapter 3)** for the $PGS_{2:3}$ fibrous mats with k = 2.5 and α = 0.6 up to 40 % strain and 0.4 MPa, whereas $PGS_{2:3}$/PVA core/shell fibrous mats could only match to 5 % strain and 4 MPa with k = 21.9 and α = 53.1. Inspection of **Eq 3.5** reveals that α is the initial slope of the stress strain curve (i.e., the Young's modulus), while k is a measure of how rapidly the stress-strain departs from a linear relationship – i.e., the extent of the J-shape. Both parameters indicate that after the PVA shell is partially removed, the fibrous mats of $PGS_{2:3}$ became much softer than its core/shell counterparts.

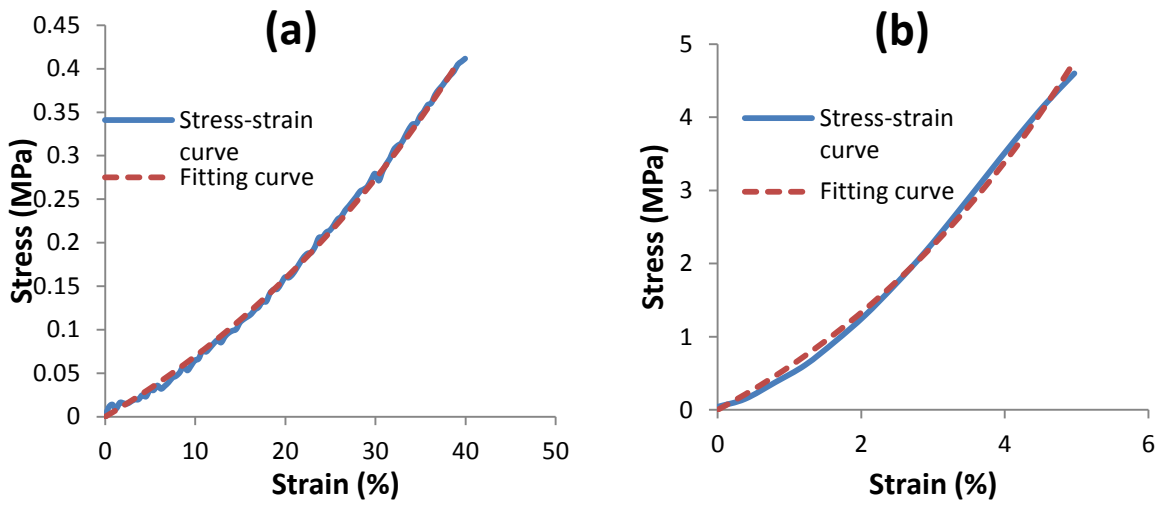

Figure 7.10 The stress-strain curve of water-saturated $PGS_{2:3}$ fibre mat (a) compared with the fit given by Equation 4 (with k=2.5, α=0.61 MPa up to 40% elongation, and of dry $PGS_{2:3}$/PVA mat (b) compared with the fitted curve using Equation 4 (where k=21.9, α=53 MPa) up to 5% elongation The PGS/PVA fibres were spun at feed rates of 0.2(core)/1.2 (shell) ml/h using PVA with a M_w of 89,000-98,000 g/mol and the PGS in the core-shell fibres cured at 130°C under vacuum for 72 h.

7.2.6.2. Dynamic tensile testing

Figures 7.11a-d show the cyclic stress-strain curves of dry $PGS_{2:3}$ solid sheets, dry $PGS_{2:3}$/PVA core/shell mats and $PGS_{2:3}$ fibre mats in dry or wet conditions. The $PGS_{2:3}$ sheet showed almost linear elastic behaviour and had the best resilience of 98% for the first cycle and 99% for the subsequent cycles (see **Figure 7.9d**), The $PGS_{2:3}$ sheet also had the most reproducible deformation cycles (see **Figures 7.11a-d**). With $PGS_{2:3}$/PVA and $PGS_{2:3}$ fibrous mats in dry condition, the stress-strain curves of the first cycle were concave to the strain

abscissa (the slope continuingly decreased with increasing strain) similar to the yielding behaviour of a thermoplastic, but then became J-shaped, concave to the strain abscissa (the slope continuingly increased with increasing strain) in the subsequent cycles, as shown in **Figure 7.11b** and **c**. This change in stress-strain behaviour may be due to the rupture of the rigid PVA shell or a remnant PVA coating upon loading, so that during subsequent strain cycles the PVA plays a much less important role in the deformation behaviour. The resiliencies for these two groups of fibrous mats were both approximately 30% for the first cycle and 45% for the subsequent cycles. The wet $PGS_{2:3}$ fibrous mats demonstrated J-shaped stress-strain curve from the first cycle, as shown in **Figure 7.11d**. The resilience of the fibrous mats in the wet condition were 70% for the first cycle and 95% for the subsequent cycles, and these are significantly higher than the values of the same materials in the dry condition (34% and 45%), presumably because the residual PVA in the water-plasticized $PGS_{2:3}$ plays no role in energy absorption whereas it is involved in viscoelastic/plastic energy loss when the mat is tested in the dry condition.

It is interesting to note that the stress-strain curves of the spun $PGS_{2:3}$ fibrous mats tested in the wet condition exhibited a jagged appearance reminiscent of a “stick-slip” phenomenon - see **Figure 7.8d**. The reason for this may be that during stretching, the fibres were held together by frictional adhesive forces, but when the applied stress finally overcame this friction the fibres spring back towards a lower stress state or the fibres may break causing a decrease in overall stress while is repeated as the sample is stretched further. Similar irregular stress-strain behaviour has also been observed in PGS:Gelatin electrospun fibrous mats [100] .

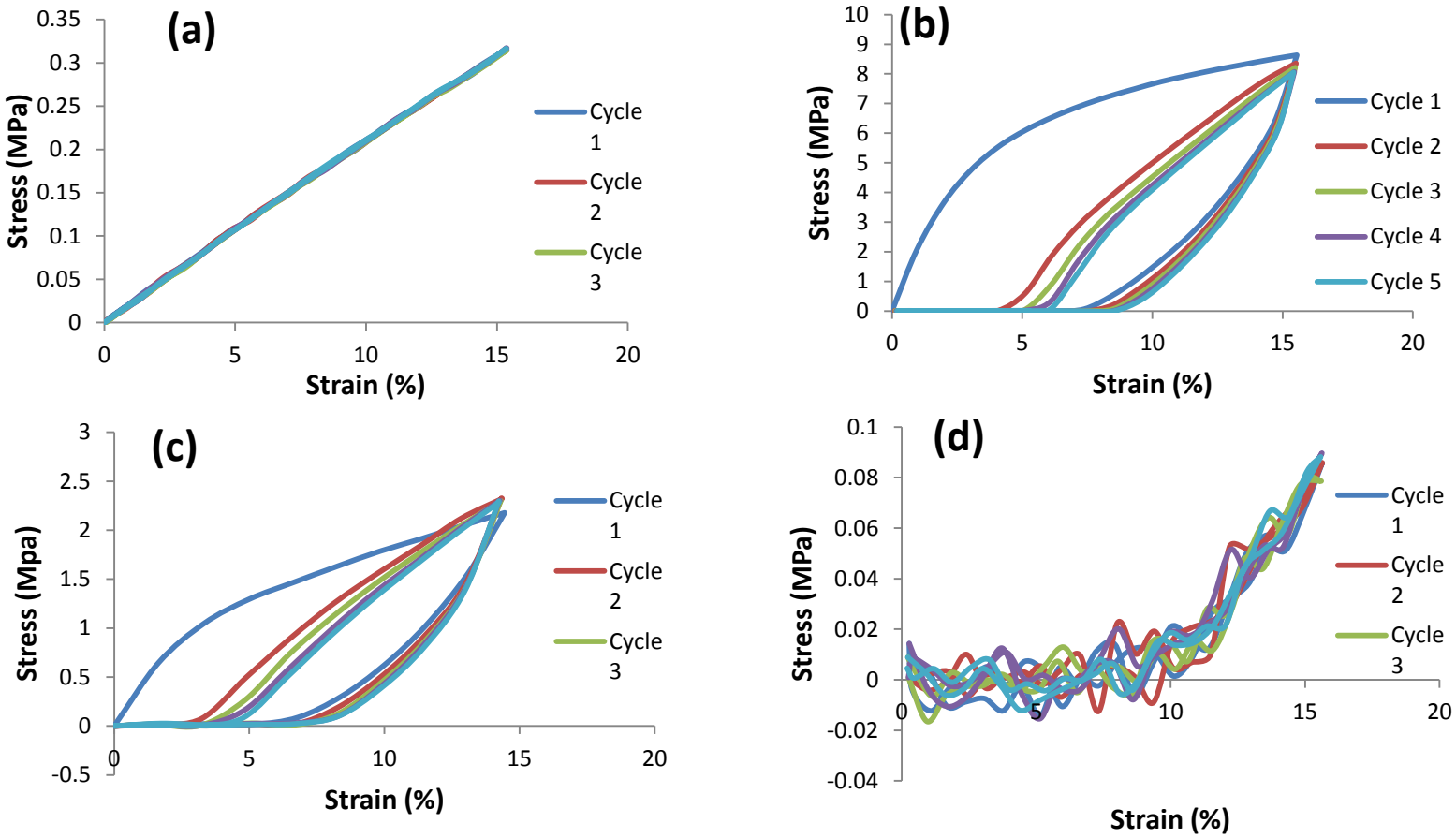

Figure 7.11 (a) Resilience tests of $PGS_{2:3}$ solid sheet (glycerol and sebacic acid, molar ratio 2:3, heated at 130°C for 3 days), (b)$PGS_{2:3}$/PVA fibre mat (glycerol and sebacic acid molar ratio 2:3, core/shell electrospinning with PVA M_w of 89,000-98,000 g/mol at feeding rates of 0.2(core)/1.2 (shell) ml/h after heated at 130°C for 3 days), (c) dry $PGS_{2:3}$ fibre mat (glycerol and sebacic acid molar ratio 2:3, core/shell electrospinning with PVA M_w of 89,000-98,000 g/mol at feeding rates of 0.2(core)/1.2 (shell) ml/h after heated at 130°C for 3 days, washed in 95°C water for 4 hours) and (d) wet $PGS_{2:3}$ fibre mat

7.2.7. *In vitro* evaluation of cytotoxicity

A visual examination of the SNL cell growth did not indicate serious cytotoxicity in any of the tested groups, as shown in **Figure 7.12**. SNL cells attached to the bottom well and proliferated in the material-free culture media and media soaked with PLLA fibre mats, $PGS_{2:3}$ solid sheets and spun $PGS_{2:3}$ fibrous mats. At day 2, the cells in each well proliferated and reached confluence, as shown in **Figure 7.12**. Quantitative LDH measurements results were showed in **Figure 7.13**, according to this figure the PGS 2:3 fibre mat has the lowest percentage of dead cells. The statistical analysis results indicated that there was no significant difference between the $PGS_{2:3}$ fibre mat,$PGS_{2:3}$ sheet or PLLA fibre mat, however the difference between the $PGS_{2:3}$ fibre mat and medium was significant (the percentage of dead cells in $PGS_{2:3}$ fibre mats were significant lower than that in medium), which demonstrated that the cytocompatibility of the $PGS_{2:3}$ fibre mats were comparable with the control groups.

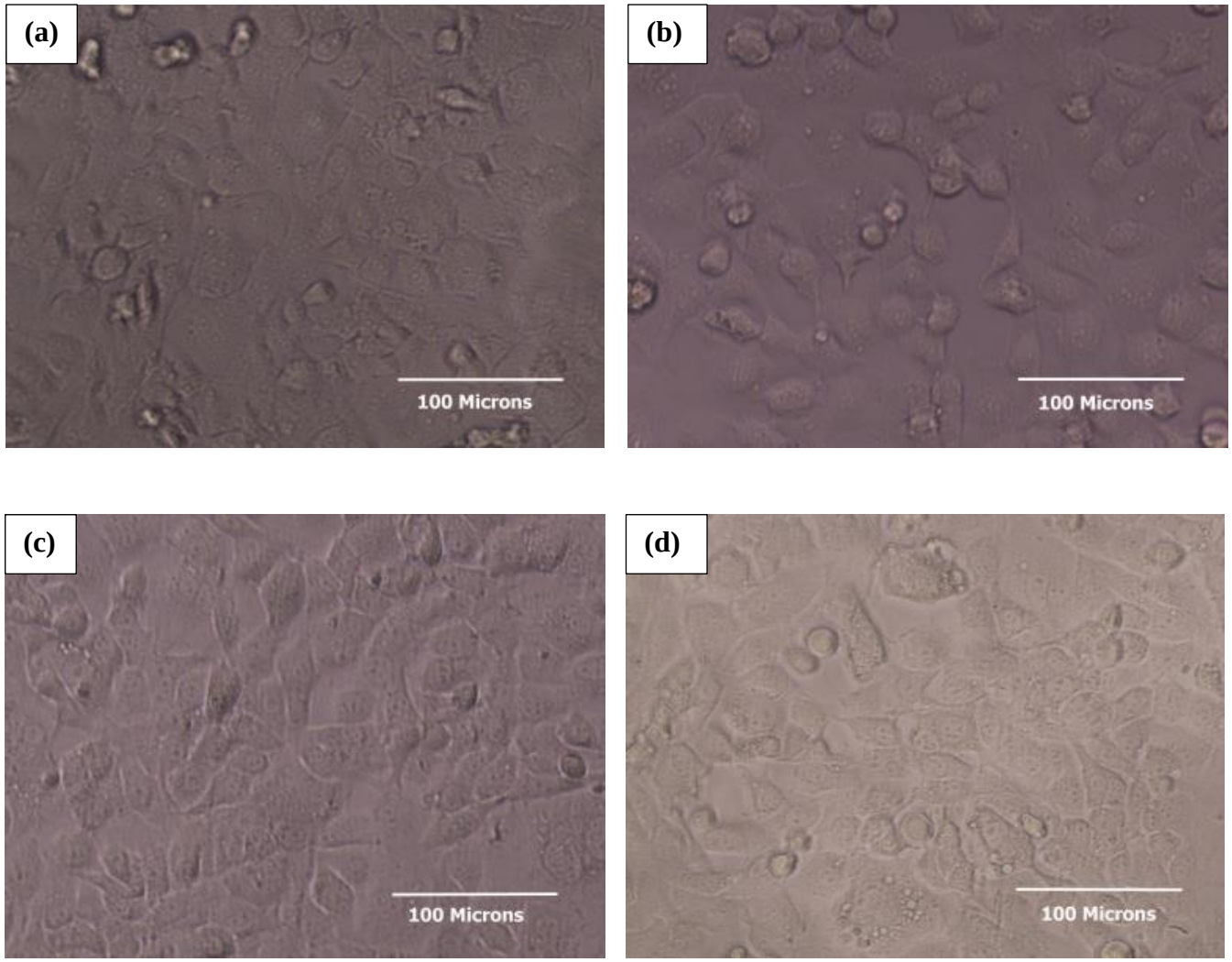

Figure 7.12 Images of SNL cells cultured for 2 days in (a) material-free culture medium (negative control), adjacent to (b) PLLA fibre mat (positive control) (c), PGS2:3 solid sheet, and (d) PGS2:3 fibre mat obtained from the core-shell fibres after removal of the PVA.

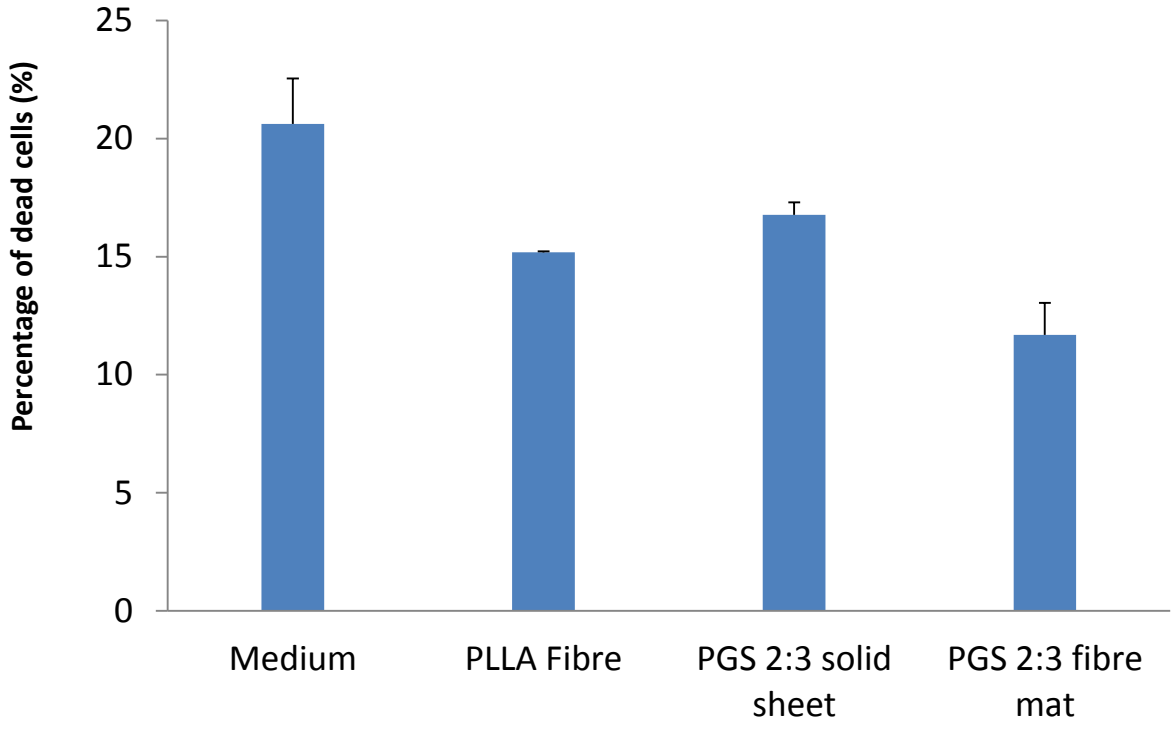

Tukey's Multiple Comparison Test	P value
Medium vs $PGS_{2:3}$ fibre mat	$P < 0.01$
PLLA fibre mat vs $PGS_{2:3}$ fibre mat	$P > 0.05$
$PGS_{2:3}$ sheet vs $PGS_{2:3}$ fibre mat	$P > 0.05$

Figure 7.13 Cytotoxicity of material-free culture medium (negative control), PLLA fibre, PGS2:3 solid sheet and PGS2:3 fibre mat (obtained from the core-shell fibres after removal of the PVA) detected by measuring the release of lactate dehydrogenase (LDH) from the cells after four days of cultivation (n=5). No significant differences existed between PGS2:3 fibre mat and PLLA fibre mat and PGS2:3 fibre mats but PGS2:3 fibre mat is better than the control.

7.3. Conclusions

In this Chapter, $PGS_{2:3}$/PVA core/shell fibres were successfully electrospun using PVA with a M_W of 89,000-98,000 as a shell material, and optimal fabrication conditions that produce uniform fibrous mats have been established. After crosslinking treatment of the $PGS_{2:3}$ core, PVA could be partially removed by soaking in hot water, resulting in a fibrous network of $PGS_{2:3}$. In a water-saturated condition, the spun porous $PGS_{2:3}$ fibrous mats demonstrated soft-tissue-like mechanical properties with J-shaped, elastic stress-strain curves. The Young's modulus, UTS, rupture elongation, and resilience of this spun PGS in wet condition were 1.1

MPa, 1.5 MPa, 98 %, and 0.95, respectively. *In vitro* evaluations indicated that the fabrication of the $PGS_{2:3}$ fibrous mats using the core/shell electrospinning technique had excellent biocompatibility which is as good as standard culture medium and PLLA material. The combination of soft, elastomeric mechanical properties and excellent cytocompatibility make the present $PGS_{2:3}$ fibrous materials very promising for applications in soft tissue engineering.

Chapter 8

Summary and future work

In this project PGS/PLLA fibre mats and $PGS_{2:3}$ fibre mats with non-linear elasticity were successfully fabricated using core/shell electrospinning technology and their mechanical properties, biocompatibility and degradation speeds were improved compared with non-fibrous PGS sheets synthesised according to the standard method [9]. In this Chapter, the major findings from the previous sections of this thesis are summarized, and then a series of recommended future work is discussed.

8.1 Summary

8.1.1 Characterization and cell culture of PGS/PLLA core/shell fibre mats

In Chapter 4, PGS/PLLA core/shell fibre mats (using PGS synthesized from glycerol and sebacic acid with a 1:1 molar ratio) were fabricated using core/shell electrospinning technology and their mechanical properties, biocompatibility and ability in cell culturing were tested. The main conclusions of this chapter are listed below:

1) The miscibility of the PLLA and the PGS solutions was shown to be very low and even if small amount of PLLA was dissolved in PGS, this does not impair the mechanical properties of PGS.
2) The optimal fabrication conditions have been established for electrospinning single component and two component core/shell fibres. A critical parameter for successful core/shell electrospinning is the ratio of the feeding rates of the core and shell solutions. If the ratio of core to shell feeding rates was smaller than 1:10, globules formed in the fibre mats because the low feed flow rate of the core solution caused accumulation of polymer solution on the needle rather than allowing a continuous flow. If the ratio of core to shell feeding rates were larger than 1:3, the amount of shell material was insufficient to fully cover the core and led to an incomplete core/shell structure. However the fibre mats fabricated at a core to shell feeding rate ratio ranging from 1:3 to 1:4 were uniform and had complete core/shell fibre structures.

3) When fabricated under optimal conditions, the PGS/PLLA fibre mats demonstrate soft tissue like mechanical properties with J-shaped, elastic stress-strain curves in tensile test and their UTS, rupture elongation and stiffness constant are 1±0.2 MPa, 25±3% and 18±2, respectively. The above findings are comparable to those of muscular tissues.
4) The results of cytocompatibility tests using either using AlamarBlue^{TM} (measuring the cell proliferation kinetics) or TOX-7 (detecting cytotoxicity) have proved that the biocompatibility of these core/shell fibre mats are as good as control groups.
5) Both human stem-cell-derived cardiomyocytes and enteric neural crest progenitor cells were successfully cultured on PGS/PLLA fibre mats. In addition, this material was capable of supporting optimal functional activity of hESC-CM for over a month and had the ability to support and foster the growth the ENC progenitor cells.

8.1.2 *In vitro* enzymatic degradation of PGS/PLLA core/shell fibre mats

A major problem associated with PGS is its rapid degradation rate, and the *in vivo* degradation rates of PGS have been found to be much faster than *in vitro* degradation due to the enzymatic activity *in vivo*. In Chapter 5, the *in vitro* degradation of PGS/PLLA fibre mats with and without enzymes were investigated and compared with pure PGS sheets. The degradation study was conducted over five weeks and the degradation rate was monitored by specimen weight loss, solution pH decrease and specimen thickness decrease. The main findings were as follows:

1) The presence of enzyme (esterase) significantly increased the degradation of PGS resulting in an increase in the weight loss from 7.7% to 61.7%. The enhanced weight loss of PGS cultured in medium and in the presence of enzyme is consistent with the high degradation speed reported *in vivo*. In contrast, the effect of enzyme on PGS/PLLA fibre mats was quite limited and the weight loss only increased from 3.9% to 4.7% after enzyme was added. Taking into account the larger surface area of porous PGS/PLLA fibre mats, the degradation properties of PGS/PLLA fibre mats were dramatically reduced compared with pure PGS.
2) The results of weight loss, pH reduction and thickness decrease monitored during the degradation of PGS were consistent. But the thickness of PGS/PLLA fibre mats decreased by 28% or 37% after exposure to culture medium or medium with enzyme,

respectively. These results are much larger than the weight losses of only 3.9% and 4.7% noted above. This indicates that the porous mats had become more compact during culture medium treatment.

8.1.3 Characterization of aligned PGS/PLLA core/shell fibre mats

PGS/PLLA core/shell fibre mats with various degrees of alignment were produced using a rotating mandrel with surface speeds of 0, 80, 160, 240 and 320 m/min. The alignment of the fibre mat was measured by the angle standard deviation, where the angle was measured as the departure of the fibres from the rotation direction. These results indicated that an increase in the collection speed from 0 to 320m/min reduced the angle standard deviation from 45° to 27°. At the same time the increase in collection rotational speed also slightly reduced the fibre diameter from 2.5 μm at 0m/min to 2.1 μm at 320 m/min. In mechanical properties tests, the fibre mats all showed J-shaped stress-strain curves and had good resilience, irrespective of the degree of alignment. However, with an increase of the fibre alignment, the stiffness constant of the fibre mats was increased from 9.3 to 15.9 MPa while the UTS, elongation and resilience were first increased with alignment then slightly decreased. The UTS was increased from 2.2 MPa at 0 m/min to 4.5MPa at 240 m/s then decreased to 3.8 MPa when collected at 340 m/min. Rupture elongation and resilience were first raised with the extent of alignment, varying from 25% and 64%, respectively for fibre mats collected at 0 m/min to maximum 53% and 68% for fibre mats collected at 160 m/min. However the UTS and elongation then decreased to 19% and 60%, respectively for fibre mats collected at 360m/min. Thus, PGS/PLLA fibrous mats with a wide range of mechanical properties were produced which could meet the requirements of a variety of soft tissue applications.

8.1.4 Fabrication and characterization of porous $PGS_{2:3}$ mats made by $PGS_{2:3}$/PVA core/shell electrospinning

Porous $PGS_{2:3}$ fibre mats (synthesized from glycerol and sebacic acid with a 2:3 molar ratio) was fabricated using water soluble PVA as an alternative and a better option than PLLA for the shell polymer, because the PVA shell can be dissolved in water with minimal swelling to the core PGS, whereas PLLA requires dissolution in organic solvents. The optimised electrospinning condition for $PGS_{2:3}$/PVA core shell electrospinning were 12 g PVA (M_W 89,000-98,000) per 100ml water/DMF (4:1) co-solvent as the shell solution, 100g prepolymer $PGS_{2:3}$ per 100ml THF as the core solution, core/shell feeding rates of 0.2:1.2 ml/h, 17kV accelerating voltage, and 18 cm collection distance. After curing, the PVA shell could be

largely washed off by soaking in hot water (95°C) for 4 hours, resulting in porous fibre mats predominantly composed of $PGS_{2:3}$. Tensile test of these $PGS_{2:3}$ fibre mats were carried out in the dry and wet state (to mimic the potential application in vivo). Under dry conditions, the $PGS_{2:3}$ fibre mats exhibited improved mechanical properties compared with cast $PGS_{2:3}$ sheets. The UTS and elongation were increased from 0.9MPa and 46%, respectively for $PGS_{2:3}$ sheets to 7MPa and 130% for $PGS_{2:3}$ fibre mats in the dry state. In the wet condition, the $PGS_{2:3}$ fibre mats exhibited J-shaped stress-strain curves and excellent elasticity (95% resilience); also its UTS and elongation at break of 1.5MPa and 97%, respectively were improved over those of $PGS_{2:3}$ solid sheets. Cytotoxicity tests indicated that the biocompatibility of these $PGS_{2:3}$ fibre mats were also very good.

8.2 Recommendations for future work

8.2.1 Improvement of the electrospinning conditions

Although $PGS_{2:3}$ fibre mats were fabricated from $PGS_{2:3}$/PVA as described in Chapter 7, the fibre structures for these mats were not uniform. In some places, the fibres were fused together, resulting in a porous structure rather than fibrous structure. The formation of fused regions of the $PGS_{2:3}$ fibre mats might be due to two reasons discussed below.

The fused regions may have occurred because the core/shell fibres were not fully dried before landing on the collector, allowing the PVA shells and even the uncrosslinked PGS cores to fuse together. This problem may be minimized by identifying a more volatile solvent mixture for the PVA and by decreasing the environment humidity by purging the electrospinning chamber with nitrogen to increase the drying speed. Also collection of $PGS_{2:3}$/PVA fibres using a rotating mandrel (as was used in the PGS/PLLA core/shell studies) may increase the solvent evaporation by turbulence caused during mandrel spinning, and also allow fabrication of aligned fibre mats.

However, the presence of the fused fibre regions may be caused by grafting reactions between PVA (which contains hydroxyl side-groups) and PGS (contains carboxyl and ester groups) during crosslinking process. Other water soluble polymers (for example polyvinylpyrrolidone) with a melting point which is high enough to resist flow at the PGS curing could be used to replace PVA. Alternatively, this problem could be solved by use of a different crosslinking processes for the PGS which does not require high temperature curing. Examples of this are incorporation of acrylate groups in the PGS which can be

photopolymerized at room temperature, or use of crosslinking agent which couples free alcohol such as isocyanides, and these methods could be applied to crosslink PGS without triggering reactions between PGS and PVA.

8.2.2 Possible future work on the degradation kinetics

The degradation rates of $PGS_{2:3}$ fibre mats have not been evaluated, however due to its higher crosslink density, the degradation of $PGS_{2:3}$ should be slower than PGS synthesized with a monomer ratio 1:1.

Although the PGS/PLLA fibre mats showed excellent degradation resistance after 5 weeks of exposure to culture medium, the general healing process for soft tissue usually lasts for over a year and occurs under cyclic tensile conditions. Thus, investigations of the degradation of these fibre mats for longer periods and under cyclic culture conditions would be an interesting extension to the present work.

8.2.2 Studies of the mechanical and cell response to $PGS_{2:3}$/PVA fibre mats

In this project, the $PGS_{2:3}$/PVA core/shell fibre mats were developed as a way of obtaining near-pure $PGS_{2:3}$ fibre mats. However, in the biological environment the PVA shell would be hydrated and highly plasticized and so it may be unnecessary to remove it from the fibres. Thus studies of the mechanical and cell response to PGS2:3/PVA fibre mats would be an interesting investigation.

8.2.3 Extension of cell culture work and *in vivo* studies

In this project, $PGS_{2:3}$/PLLA fibre mats with a wide range of mechanical properties have been fabricated, and these materials have the potential to be used in various soft tissues engineering such as tendon, ligament, lung epithelium, neural tissue and vascular tissue. But up to now, only hESC-derived cardiomyocytes and ENC cells have been cultured on these fibrous materials. Also no cell culture work has been done on aligned PGS/PLLA fibre mats. Since the aligned fibre mats could mimic the 3D anisotropic structure of natural ECM, aligned fibre mats may guide the growth and increase the alignment of cells cultured on them. So extending the study to the *in vivo* performance of oriented fibrous mats could lead to promising developments.

8.2.4 Development of additional electrospun core/shell polymer systems

In this work, PGS has been successfully used as the core material and we have fabricated core/shell fibre mats with desirable elasticity. However PGS is not the only member from the PPS family, and so other crosslinked elastomers that could not be fabricated into fibres using the conventional electrospinning process could be used as the core in core/shell electrospinning and provide required elasticity in the resultant fibre mats. Also besides PLLA and PVA, other widely used biodegradable thermoplastic polymer such as polyglycolides and polyvinylpyrrolidone could be used as the shell materials also. By changing the combination of core and shell materials, elastic fibre mats with predicable mechanical properties and degradation properties could be made.

References

1. Beachley, V., Katsanevakis, E., Zhang, N., and Wen, X., *Highly Aligned Polymer Nanofiber Structures: Fabrication and Applications in Tissue Engineering*, in *Biomedical Applications of Polymeric Nanofibers*, R. Jayakumar and S. Nair, Editors. 2012, Springer Berlin Heidelberg. p. 171-212.
2. Lee, C.H., Shin, H.J., Cho, I.H., Kang, Y.M., Kim, I.A., Park, K.D., and Shin, J.W., *Nanofiber alignment and direction of mechanical strain affect the ECM production of human ACL fibroblast.* Biomaterials, 2005. **26**(11): p. 1261-1270.
3. Mirsky, I. and Parmley, W.W., *Assessment of passive elastic stiffness for isolated heart muscle and the intact heart.* Circulation Research, 1973. **33**(2): p. 233-243.
4. Chen, Q.-Z., Harding, S.E., Ali, N.N., Lyon, A.R., and Boccaccini, A.R., *Biomaterials in cardiac tissue engineering: Ten years of research survey.* Materials Science and Engineering: R: Reports, 2008. **59**(1-6): p. 1-37.
5. Freed, L.E., Engelmayr, G.C., Jr., Borenstein, J.T., Moutos, F.T., and Guilak, F., *Advanced Material Strategies for Tissue Engineering Scaffolds.* Advanced Materials, 2009. **21**(32-33): p. 3410-3418.
6. Freed, L.E., Guilak, F., Guo, X.E., Gray, M.L., Tranquillo, R., Holmes, J.W., Radisic, M., Sefton, M.V., Kaplan, D., and Vunjak-Novakovic, G., *Advanced tools for tissue engineering: Scaffolds, bioreactors, and signaling.* Tissue engineering, 2006. **12**(12): p. 3285-3305.
7. Wang, Y., Ameer, G.A., Sheppard, B.J., and Langer, R., *A tough biodegradable elastomer.* Nat Biotech, 2002. **20**(6): p. 602-606.
8. Bettinger, C.J., Orrick, B., Misra, A., Langer, R., and Borenstein, J.T., *Microfabrication of poly (glycerol-sebacate) for contact guidance applications.* Biomaterials, 2006. **27**(12): p. 2558-2565.
9. Chen, Q.-Z., Bismarck, A., Hansen, U., Junaid, S., Tran, M.Q., Harding, S.E., Ali, N.N., and Boccaccini, A.R., *Characterisation of a soft elastomer poly(glycerol sebacate) designed to match the mechanical properties of myocardial tissue.* Biomaterials, 2008. **29**(1): p. 47-57.
10. Wang, Y.D., Kim, Y.M., and Langer, R., *In vivo degradation characteristics of poly(glycerol sebacate).* Journal of Biomedical Materials Research Part A, 2003. **66A**(1): p. 192-197.
11. Stuckey, D.J., Ishii, H., Chen, Q.Z., Boccaccini, A.R., Hansen, U., Carr, C.A., Roether, J.A., Jawad, H., Tyler, D.J., Ali, N.N., Clarke, K., and Harding, S.E., *Magnetic resonance imaging evaluation of remodeling by cardiac elastomeric tissue scaffold biomaterials in a rat model of myocardial infarction.* Tissue Engineering - Part A, 2010. **16**(11): p. 3395-3402.
12. Chen, Q., Liang, S., and Thouas, G.A., *Elastomeric biomaterials for tissue engineering.* Progress in Polymer Science, 2013. **38**(3-4): p. 584-671.
13. Yi, F. and LaVan, D.A., *Poly(glycerol sebacate) Nanofiber Scaffolds by Core/Shell Electrospinning.* Macromolecular Bioscience, 2008. **8**(9): p. 803-806.
14. Ravichandran, R., Venugopal, J.R., Sundarrajan, S., Mukherjee, S., and Ramakrishna, S., *Poly(Glycerol Sebacate)/Gelatin Core/Shell Fibrous Structure for Regeneration of Myocardial Infarction.* Tissue Engineering Part A, 2011. **17**(9-10): p. 1363-1373.
15. Langer, R. and Vacanti, J.P., *Tissue engineering. (methods of replacing or substituting for damaged or diseased tissues).* Science, 1993. **v260**(n5110): p. p920(7).

16. Kusama, K., Donegan, W., and Samter, T., *An investigation of colon cancer associated with urinary diversion.* Diseases of the Colon & Rectum, 1989. **32**(8): p. 694-697.
17. Kolff, W.J., Berk, H.T.J., Welle, N.M., van der Ley, A.J.W., van Dijk, E.C., and van Noordwijk, J., *The Artificial Kidney: a dialyser with a great area.* Acta Medica Scandinavica, 1944. **117**(2): p. 121-134.
18. Murray, J.E., Merrill, J.P., and Harrison, J.H., *Renal Homotransplantation in Identical Twins.* J Am Soc Nephrol, 2001. **12**(1): p. 201-204.
19. Black, K.S. and Dawson, P.E., *Allografts*, in *Encyclopedia of Biomaterials and Biomedical Engineering*2004. p. 11-18.
20. Vacanti, J.P. and Langer, R., *Tissue engineering: the design and fabrication of living replacement devices for surgical reconstruction and transplantation.* Lancet, 1999. **354**: p. SI32-SI34.
21. Li, Y., Thouas, G.A., and Chen, Q.-Z., *Biodegradable soft elastomers: synthesis/properties of materials and fabrication of scaffolds.* RSC Advances, 2012. **2**(22): p. 8229-8242.
22. Niklason, L.E., Gao, J., Abbott, W.M., Hirschi, K.K., Houser, S., Marini, R., and Langer, R., *Functional arteries grown in vitro.* Science, 1999. **284**(5413): p. 489-493.
23. Yang, J., Webb, A.R., Pickerill, S.J., Hageman, G., and Ameer, G.A., *Synthesis and evaluation of poly(diol citrate) biodegradable elastomers.* Biomaterials, 2006. **27**(9): p. 1889-1898.
24. Lu, L.C. and Mikos, A.G., *The importance of new processing techniques in tissue engineering.* Mrs Bulletin, 1996. **21**(11): p. 28-32.
25. Thomas, R.C., Shung, A.K., and Yaszemski, M.J., *Polymer scaffold processing*, in *Principles of Tissue Engineering*, R.P. Lanza, R. Langer, and J.P. Vacanti, Editors. 2000, Academic Press: California, USA. p. 251-262.
26. Widmer, M.S. and Mikos, A.G., *Fabrication of biodegradable polymer scaffolds for tissue engineering*, in *Frontier in Tissue Engineering*, C.W. Patrick Jr, A.G. Mikos, and L.V. Mcintire, Editors. 1998, Elsevier Science: New York. p. 107-120.
27. Atala, A., Lanza, R.P., and (eds), *Methods of Tissue Engineering*, ed. .2002, p.681-740, California: Academic Press.
28. Hutmacher, D.W., *Scaffolds in tissue engineering bone and cartilage.* Biomaterials, 2000. **21**(24): p. 2529-2543.
29. Karageorgiou, V. and Kaplan, D., *Porosity of 3D biormaterial scaffolds and osteogenesis.* Biomaterials, 2005. **26**(27): p. 5474-5491.
30. Du, C., Cui, F.Z., Zhu, X.D., and De Groot, K., *Three-dimensional nano-HAp/collagen matrix loading with osteogenic cells in organ culture.* Journal of Biomedical Materials Research, 1999. **44**(4): p. 407-415.
31. Li, D. and Xia, Y., *Electrospinning of Nanofibers: Reinventing the Wheel?* Advanced Materials, 2004. **16**(14): p. 1151-1170.
32. Yaylaoglu, M.B., Yildiz, C., Korkusuz, F., and Hasirci, V., *A novel osteochondral implant.* Biomaterials, 1999. **20**(16): p. 1513-1520.
33. Christman, K.L. and Lee, R.J., *Biomaterials for the treatment of myocardial infarction.* Journal of the American Collage of Cardiology, 2006. **48**(5): p. 907-913.
34. Seal, B.L., Otero, T.C., and Panitch, A., *Polymeric biomaterials for tissue and organ regeneration.* Materials Science and Engineering: R: Reports, 2001. **34**(4–5): p. 147-230.
35. Vacanti, C.A., Bonassar, L.J., and Vacanti, J.P., *Chapter 47 - Structural Tissue Engineering*, in *Principles of Tissue Engineering (Second Edition)*, P.L. Robert, L.

Robert, R.L. Joseph VacantiA2 - Robert P. Lanza, and V. Joseph, Editors. 2000, Academic Press: San Diego. p. 671-682.
36. Williams, D.F., *Biomaterials and tissue engineering in reconstructive surgery.* Sadhana - Academy Proceedings in Engineering Sciences, 2003. **28**(3-4): p. 563-574.
37. Yang, S., Leong, K.F., Du, Z., and Chua, C.K., *The design of scaffolds for use in tissue engineering. Part 1. Traditional factors.* Tissue engineering, 2001. **7**(6): p. 679-689.
38. Peter, B.M. and Christopher, C.K., *Bioabsorbable implant material review.* Operative Techniques in Sports Medicine, 2004. **12**(3): p. 158-160.
39. Bursac, N., Papadaki, M., Cohen, R.J., Schoen, F.J., Eisenberg, S.R., Carrier, R., Vunjak-Novakovic, G., and Freed, L.E., *Cardiac muscle tissue engineering: toward an in vitro model for electrophysiological studies*. Vol. 277. 1999. H433-H444.
40. Middleton, J.C. and Tipton, A.J., *Synthetic biodegradable polymers as orthopedic devices.* Biomaterials, 2000. **21**(23): p. 2335-2346.
41. Cooper, J.A., Lu, H.H., Ko, F.K., Freeman, J.W., and Laurencin, C.T., *Fiber-based tissue-engineered scaffold for ligament replacement: design considerations and in vitro evaluation.* Biomaterials, 2005. **26**(13): p. 1523-1532.
42. Miller, R.A., Brady, J.M., and Cutright, D.E., *Degradation rates of oral resorbable implants (polylactates and polyglycolates): Rate modification with changes in PLA/PGA copolymer ratios.* Journal of Biomedical Materials Research, 1977. **11**(5): p. 711-719.
43. Nair, L.S. and Laurencin, C.T., *Biodegradable polymers as biomaterials.* Progress in Polymer Science, 2007. **32**(8-9): p. 762-798.
44. Shin, M., Ishii, O., Sueda, T., and Vacanti, J.P., *Contractile cardiac grafts using a novel nanofibrous mesh.* Biomaterials, 2004. **25**(17): p. 3717-3723.
45. Stankus, J.J., Guan, J., Fujimoto, K., and Wagner, W.R., *Microintegrating smooth muscle cells into a biodegradable, elastomeric fiber matrix.* Biomaterials, 2006. **27**(5): p. 735-744.
46. Nagata, M., Machida, T., Sakai, W., and Tsutsumi, N., *Synthesis, characterization, and enzymatic degradation of network aliphatic copolyesters.* Journal of Polymer Science Part A: Polymer Chemistry, 1999. **37**(13): p. 2005-2011.
47. Martin, D.P. and Williams, S.F., *Medical applications of poly-4-hydroxybutyrate: a strong flexible absorbable biomaterial.* Biochemical Engineering Journal, 2003. **16**(2): p. 97-105.
48. Chen, Q., Zhu, C., and Thouas, G., *Progress and challenges in biomaterials used for bone tissue engineering: bioactive glasses and elastomeric composites.* Progress in Biomaterials, 2012. **1**(1): p. 2.
49. Doi, Y., *Biotechnology: Unnatural biopolymers.* Nat Mater, 2002. **1**(4): p. 207-208.
50. Engelmayr, G.C., Cheng, M., Bettinger, C.J., Borenstein, J.T., Langer, R., and Freed, L.E., *Accordion-like honeycombs for tissue engineering of cardiac anisotropy.* Nat Mater, 2008. **7**(12): p. 1003-1010.
51. Lu, L.C. and Mikos, A.G., *Poly (lactic acid),* in *Polymer data handbook*, J.E. Mark, Editor 1999, Oxford Press: Oxford. p. 527-33.
52. Webb, A.R., Yang, J., and Ameer, G.A., *Biodegradable polyester elastomers in tissue engineering.* Expert Opinion on Biological Therapy, 2004. **4**(6): p. 801-812.
53. Narine, S.S., Kong, X., Bouzidi, L., and Sporns, P., *Physical properties of polyurethanes produced from polyols from seed oils: I. Elastomers.* JAOCS, Journal of the American Oil Chemists' Society, 2007. **84**(1): p. 55-63.
54. Gosline, J., Lillie, M., Carrington, E., Guerette, P., Ortlepp, C., and Savage, K., *Elastic proteins: Biological roles and mechanical properties.* Philosophical

Transactions of the Royal Society B: Biological Sciences, 2002. **357**(1418): p. 121-132.
55. Amler, E., Mickova, A., and Buzgo, M., *Electrospun core/shell nanofibers: A promising system for cartilage and tissue engineering?* Nanomedicine, 2013. **8**(4): p. 509-512.
56. Ramakrishna, S., Fujihara, k., Teo, W.E., Lim, T.C., and Ma, Z.W., *An introduction to electrospinning and nanofibers*2005: Singapore: World Scientific.
57. Casper, C.L., Stephens, J.S., Tassi, N.G., Chase, D.B., and Rabolt, J.F., *Controlling Surface Morphology of Electrospun Polystyrene Fibers: Effect of Humidity and Molecular Weight in the Electrospinning Process.* Macromolecules, 2003. **37**(2): p. 573-578.
58. Shanmuganathan, K., Sankhagowit, R.K., Iyer, P., and Ellison, C.J., *Thiol–Ene Chemistry: A Greener Approach to Making Chemically and Thermally Stable Fibers.* Chemistry of Materials, 2011. **23**(21): p. 4726-4732.
59. Lyons, J., Li C., Ko F., *Melt-electrospinning part 1: processing parameters and geometric properties.* polymer, 2004. **45**: p. 7597-7603.
60. Son, W.K., Youk, J.H., Lee, T.S., and Park, W.H., *The effects of solution properties and polyelectrolyte on electrospinning of ultrafine poly(ethylene oxide) fibers.* Polymer, 2004. **45**(9): p. 2959-2966.
61. Dersch, R., Steinhart, M., Boudriot, U., Greiner, A., and Wendorff, J.H., *Nanoprocessing of polymers: applications in medicine, sensors, catalysis, photonics.* Polymers for Advanced Technologies, 2005. **16**(2-3): p. 276-282.
62. Bognitzki, M., Czado, W., Frese, T., Schaper, A., Hellwig, M., Steinhart, M., Greiner, A., and Wendorff, J.H., *Nanostructured Fibers via Electrospinning.* Advanced Materials, 2001. **13**(1): p. 70-72.
63. Ou, K.-L., Chen, C.-S., Lin, L.-H., Lu, J.-C., Shu, Y.-C., Tseng, W.-C., Yang, J.-C., Lee, S.-Y., and Chen, C.-C., *Membranes of epitaxial-like packed, super aligned electrospun micron hollow poly(l-lactic acid) (PLLA) fibers.* European Polymer Journal, 2011. **47**(5): p. 882-892.
64. Caruso, R.A., Schattka, J.H., and Greiner, A., *Titanium dioxide tibes from sol-gel coating of electrospun polymer fibers.* Advanced Materials, 2001. **13**(20): p. 1577-1579.
65. Tsuji, H., Nakano, M., Hashimoto, M., Takashima, K., Katsura, S., and Mizuno, A., *Electrospinning of Poly(lactic acid) Stereocomplex Nanofibers.* Biomacromolecules, 2006. **7**(12): p. 3316-3320.
66. Sun, B., Duan, B., and Yuan, X., *Preparation of core/shell PVP/PLA ultrafine fibers by coaxial electrospinning.* Journal of Applied Polymer Science, 2006. **102**(1): p. 39-45.
67. Buchko, C.J., Chen, L.C., Shen, Y., and Martin, D.C., *Processing and microstructural characterization of porous biocompatible protein polymer thin films.* Polymer, 1999. **40**(26): p. 7397-7407.
68. Shenoy, S.L., Bates, W.D., Frisch, H.L., and Wnek, G.E., *Role of chain entanglements on fiber formation during electrospinning of polymer solutions: good solvent, non-specific polymer–polymer interaction limit.* Polymer, 2005. **46**(10): p. 3372-3384.
69. Kameoka, J., Czaplewski, D., Liu, H., and Craighead, H.G., *Polymeric nanowire architecture.* Journal of Materials Chemistry, 2004. **14**(10): p. 1503-1505.
70. Megelski, S., Stephens, J.S., Chase, D.B., and Rabolt, J.F., *Micro- and Nanostructured Surface Morphology on Electrospun Polymer Fibers.* Macromolecules, 2002. **35**(22): p. 8456-8466.

71. Shim, I.K., Jung, M.R., Kim, K.H., Seol, Y.J., Park, Y.J., Park, W.H., and Lee, S.J., *Novel three-dimensional scaffolds of poly(L-lactic acid) microfibers using electrospinning and mechanical expansion: Fabrication and bone regeneration.* Journal of Biomedical Materials Research Part B: Applied Biomaterials, 2010. **95B**(1): p. 150-160.
72. Demir, M.M., Yilgor, I., Yilgor, E., and Erman, B., *Electrospinning of polyurethane fibers.* Polymer, 2002. **43**(11): p. 3303-3309.
73. Reneker, D.H., Yarin, A.L., Fong, H., and Koombhongse, S., *Bending instability of electrically charged liquid jets of polymer solutions in electrospinning.* Journal of Applied Physics, 2000. **87**(9): p. 4531-4547.
74. Zhao, S., Wu, X., Wang, L., and Huang, Y., *Electrospinning of ethyl–cyanoethyl cellulose/tetrahydrofuran solutions.* Journal of Applied Polymer Science, 2004. **91**(1): p. 242-246.
75. Supaphol, P., Mit-Uppatham, C., and Nithitanakul, M., *Ultrafine electrospun polyamide-6 fibers: Effect of emitting electrode polarity on morphology and average fiber diameter.* Journal of Polymer Science Part B: Polymer Physics, 2005. **43**(24): p. 3699-3712.
76. Hao, F., *Electrospun nylon 6 nanofiber reinforced BIS-GMA/TEGDMA dental restorative composite resins.* Polymer, 2004. **45**(7): p. 2427-2432.
77. Zeng, J., Xu, X., Chen, X., Liang, Q., Bian, X., Yang, L., and Jing, X., *Biodegradable electrospun fibers for drug delivery.* Journal of Controlled Release, 2003. **92**(3): p. 227-231.
78. Huang, Z.-M., Zhang, Y.Z., Ramakrishna, S., and Lim, C.T., *Electrospinning and mechanical characterization of gelatin nanofibers.* Polymer, 2004. **45**(15): p. 5361-5368.
79. Zong, X.H., Kim, K., Fang, D.F., Ran, S.F., Hsiao, B.S., and Chu, B., *Structure and process relationship of electrospun bioabsorbable nanofiber membranes.* Polymer, 2002. **43**(16): p. 4403-4412.
80. Tong, L., Hongxia, W., Huimin, W., and Xungai, W., *The charge effect of cationic surfactants on the elimination of fibre beads in the electrospinning of polystyrene.* Nanotechnology, 2004. **15**(9): p. 1375.
81. Deitzel, J.M., Kleinmeyer, J., Harris, D., and Beck Tan, N.C., *The effect of processing variables on the morphology of electrospun nanofibers and textiles.* Polymer, 2001. **42**(1): p. 261-272.
82. Demir, M.M., Gulgun, M.A., Menceloglu, Y.Z., Erman, B., Abramchuk, S.S., Makhaeva, E.E., Khokhlov, A.R., Matveeva, V.G., and Sulman, M.G., *Palladium Nanoparticles by Electrospinning from Poly(acrylonitrile-co-acrylic acid)−PdCl2 Solutions. Relations between Preparation Conditions, Particle Size, and Catalytic Activity.* Macromolecules, 2004. **37**(5): p. 1787-1792.
83. Mo, X.M., Xu, C.Y., Kotaki, M., and Ramakrishna, S., *Electrospun P(LLA-CL) nanofiber: a biomimetic extracellular matrix for smooth muscle cell and endothelial cell proliferation.* Biomaterials, 2004. **25**(10): p. 1883-1890.
84. Lee, J.S., Choi, K.H., Do Ghim, H., Kim, S.S., Chun, D.H., Kim, H.Y., and Lyoo, W.S., *Role of molecular weight of atactic poly(vinyl alcohol) (PVA) in the structure and properties of PVA nanofabric prepared by electrospinning.* Journal of Applied Polymer Science, 2004. **93**(4): p. 1638-1646.
85. Yarin, A.L., *Coaxial electrospinning and emulsion electrospinning of core-shell fibers.* Polymers for Advanced Technologies, 2011. **22**(3): p. 310-317.
86. Lukáš, D., Sarkar, A., Martinová, L., Vodsed'álková, K., Lubasová, D., Chaloupek, J., Pokorný, P., Mikeš, P., Chvojka, J., and Komárek, M., *Physical principles of*

electrospinning (electrospinning as a nano-scale technology of the twenty-first century). Textile Progress, 2009. **41**(2): p. 59-140.
87. Bazilevsky, A.V., Yarin, A.L., and Megaridis, C.M., *Co-electrospinning of Core−Shell Fibers Using a Single-Nozzle Technique.* Langmuir, 2007. **23**(5): p. 2311-2314.
88. Zhang, Y., Huang, Z.-M., Xu, X., Lim, C.T., and Ramakrishna, S., *Preparation of Core−Shell Structured PCL-r-Gelatin Bi-Component Nanofibers by Coaxial Electrospinning.* Chemistry of Materials, 2004. **16**(18): p. 3406-3409.
89. Li, Y., Thouas, G.A., and Chen, Q., *Novel elastomeric fibrous networks produced from poly(xylitol sebacate)2:5 by core/shell electrospinning: Fabrication and mechanical properties.* Journal of the Mechanical Behavior of Biomedical Materials, 2014. **40**(0): p. 210-221.
90. Wang, C., Yan, K.-W., Lin, Y.-D., and Hsieh, P.C.H., *Biodegradable Core/Shell Fibers by Coaxial Electrospinning: Processing, Fiber Characterization, and Its Application in Sustained Drug Release.* Macromolecules, 2010. **43**(15): p. 6389-6397.
91. Kayaci, F., Ozgit-Akgun, C., Donmez, I., Biyikli, N., and Uyar, T., *Polymer-inorganic core-shell nanofibers by electrospinning and atomic layer deposition: Flexible nylon-ZnO core-shell nanofiber mats and their photocatalytic activity.* ACS Applied Materials and Interfaces, 2012. **4**(11): p. 6185-6194.
92. Li, X.H., Shao, C.L., and Liu, Y.C., *A Simple Method for Controllable Preparation of Polymer Nanotubes via a Single Capillary Electrospinning.* Langmuir, 2007. **23**(22): p. 10920-10923.
93. Zhang, J.-F., Yang, D.-Z., Xu, F., Zhang, Z.-P., Yin, R.-X., and Nie, J., *Electrospun Core−Shell Structure Nanofibers from Homogeneous Solution of Poly(ethylene oxide)/Chitosan.* Macromolecules, 2009. **42**(14): p. 5278-5284.
94. Angeles, M., Cheng, H.-L., and Velankar, S.S., *Emulsion electrospinning: composite fibers from drop breakup during electrospinning.* Polymers for Advanced Technologies, 2008. **19**(7): p. 728-733.
95. Lisunova, M., Hildmann, A., Hatting, B., Datsyuk, V., and Reich, S., *Nanofibres of CA/PAN with high amount of carbon nanotubes by core-shell electrospinning.* Composites Science and Technology, 2010. **70**(11): p. 1584-1588.
96. Li, D., Wang, Y., and Xia, Y., *Electrospinning of polymeric and ceramic nanofibers as uniaxially aligned arrays.* Nano Letters, 2003. **3**(8): p. 1167-1171.
97. Jalili, R., Morshed, M., and Ravandi, S.A.H., *Fundamental parameters affecting electrospinning of PAN nanofibers as uniaxially aligned fibers.* Journal of Applied Polymer Science, 2006. **101**(6): p. 4350-4357.
98. Edwards, M.D., Mitchell, G.R., Mohan, S.D., and Olley, R.H., *Development of orientation during electrospinning of fibres of poly(e-caprolactone).* European Polymer Journal, 2010. **46**(6): p. 1175-1183.
99. Wang, H.B., Mullins, M.E., Cregg, J.M., Hurtado, A., Oudega, M., Trombley, M.T., and Gilbert, R.J., *Creation of highly aligned electrospun poly-L-lactic acid fibers for nerve regeneration applications.* Journal of Neural Engineering, 2009. **6**(1): p. 016001.
100. Kharaziha, M., Nikkhah, M., Shin, S.R., Annabi, N., Masoumi, N., Gaharwar, A.K., Camci-Unal, G., and Khademhosseini, A., *PGS:Gelatin nanofibrous scaffolds with tunable mechanical and structural properties for engineering cardiac tissues.* Biomaterials, 2013. **34**(27): p. 6355-6366.
101. Li, W.-J., Mauck, R.L., Cooper, J.A., Yuan, X., and Tuan, R.S., *Engineering controllable anisotropy in electrospun biodegradable nanofibrous scaffolds for*

musculoskeletal tissue engineering. Journal of Biomechanics, 2007. **40**(8): p. 1686-1693.
102. Ayres, C., Bowlin, G.L., Henderson, S.C., Taylor, L., Shultz, J., Alexander, J., Telemeco, T.A., and Simpson, D.G., *Modulation of anisotropy in electrospun tissue-engineering scaffolds: Analysis of fiber alignment by the fast Fourier transform.* Biomaterials, 2006. **27**(32): p. 5524-5534.
103. Shang, S., Yang, F., Cheng, X., Frank Walboomers, X., and Jansen, J.A., *The effect of electrospun fibre alignment on the behaviour of rat periodontal ligament cells.* European Cells and Materials, 2010. **19**: p. 180-192.
104. Alexander, J.K., Fuss, B., and Colello, R.J., *Electric field-induced astrocyte alignment directs neurite outgrowth.* Neuron Glia Biology, 2006. **2**(2): p. 93-103.
105. Karlon, W.J., Hsu, P.P., Song, L.I., Chien, S., McCulloch, A.D., and Omens, J.H., *Measurement of Orientation and Distribution of Cellular Alignment and Cytoskeletal Organization.* Annals of Biomedical Engineering, 1999. **27**(6): p. 712-720.
106. Fisher, N., I., *Statistical analysis of circular data*, 1993, Cambridge University Press: New York.
107. Mirsky, I., *Assessment of passive elastic stiffness of cardiac muscle: mathematical concepts, physiologic and clinical considerations, directions of future research.* Progress in Cardiovascular Diseases, 1976. **18**(4): p. 277-308.
108. Chen, Q.Z., Liang, S.L., and Thouas, G.A., *Synthesis and characterisation of poly(glycerol sebacate)-co-lactic acid as surgical sealants.* Soft Matter, 2011. **7**(14): p. 6484-6492.
109. Liang, S.-L., Cook, W.D., Thouas, G.A., and Chen, Q.-Z., *The mechanical characteristics and in vitro biocompatibility of poly(glycerol sebacate)-Bioglass® elastomeric composites.* Biomaterials, 2010. **31**(33): p. 8516-8529.
110. Chen, Q.Z., Jin, L.Y., Cook, W.D., Mohn, D., Lagerqvist, E.L., Elliott, D.A., Haynes, J.M., Boyd, N., Stark, W.J., Pouton, C.W., Stanley, E.G., and Elefanty, A.G., *Elastomeric nanocomposites as cell delivery vehicles and cardiac support devices.* Soft Matter, 2010. **6**(19): p. 4715-4726.
111. Li, Y., Cook, W.D., Moorhoff, C., Huang, W.C., and Chen, Q.Z., *Synthesis, characterization and properties of biocompatible poly(glycerol sebacate) pre-polymer and gel.* Polymer International, 2013. **62**(4): p. 534-547.
112. Gupta, P., Elkins, C., Long, T.E., and Wilkes, G.L., *Electrospinning of linear homopolymers of poly(methyl methacrylate): exploring relationships between fiber formation, viscosity, molecular weight and concentration in a good solvent.* Polymer, 2005. **46**(13): p. 4799-4810.
113. Tiwari, S.K. and Venkatraman, S.S., *Importance of viscosity parameters in electrospinning: Of monolithic and core–shell fibers.* Materials Science and Engineering: C, 2012. **32**(5): p. 1037-1042.
114. Pinner, S.H., *A ractical course in Polymer Chemistry*1961, New York: Pergamon Press.
115. Veress, A.I., Gullberg, G.T., and Weiss, J.A., *Measurement of strain in the left ventricle during diastole with cine-MRI and deformable image registration.* Journal of Biomechanical Engineering-Transactions of the Asme, 2005. **127**(7): p. 1195-1207.
116. Lv, S., Dudek, D.M., Cao, Y., Balamurali, M.M., Gosline, J., and Li, H.B., *Designed biomaterials to mimic the mechanical properties of muscles.* Nature, 2010. **465**(7294): p. 69-73.
117. Flory, P.J., *Principles of polymer chemistry*, 1953, Ithaca: Cornell Univ. Pr.
118. Bellingham, C.M., Lillie, M.A., Gosline, J.M., Wright, G.M., Starcher, B.C., Bailey, A.J., Woodhouse, K.A., and Keeley, F.W., *Recombinant human elastin polypeptides*

self-assemble into biomaterials with elastin-like properties. Biopolymers, 2003. **70**(4): p. 445-455.
119. Fung, Y.C.B., *Elasticity of soft tissues in simple elongation.* American Journal of Physiology, 1967. **213**(6): p. 1532-1544.
120. Stromberg, D.D. and Wiederhi, C.A., *Viscoelastic description of a collagenous tissue in simple elongation.* Journal of Applied Physiology, 1969. **26**(6): p. 857-862.
121. Haut, R.C. and Little, R.W., *A constitutive equation for collagen fibers.* Journal of Biomechanics, 1972. **5**(5): p. 423-424,IN1,425-430.
122. Mirsky, I., Cohn, P.F., Levine, J.A., Gorlin, R., Herman, M.V., Kreulen, T.H., and Sonnenblick, E.H., *Assessment of left ventricular stiffness in primary myocardial disease and coronary artery disease.* Circulation, 1974. **50**(1): p. 128-136.
123. Fester, A. and Samet, P., *Passive elasticity of the human left ventricle. The 'parallel elastic element'.* Circulation, 1974. **50**(3): p. 609-618.
124. Takaoka, H., Esposito, G., Mao, L., Suga, H., and Rockman, H.A., *Heart size-independent analysis of myocardial function in murine pressure overload hypertrophy.* American Journal of Physiology-Heart and Circulatory Physiology, 2002. **282**(6): p. H2190-H2197.
125. Liang, S., Cook, W.D., and Chen, Q., *Physical characterization of poly(glycerol sebacate)/Bioglass® composites.* Polymer International, 2012. **61**(1): p. 17-22.
126. Chen, Q.-Z., Ishii, H., Thouas, G.A., Lyon, A.R., Wright, J.S., Blaker, J.J., Chrzanowski, W., Boccaccini, A.R., Ali, N.N., Knowles, J.C., and Harding, S.E., *An elastomeric patch derived from poly(glycerol sebacate) for delivery of embryonic stem cells to the heart.* Biomaterials, 2010. **31**(14): p. 3885-3893.
127. Chen, Q.-Z., Li, Y., Jin, L.-Y., Quinn, J.M.W., and Komesaroff, P.A., *A new sol–gel process for producing Na2O-containing bioactive glass ceramics.* Acta Biomaterialia, 2010. **6**(10): p. 4143-4153.
128. Nishiyama, C., Uesaka, T., Manabe, T., Yonekura, Y., Nagasawa, T., Newgreen, D.F., Young, H.M., and Enomoto, H., *Trans-mesenteric neural crest cells are the principal source of the colonic enteric nervous system.* Nature Neuroscience, 2012. **15**(9): p. 1211-1218.
129. Chen, Q., Yang, X., and Li, Y., *A comparative study on in vitro enzymatic degradation of poly(glycerol sebacate) and poly(xylitol sebacate).* RSC Advances, 2012. **2**(10): p. 4125-4134.
130. Li, Y., Thouas, G.A., Shi, H., and Chen, Q., *Enzymatic and oxidative degradation of poly(polyol sebacate).* Journal of Biomaterials Applications, 2013.
131. Liang, S.-L., Yang, X.-Y., Fang, X.-Y., Cook, W.D., Thouas, G.A., and Chen, Q.-Z., *In Vitro enzymatic degradation of poly (glycerol sebacate)-based materials.* Biomaterials, 2011. **32**(33): p. 8486-8496.
132. Bettinger, C.J., Weinberg, E.J., Kulig, K.M., Vacanti, J.P., Wang, Y., Borenstein, J.T., and Langer, R., *Three-dimensional microfluidic tissue-engineering scaffolds using a flexible biodegradable polymer.* Advanced Materials, 2006. **18**(2): p. 165-169.
133. Sun, Z.C., Zussman, E., Yarin, A.L., Wendorff, J.H., and Greiner, A., *Compound core-shell polymer nanofibers by co-electrospinning.* Advanced Materials, 2003. **15**(22): p. 1929-+.
134. Zhang, Y.Z., Huang, Z.M., Xu, X.J., Lim, C.T., and Ramakrishna, S., *Preparation of core-shell structured PCL-r-gelatin Bi-component nanofibers by coaxial electrospinning.* Chemistry of Materials, 2004. **16**(18): p. 3406-3409.
135. Jiang, H.L., Hu, Y.Q., Zhao, P.C., Li, Y., and Zhu, K.J., *Modulation of protein release from biodegradable core-shell structured fibers prepared by coaxial*

electrospinning. Journal of Biomedical Materials Research Part B-Applied Biomaterials, 2006. **79B**(1): p. 50-57.
136. Anseth, K.S., Shastri, V.R., and Langer, R., *Photopolymerizable degradable polyanhydrides with osteocompatibility.* Nat Biotech, 1999. **17**(2): p. 156-159.
137. Malberg, S., Basalp, D., Finne-Wistrand, A., and Albertsson, A.C., *Bio-Safe Synthesis of Linear and Branched PLLA.* Journal of Polymer Science Part a-Polymer Chemistry, 2010. **48**(5): p. 1214-1219.
138. Sun, Z.-J., Wu, L., Huang, W., Zhang, X.-L., Lu, X.-L., Zheng, Y.-F., Yang, B.-F., and Dong, D.-L., *The influence of lactic on the properties of Poly (glycerol–sebacate–lactic acid).* Materials Science and Engineering: C, 2009. **29**(1): p. 178-182.
139. Rowland, S.P., Brannan, M.A.F., Janssen, H.J., and Pittman, P.F., *A kinetic analysis of the reactivities of the hydroxyl groups in formylation of the D-glucopyranosyl residues in dextrin.* Carbohydrate Research, 1967. **3**(3): p. 361-368.
140. Stochmayer, W.H., ed. *Advancing Fronts in Chemistry*. 1945, Reinhold Publishing Company: New York.
141. Taylor, G.R. and Darin, S.R., *The tensile strength of elastomers.* Journal of Polymer Science, 1955. **17**(86): p. 511-525.
142. Szczesny, S.E., Peloquin, J.M., Cortes, D.H., Kadlowec, J.A., Soslowsky, L.J., and Elliott, D.M., *Biaxial tensile testing and constitutive modeling of human supraspinatus tendon.* Journal of biomechanical engineering, 2012. **134**(2): p. 021004-021004.
143. Hackett-Jones, E.J., Landman, K.A., Newgreen, D.F., and Zhang, D., *On the role of differential adhesion in gangliogenesis in the enteric nervous system.* Journal of Theoretical Biology, 2011. **287**(1): p. 148-159.
144. Hotta, R., Anderson, R.B., Kobayashi, K., Newgreen, D.F., and Young, H.M., *Effects of tissue age, presence of neurones and endothelin-3 on the ability of enteric neurone precursors to colonize recipient gut: Implications for cell-based therapies.* Neurogastroenterology and Motility, 2010. **22**(3): p. 331-340+e86.
145. Bruggeman, J.P., de Bruin, B.-J., Bettinger, C.J., and Langer, R., *Biodegradable poly(polyol sebacate) polymers.* Biomaterials, 2008. **29**(36): p. 4726-4735.
146. Hamid, S.H., Amin, M.B., and Maadhah, A.G., *Handbook of Polymer Degradation*1992: Marcel Dekker.
147. Scott, G., ed. *Degradable Polymers: Principles and Applications*. 2003, Kluwer Academic Publishers The Netherlands: Dordrecht.
148. Shtilman, M.I., *Polymeric biomaterials part I polymer implants*2003: VSP BV, The Netherlands.
149. Hutmacher, D.W., Schantz, J.T., Lam, C.X.F., Tan, K.C., and Lim, T.C., *State of the art and future directions of scaffold-based bone engineering from a biomaterials perspective.* Journal of Tissue Engineering and Regenerative Medicine, 2007. **1**(4): p. 245-260.
150. Kretlow, J.D. and Mikos, A.G., *From material to tissue: Biomaterial development, scaffold fabrication, and tissue engineering.* AIChE Journal, 2008. **54**(12): p. 3048-3067.
151. Navarro, M., Michiardi, A., Castaño, O., and Planell, J.A., *Biomaterials in orthopaedics.* Journal of the Royal Society Interface, 2008. **5**(27): p. 1137-1158.
152. Bergsma, J.E., Rozema, F.R., Bos, R.R.M., Boering, G., De Bruijn, W.C., and Pennings, A.J., *In vivo degradation and biocompatibility study of in vitro pre-degraded as-polymerized polylactide particles.* Biomaterials, 1995. **16**(4): p. 267-274.
153. Smith, R., Oliver, C., and Williams, D.F., *The enzymatic degradation of polymers in vitro.* Journal of Biomedical Materials Research, 1987. **21**(8): p. 991-1003.

154. Williams, D.F., *Enzymic Hydrolysis of Polylactic Acid.* Engineering in Medicine, 1981. **10**(1): p. 5-7.
155. Visscher, G.E., Robison, R.L., Maulding, H.V., Fong, J.W., Pearson, J.E., and Argentieri, G.J., *Biodegradation of and tissue reaction to poly(DL-Lactide) Microcapsules.* Journal of Biomedical Materials Research, 1986. **20**(5): p. 667-676.
156. Pietzsch, M., Vielhauer, O., Pamperin, D., Ohse, B., and Hopf, H., *On the kinetics of the enzyme-catalyzed hydrolysis of axial chiral alkyl allenecarboxylates: Preparation of optically active R-(-)-2-ethyl-4-phenyl- 2,3-hexadiene-carboxylic acid and its optically pure S-(+)-methylester.* Journal of Molecular Catalysis - B Enzymatic, 1999. **6**(1-2): p. 51-57.
157. Kai, D., Prabhakaran, M.P., Jin, G., and Ramakrishna, S., *Guided orientation of cardiomyocytes on electrospun aligned nanofibers for cardiac tissue engineering.* Journal of Biomedical Materials Research - Part B Applied Biomaterials, 2011. **98 B**(2): p. 379-386.
158. Riboldi, S.A., Sadr, N., Pigini, L., Neuenschwander, P., Simonet, M., Mognol, P., Sampaolesi, M., Cossu, G., and Mantero, S., *Skeletal myogenesis on highly orientated microfibrous polyesterurethane scaffolds.* Journal of Biomedical Materials Research - Part A, 2008. **84**(4): p. 1094-1101.
159. Bashur, C.A., Dahlgren, L.A., and Goldstein, A.S., *Effect of fiber diameter and orientation on fibroblast morphology and proliferation on electrospun poly(d,l-lactic-co-glycolic acid) meshes.* Biomaterials, 2006. **27**(33): p. 5681-5688.
160. Lee, J.Y., Bashur, C.A., Gomez, N., Goldstein, A.S., and Schmidt, C.E., *Enhanced polarization of embryonic hippocampal neurons on micron scale electrospun fibers.* Journal of Biomedical Materials Research - Part A, 2010. **92**(4): p. 1398-1406.
161. Bashur, C.A., Shaffer, R.D., Dahlgren, L.A., Guelcher, S.A., and Goldstein, A.S., *Effect of fiber diameter and alignment of electrospun polyurethane meshes on mesenchymal progenitor cells.* Tissue engineering. Part A, 2009. **15**(9): p. 2435-2445.
162. Renouf-Glauser, A.C., Rose, J., Farrar, D.F., and Cameron, R.E., *The effect of crystallinity on the deformation mechanism and bulk mechanical properties of PLLA.* Biomaterials, 2005. **26**(29): p. 5771-5782.
163. Pham, Q.P., Sharma, U., and Mikos, A.G., *Electrospinning of polymeric nanofibers for tissue engineering applications: A review.* Tissue engineering, 2006. **12**(5): p. 1197-1211.
164. Yao, L., Haas, T.W., Guiseppi-Elie, A., Bowlin, G.L., Simpson, D.G., and Wnek, G.E., *Electrospinning and Stabilization of Fully Hydrolyzed Poly(Vinyl Alcohol) Fibers.* Chemistry of Materials, 2003. **15**(9): p. 1860-1864.
165. Zhang, C., Yuan, X., Wu, L., Han, Y., and Sheng, J., *Study on morphology of electrospun poly(vinyl alcohol) mats.* European Polymer Journal, 2005. **41**(3): p. 423-432.
166. Zeng, J., Aigner, A., Czubayko, F., Kissel, T., Wendorff, J.H., and Greiner, A., *Poly(vinyl alcohol) Nanofibers by Electrospinning as a Protein Delivery System and the Retardation of Enzyme Release by Additional Polymer Coatings.* Biomacromolecules, 2005. **6**(3): p. 1484-1488.
167. Slaughter, B.V., Khurshid, S.S., Fisher, O.Z., Khademhosseini, A., and Peppas, N.A., *Hydrogels in Regenerative Medicine.* Advanced Materials, 2009. **21**(32-33): p. 3307-3329.
168. Kobayashi, M., Toguchida, J., and Oka, M., *Development of Polyvinyl Alcohol-Hydrogel (PVA-H) Shields With A High Water Content For Tendon Injury Repair.* The Journal of Hand Surgery: British & European Volume, 2001. **26**(5): p. 436-440.

169. Graessley, W., *The entanglement concept in polymer rheology*, in *The Entanglement Concept in Polymer Rheology*1974, Springer Berlin Heidelberg. p. 1-179.
170. Crawford, R.J., *Plastics Engineering 3rd edition*, 1998, Butterworth Heinemann: Oxford.
171. Koski, A., Yim, K., and Shivkumar, S., *Effect of molecular weight on fibrous PVA produced by electrospinning.* Materials Letters, 2004. **58**(3–4): p. 493-497.
172. Jarusuwannapoom, T., Hongrojjanawiwat, W., Jitjaicham, S., Wannatong, L., Nithitanakul, M., Pattamaprom, C., Koombhongse, P., Rangkupan, R., and Supaphol, P., *Effect of solvents on electro-spinnability of polystyrene solutions and morphological appearance of resulting electrospun polystyrene fibers.* European Polymer Journal, 2005. **41**(3): p. 409-421.
173. Assender, H.E. and Windle, A.H., *Crystallinity in poly(vinyl alcohol). 1. An X-ray diffraction study of atactic PVOH.* Polymer, 1998. **39**(18): p. 4295-4302.
174. Socrates, G., *Infrared and Raman Characteristic Group Frequencies: Tables and Charts*, 2001, John Wiley & Sons, Ltd.: Chichester.
175. Jaafar, I., Ammar, M., Jedlicka, S., Pearson, R., and Coulter, J., *Spectroscopic evaluation, thermal, and thermomechanical characterization of poly(glycerol-sebacate) with variations in curing temperatures and durations.* Journal of Materials Science, 2010. **45**(9): p. 2525-2529.
176. Montserrat, S., *Effect of crosslinking density on ΔCp(Tg) in an epoxy network.* Polymer, 1995. **36**(2): p. 435-436.
177. Peijs, T., van Vught, R.J.M., and Govaert, L.E., *Mechanical properties of poly(vinyl alcohol) fibres and composites.* Composites, 1995. **26**(2): p. 83-90.
178. Hodge, R.M., Bastow, T.J., Edward, G.H., Simon, G.P., and Hill, A.J., *Free volume and the mechanism of plasticization in water-swollen poly(vinyl alcohol).* Macromolecules, 1996. **29**(25): p. 8137-8143.